WAVE ENVELOPE ELEMENTS FOR ACOUSTICS

A THESIS PRESENTED FOR THE DEGREE
OF
DOCTOR OF PHILOSOPHY
IN
MECHANICAL ENGINEERING
AT THE
UNIVERSITY OF CANTERBURY
by
Gavin John Macaulay

University of Canterbury
1994

To my parents.

The illustration on the previous page is a solid colour version of that presented in figure 31

Abstract

This thesis develops and extends a method for modelling acoustical propagation in unbounded domains. This *wave envelope* method is ideally suited for inclusion into existing acoustic finite element formulations. Results are presented for test cases which show close agreement between the wave envelope results and analytical results. Basis function interpolation in the wave envelope elements can be varied from order 2 to order 10, allowing for modelling of complicated pressure fields solely with wave envelope elements. The system to be solved consists of three frequency independent matrices, allowing easy generation of frequency response data. For large systems a frequency response calculation can consume considerable CPU time and a modal decomposition procedure using *Ritz vectors* is presented that can significantly reduce computation times, with minimal loss in accuracy. The use of Ritz vectors was also found to give better results than the full solution for some situations.

Acknowledgements

The support and guidance provided by my supervisor, Professor R.J. Astley, is gratefully acknowledged.

Profuse thanks go to Wayne Munro for the many mathematical discussions we had, as well as for his readiness to consider any problems that I encountered.

I would like to thank Phillip Smith for his help in all matters concerned with computers, and the Computer Services Centre of the University of Canterbury for providing ever improving computing resources.

I wish to acknowledge the financial support of the Royal Aeronautical Society of New Zealand in the form of the Mercer Memorial Scholarship.

Many thanks go to Numerical Integration Technologies of Belgium for the use of their SYSNOISE acoustical analysis software.

Finally I wish to thank fellow students and friends, especially Debbie, Nicky, Dave and Katharine.

Contents

List of Figures

List of Tables

List of Symbols

Symbol	Description	Units
$\mathbf{A}$	matrix used in Ritz algorithm	
$\mathbf{B}$	matrix used in Ritz algorithm	
A	complex wave amplitude	
$\mathbf{C}$	final assembled damping matrix	
$\hat{\mathbf{C}}$	reduced, assembled damping matrix	
$\mathbf{c}$	assembled damping matrix	
c	wave speed ($c = f\lambda$)	m/s
c_j	inner product used in Ritz algorithm	
D	wave envelope basis function factor	
$\mathbf{f}$	assembled forcing vector	
$\hat{\mathbf{f}}$	reduced, assembled forcing vector	
f	frequency	Hz
i	$\sqrt{-1}$	
i, j	integer counters	
J	Jacobian matrix	
$\mathbf{K}$	final assembled stiffness matrix	
$\hat{\mathbf{K}}$	reduced, assembled stiffness matrix	
$\mathbf{k}$	assembled stiffness matrix	
k	acoustical wavenumber ($k = 2\pi f/c = \omega/c$)	1/m
$\mathbf{M}$	final assembled mass matrix	
$\hat{\mathbf{M}}$	reduced assembled mass matrix	
$\mathbf{m}$	assembled mass matrix	
M	mapping function	
$\mathbf{n}$	normal to surface	
$\hat{\mathbf{n}}$	unit normal to surface	
n	integer counter	
$\mathbf{P}$	Ritz basis	
P	conventional component of basis function	
$\mathbf{p}$	acoustical pressure vector	Pa
$\hat{\mathbf{p}}$	reduced acoustical pressure vector	Pa

p	Ritz vector	
$\dot{p}$	derivative of a Ritz vector	
p	acoustical pressure	Pa
p'	finite element approximation to pressure, p	Pa
$\mathbf{q}$	nodal pressure vector	Pa
q	nodal pressure	Pa
$\mathbf{r}$	assembled damping matrix	
R	finite element residual equation	
$\hat{\mathbf{r}}$	cylindrical coordinate radial unit vector	
r	radial distance	
S	surface area	m^2
S^e	surface area of an element	m^2
t	time	seconds
U	normal velocity to a surface	
V	volume	m^3
V^e	volume of an element	m^3
W	finite element weighting function	
w	Gaussian weighting constant	
$\mathbf{x}$	Ritz vector	
x, y, z	coordinates in real space	m
$\mathbf{y}$	Ritz forcing vector	
$\mathbf{z}$	combined Ritz vector and it's derivative	
$\dot{\mathbf{z}}$	derivative of $\mathbf{z}$	

Greek letters

ε	local element coordinate	
η	local element coordinate	
$\hat{\theta}$	cylindrical coordinate angular unit vector	
λ	wavelength	m
μ	wave envelope basis function factor	
ρ	fluid density	kg/m^3
ϕ	basis function	
ψ	local element coordinate	
ω	frequency ($\omega = 2\pi f$)	radians/s

Chapter 1

Introduction

1.1 Introduction

This thesis investigates and extends a method that permits the modelling of unbounded domains when using the finite element method for acoustical radiation and scattering. This *wave envelope* method is ideally suited to inclusion in existing acoustic finite element procedures.

Wave envelope elements are presented for two- and three-dimensional analyses, and their behaviour is illustrated with several test cases. High interpolation order in the radial basis functions is introduced and the effect of increasing this interpolation order on otherwise identical models is studied. Limitations of the method are shown to be consistent with the known behaviour of analytic test solutions. An absolute limit on the highest interpolation order was found to be related to computational precision, and this places a corresponding limit on the highest frequency usable in an analysis. The geometries that wave envelope elements will mesh without requiring the use of conventional elements is also discussed.

A mode superposition technique (using *Ritz vectors*) is investigated that reduces the CPU time for calculating frequency response curves. Ritz vectors have been successfully applied to structural systems, and are now adapted to the systems obtained with wave envelope elements. The accuracy and CPU time savings realised by the use of Ritz vectors are assessed on radiation and scattering problems.

All results in this thesis have been calculated with a fluid density of 1.2 kg/m^3 and a wave speed of 340 m/s on a SUN SPARCcenter 2000 computer (containing two CPUs, each capable of approximately 100 MIPS), with 256 MB of RAM.

1.2 Assumed background

This thesis assumes that the reader has a reasonable knowledge of the finite element method. If not, there is a large selection of reference books available. Most finite element

books deal with structural, solid mechanics and heat transfer formulations, devoting little space to wave-type formulations. A book which does discuss wave-type problems clearly and in detail is *Finite Element Analysis* by Burnett [26]. Two books of encyclopedic proportions which deal with a very broad base of applications including solution of wave-like equations are *The Finite Element Method* by Zienkiewicz and Taylor [100, 101] and *The Finite Element Handbook* edited by Kardestuncer [63].

1.3 Historical development

1.3.1 Acoustics

Acoustics is the science of sound. The study of acoustics originated from interest in music and musical instruments as far back as 3000BC when the Chinese philosopher Fohi attempted to find a link between the pitch of a sound and the five elements: earth, water, air, fire and wind. Many of the ancient societies formed theories on the causes of sound, including the Hindus, the Arabs and the Greeks. Real progress was not made on the theoretical foundations of acoustics until the seventeenth century, when Galilei and Mersenne produced work on vibrating strings.

In 1678 Hooke proposed his law relating force to deformation. This formed the basis of the theory of vibrations, and subsequently acoustics. Experimental acoustics was founded in 1802 with the publication of *Die Akustik* by Chladni. The eighteenth century saw the development of mathematical methods applicable to acoustics, some important discoveries were Euler's theory of standing waves in ropes, Fourier's series, and the many contributions from d'Alembert, the Bernoulli brothers, Laplace and Lagrange. The nineteenth century saw contributions by Hertz, Maxwell, Faraday, Ohm and Helmholtz. A major contribution was made by Rayleigh, who's book *Theory of Sound* (1877) laid the theoretical foundations of acoustics in a thorough and complete manner.

Analytical solutions to the wave equation have been developed to describe the interaction of sound fields with mathematically simple geometries such as plane baffles, spheres and cylinders. Extension of analytic solutions to more complicated geometries and boundary conditions is difficult, and solutions must generally be obtained via other techniques. Finite element and boundary element numerical techniques are popular and are able to deal with arbitrary geometries with complicated boundary conditions. Acoustical ray theory can be used at high frequencies where conventional discrete numerical methods become unwieldy.

1.3.2 Finite elements

Beginning in the 1940's, the ideas that form the finite element method evolved gradually from contributors in the fields of applied mathematics, physics and engineering. By making possible the quick solution of large systems of simultaneous equations, digital

computers (first available in the 1950's) accelerated the development of the finite element method.

The idea of dividing a continuum into small sections was first suggested by Courant [31] in 1943. In 1956 Turner *et al.* [89] modelled a simple wing-like (box-beam) structure using an assemblage of triangular elements and obtained good results (within 2% of analytical in the best case). This was the first practical implementation of what came to be known as the finite element method. In the abstract of Turner's paper it was stated that "considerable extension of the material presented in this paper is possible".

The finite element method was developed and used only in the structural context until 1965, when Zienkiewicz and Cheung [98] demonstrated the use of the finite element method for field problems which could be placed in variational form. This greatly increased the scope of the method. A further advance in the widespread application of the finite element method was the discovery by Szabo and Lee [87] that "piecewise polynomial approximation of the displacement field in conjunction with Galerkin's error distribution" could be used to formulate almost any partial differential equation into a form amenable to finite element analysis.

The finite element method is today used for a multitude of problem types. These include static and dynamic analysis of aircraft, automotive, marine, and building structures; earthquake response of buildings and structures; fracture mechanics and solid mechanics; composites, and fibres; all manner of fluid flow problems including supersonic flows, pollutant dispersion, surface waves, ignition and combustion; acoustic and electromagnetic fields; heat conduction; coupled problems involving different problem types, and even chemical reactions. Many of these topics are covered in *The Finite Element Method* [100, 101] and *The Finite Element Handbook* [63].

1.3.3 Finite elements for acoustics

The finite element method was first applied to acoustical problems in the mid 1960's by Gladwell [46, 47]. Two formulations were developed with the aim of modelling structural-acoustic problems, one involving displacements and the other "force-like" quantities, such as stress or pressure . These ideas were extended to three-dimensional finite elements by Craggs [33], who modelled a simple window-room system. In a subsequent paper [34] tetrahedra elements were used to model the natural modes of complex shaped enclosures (in this case a car). The degrees of freedom at each node were reduced to one, namely the acoustic pressure, whereas previous formulations had used the spatial derivatives of the pressure as well, giving four degrees-of-freedom at each node.

An isoparametric twenty node element was borrowed from solid mechanics finite element formulations for use in acoustics by Petyt [80] in 1976. Pressure was the only degree-of-freedom. This element was used to model the mode shapes and frequencies of the interior of a van. The results agreed well with experiments performed.

A review of structural-acoustic finite element analysis with an emphasis on automobile

passenger compartments was published by Nefske in 1982 [74], and a review of acoustic finite elements including formulations for absorption was presented by Craggs [36].

The use of finite elements for acoustical modelling of enclosures is now commonplace. Many finite element packages include acoustical elements, and allow coupling of these to other, mainly structural, elements (ANSYS, ABAQUS, and NASTRAN, for example, are three commercial codes which offer this facility). The use of finite elements in enclosures is limited when the enclosure becomes large and/or the frequency of interest becomes high, since a large mesh is then required to adequately resolve the pressure field. Acoustical ray theory is used for high frequency analyses, predominately in 'architectural' situations [77].

Other uses of acoustic finite elements include muffler design [35], loudspeaker design [59] and modelling sound propagation in ducting [8]. Duct acoustics is an important field, an obvious application being the modelling of sound absorption, with the aim of increasing the absorption by changes in duct design.

The method can also be used to model wave propagation in non-homogeneous media, or media with inclusions. Gan *et al.* [44] present a finite element formulation of scattering in non-homogeneous mediums and Teng presents examples of scattering of waves by an inclusion [88], with a geophysics emphasis.

1.3.4 Infinite domains

Conventional finite element techniques do not cope well with large or infinite domains. A rule of thumb used when constructing an acoustical finite element mesh for a large but bounded domain is that there should be seven to ten nodes per wavelength to adequately resolve acoustic waves. Figure 1 illustrates the errors possible when approximating a one-dimensional wave, as occurs in a finite element representation of a wave-type disturbance. Parts (a) and (b) compare discrete linear approximations to the exact wave solution, with five and ten nodes respectively. Part (c) shows a five node approximation with quadratic interpolation. In terms of quality of approximation for a given number of nodes, part (c) is clearly preferable to parts (a) or (b).

The number of nodes required for analysis at even moderate frequencies can quickly exceed computer storage limits. For example, an adequate mesh of 10 nodes per wavelength for 1 cubic metre of air with a density of 1.2 kg/m^3 and a wave speed of 340 m/s would require the use of approximately 27 000 nodes for analysis in the frequency range 0–1000 Hz.

A more fundamental difficulty occurs when an acoustical problem involves an infinite or unbounded domain. These occur frequently in nature, and obviously are impossible to mesh using conventional finite elements. An initial approximation to modelling an unbounded region has been to construct a mesh extending for many wavelengths from the radiating or scattering body and then apply some form of non-reflecting boundary condition (NRBC) to the outer boundary of the mesh. The purpose of the NRBC is to absorb all radiation reaching it, not permitting any reflection back into the meshed region. The least

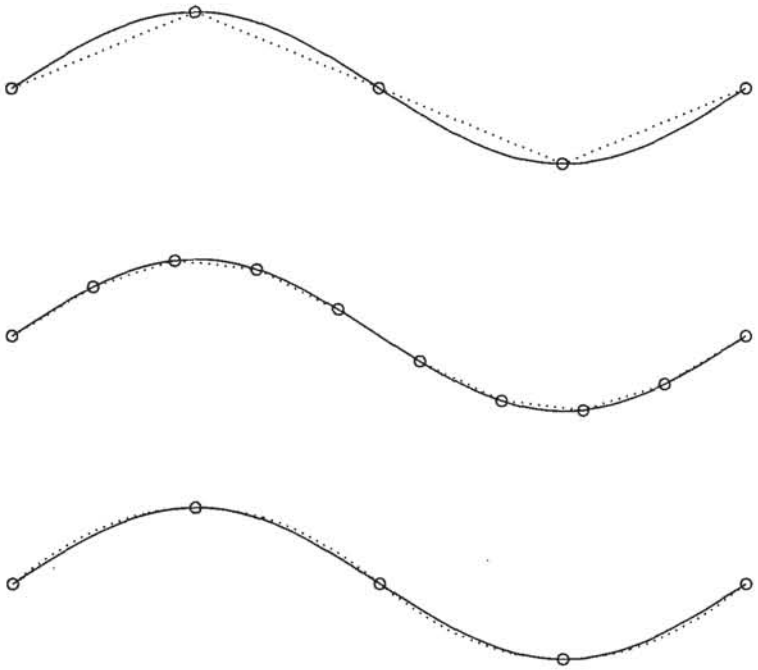

Figure 1: Finite element representations of waves. Dotted lines represent the finite element approximation to a sine curve (solid line). (a) five nodes with linear interpolation; (b) ten nodes with linear interpolation; (c) five nodes with quadratic interpolation.

complex of these is the Sommerfeld radiation condition, which will be discussed more fully in section 2.3.2. Many more advanced NRBC techniques of varying success and generality exist. An early NRBC was developed by Engquist and Majda [40, 41] who proposed a sequence of local approximate boundary conditions of increasing order. Bayliss and Turkel [14] developed a sequence of NRBC's for the wave equation, based on an asymptotic expansion of the solution at large distances. Subsequent enhancements were presented in [16] and [15]. Many other NRBCs have been developed for a multitude of problem types including acoustics, fluid-solid interaction, gasdynamics, hydrodynamics, meteorology, elasticity and electromagnetism. A discussion of the NRBCs for these problem types is given in *Numerical Methods for Problems in Infinite Domains* by Givoli [45]. This book introduces the most recent addition to these, the DtN NRBC. The DtN method uses a modal expansion in the outer region to define a relationship between the acoustic pressure and its directional derivatives on the outer edge of the inner region. These values are then used as boundary conditions on the inner region. Accuracy is dependent upon the number of modes taken into account when formulating the DtN boundary conditions. The shape of the inner region must be such that a separable eigenmode expansion can be calculated—that is to say must be cylindrical, spherical or ellipsoidal. The DtN method has been applied to the Helmholtz equation by Harari and Hughes [49].

Boundary element method

An alternative method for modelling unbounded domains is the boundary integral (BI) method. This method makes use of fundamental solutions associated with the governing equation of the problem of interest. The fundamental solutions can be selected to exhibit the characteristics of the desired solution and can deal implicitly with unbounded domains. Fundamental solutions cannot be found for all governing equations, limiting the problem types to which BI formulations can be applied.

In 1963 Symm and Jawson presented a numerical method that solved BI equations for potential problems with Dirichlet, Neumann and Cauchy boundary conditions [86, 55].

A numerical procedure based on discrete "boundary elements"—similar to finite elements, but existing only on the bounding surface of the domain of interest—was adapted by Brebbia to BI formulations. This work was carried out in the years leading up to 1978, when the first book on boundary element methods was published [25]. The term "boundary element" (BE) method was coined at this time.

The application of the BI/BE method to wave-type problems was first proposed by Friedman and Shaw [43], Cruse and Rizzo [39] and Cruse [38]. The exterior BE method (BEM) was found to have a problem with uniqueness at frequencies that correspond to eigenvalues of the corresponding interior problem. This issue is discussed in the review paper by Klienman and Roach [65].

Various remedies have been proposed for this difficulty. The Combined Helmholtz Integral Equation Formulation (CHIEF) method was proposed by Schenck [83], and uses

auxiliary points located in the interior problem, leading to an overdetermined system of linear equations. The eigenfunctions of the interior problem must not be zero at the interior points. In practice, placing the interior points is a difficult task, and is the main drawback of the CHIEF method. It is widely used however and is regarded as a robust method.

Burton and Miller [27] proposed an alternative approach that uses a combination of two integral equations—the usual BI equation and its normal derivative. The normal derivative integral equation involves hypersingular integrals, and numerical evaluation is difficult. Developments in the evaluation of hypersingular integrals is reviewed by Chien *et al.* [29].

All boundary element formulations require a mesh to be constructed on the boundary of the domain, unlike the finite element method which requires a mesh throughout the entire domain. This leads to a reduction in the dimensionality but does not necessarily give an associated computational benefit over the finite element method [50].

The use of the BEM for inhomogeneous, anisotropic or non-linear problems is not well developed.

Method of fundamental solutions

A recent method for modelling radiation and scattering from objects into an infinite medium is the method of fundamental solutions (also called the wave superposition or collocation method). The method originated in the study of electromagnetic scattering [70, 71], and was subsequently applied to acoustical radiation and scattering by the same authors [24]. The scattered field is generated by a set of sources placed inside the scatterer and the amplitude of the sources are constrained to satisfy a set of given boundary conditions on the surface of the scatterer. This gives a set of simultaneous equations, which can be solved to yield the source amplitudes. Pressures in the exterior region can then be calculated by superposition of the contributions from each source. The location of the sources can be specified or unspecified, leading to a set of linear or non-linear simultaneous equations respectively. The interior acoustic field of the scatterer can be modelled by placing sources outside the scatterer and the source type can be selected to suit the problem type.

A subsequent paper by Koopmann [67] established that this method was equivalent to the Helmholtz-integral formulation (as used in many boundary element formulations for acoustics), giving the method a sound mathematical parentage. The evidence to date suggests that the method of fundamental solutions does not exhibit the same problems associated with non-uniqueness at particular frequencies that Helmholtz integral boundary element formulations have. However the method of fundamental solutions does present numerical problems when applied to scatterers with high aspect ratios (see [67]). The method has also been used to model radiation and scattering in fields other than acoustics, such as elastic solids with inclusions. It has also been used to model potential-flow problems, elastostatics and elliptic boundary value problems. References to these topics

and a discussion of the modelling of elastic waves appears in [66].

Infinite elements

Infinite elements are similar to conventional finite elements, but are infinite in one or possibly two directions. Infinite elements were developed independently by Ungless and Anderson in 1973 [1, 90] and by Zienkiewicz and Bettess in 1975 [96]. The work of Ungless and Anderson, which was not published until 1977, used a basis function that varied as $1/(1+r)$ in the radial direction. The infinite elements of Zeinkiewicz and Bettess [23, 96] used an exponential decay term and a harmonic wave-like term in the basis functions to generate solutions of the Helmholtz equation. Bettess [19, 20] in 1977 presented an infinite element in which the basis functions from ordinary finite elements are multiplied by a decay function appropriate to the problem. Bettess employed an exponential decay function and used the elements to solve a simple two-dimensional viscous flow problem.

A comprehensive coverage of the development of infinite element techniques is presented by Bettess [22]. He divides infinite element formulations into two main types;

- those that define a mapping of the parent element from the finite to the infinite domain, with basis functions defined over the *parent* region, and
- those that use basis functions defined globally over the *infinite* region, augmented by decay functions, also defined over the infinite region.

Considerable overlap exists between these two classifications. The mapping method was first described by Beer and Meek [18] who used a two-part linear and non-linear mapping to transform the parent element from a finite ε domain to an infinite x domain. Zienkiewicz [95, 97, 99] later developed a simpler mapping function, which for [97] and [99] allowed the use of standard Gauss-Legendre integration rules (Note that [5] corrects an erroneous explanation regarding some integrals over an unbounded domain in [95], however the results obtained by the algorithm in [95] are not affected). Zienkiewicz's mapping functions have been tabulated by Marques and Owen [72] for one-, two- and three-dimensional elements, including two-dimensional elements mapped to infinity in two directions. The same mapping functions have been used in the wave envelope elements developed in this thesis. Infinite elements have been used to model electrical potential problems, acoustic fields, diffusion problems, fluid-structure interaction, surface waves, soil-structure interaction and with some adjustments transient problems (see [22], mainly chapters 8 and 11).

Wave envelope elements

The wave envelope concept was first suggested by Baumeister [10, 11, 12] in 1974, and was used to model the steady-state behaviour of high-frequency sound propagation in ducts.

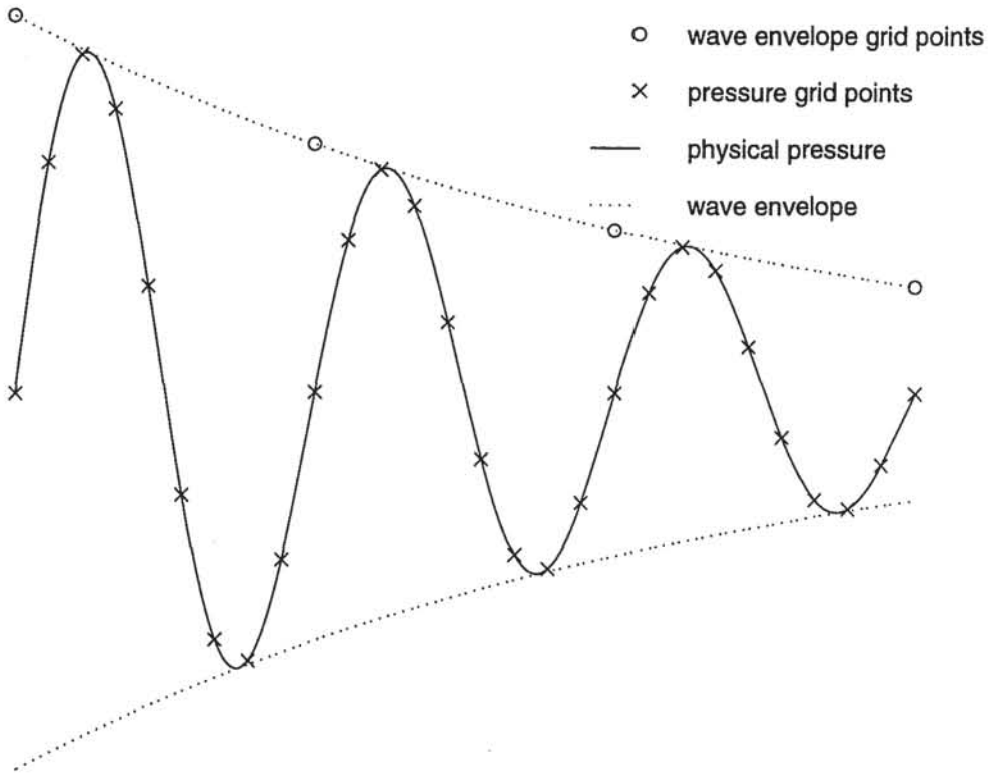

Figure 2: Wave envelope concept

Baumeister made the assumption that the acoustical pressure $P(x)$ (in the one-dimensional case) could be written as

$$P(x) = p(x)e^{-i2\pi x/\lambda}, \tag{1}$$

where λ denotes the axial wavelength. He substituted this expression into the Helmholtz equation to obtain a modified form of the wave equation which he called the 'wave envelope equation'. The wave envelope equation was then solved for duct geometries using the finite difference technique. Equation 1 removed the oscillatory part of the acoustic wave leaving only the envelope of the acoustic wave to be modelled. Figure 2 illustrates the significant reduction in the number of finite difference grid points required to model the full wave compared to the wave envelope. The figure also illustrates the origin of the term 'wave envelope'. Implicit in the wave envelope formulation is the requirement that the local direction of wave propagation is known in advance, at least in an approximate sense. This requirement is trivial for duct studies, but can become difficult to satisfy for more complex geometries. Baumeister later extended the wave envelope concept to model transient sound propagation [13] in ducting. Nayfeh and Kaiser [60, 73] used the wave envelope concept to model sound propagation in non-uniform ducts with sheared flow, although they stated that "in most respects it bears little resemblance to the procedure

used by Baumeister". Their method used the superposition of quasiparallel duct modes to represent the acoustic signal and subsequently only required the calculation of the slowly varying mode amplitudes and phases of the sound field. Baumeister used the finite difference technique in his work, but mentioned that the wave envelope method could be used with finite elements.

Astley and Eversman [7, 42] in 1981 applied the wave envelope concept to finite element analysis of acoustic duct transmission and found that significant increases in efficiency over conventional finite element techniques were possible. A subsequent paper [9] proposed a modified wave envelope scheme for a conical expansion differing in two main aspects. The weighting functions used in the Galerkin finite element scheme which had previously been chosen to be the same as the element basis functions were defined as

$$N_j(x) = (x_j/x)e^{-ik(x-x_j)}N_j'(x),$$

where N_j' is a conventional basis function for node j, and x the axial coordinate. This represented the asymptotic behaviour of propagating waves correctly for large values of x. The second change was the selection of the weighting functions as *complex conjugates* of the basis functions. This removed all oscillatory terms from the system integrals, permitting the use of standard Gauss-Lengendre integration rules. Previous forms of the wave envelope concept had required integrations of oscillatory terms. These elements were used to solve Webster's horn equation and were coupled with conventional acoustic finite elements.

The same authors then applied wave envelope finite elements and conventional finite elements to the modelling of sound radiation from axisymmetric duct openings and jet engine intake geometries [3]. This involved computation over a three-dimensional axi-symmetric unbounded domain. The unbounded region was dealt with by applying the Sommerfeld radiation condition on the outer boundary of the wave envelope mesh. Comparisons were made between conventional, infinite and wave envelope schemes. It was concluded that the wave envelope method incorporated most of the advantages of the infinite element scheme, and accurately represented the behaviour in the far-field. A wave envelope element that allowed for non-uniform mean flows was also introduced by Astley [4] and Parrett [79].

The wave envelope elements in the above discussion were of a finite size. An extension of the wave envelope concept to elements of infinite length (in one direction) was proposed by Bettess [21] (for a simple one-dimensional case). Bettess then proposed the use of mapped infinite wave envelope elements in unbounded problems in a private communication to Coyette in 1988. The formulation selected by Bettess, however, would not have worked because of the incorrect treatment of some integrals over an unbounded domain (this omission was discussed in [5]). The application of infinite mapped wave envelope elements to two- and three-dimensional acoustical problems (with the correct treatment of the integrals over an unbounded domain) was carried out by Astley *et al.* [6] and later investigated by Cremers *at al.* [37]. The mapping developed for infinite elements

by Zienkiewicz *et al.* was used to transform the finite wave envelope elements into infinite wave envelope elements. This made the wave envelope element method almost identical to the infinite element approach, the difference being in the specification of the weighting functions. Astley's weighting functions, beside being complex conjugates of the shape functions, possess in their mapped version an additional factor that removes the need to calculate an integral over the far-field boundary.

It will be shown later in this thesis that the mapped infinite wave envelope formulation yields a system of linear equations of the form

$$\left[\mathbf{K} + ik\mathbf{C} - k^2\mathbf{M}\right]\mathbf{q} = \mathbf{f}, \tag{2}$$

where $\mathbf{K}$, $\mathbf{M}$ and $\mathbf{C}$ are constant matrices which do not depend upon the frequency parameter, k. This eases the calculation of solutions at multiple frequencies. Most other methods for unbounded domains, notably the boundary element method, do not have this feature and require the full coefficient matrix of equation 2 to be assembled at each frequency interval. This frequency independence of the acoustical stiffness, damping and mass matrices is also essential to the use of Ritz vectors.

Wave envelope elements fit in well with the techniques used in conventional finite elements and allow the modelling of unbounded domains without any of the uniqueness problems that the boundary element method suffers from. Finding the pressure at a given point in the domain is numerically trivial, allowing the calculation of pressures at a large number of points in a short time. This is in contrast to the boundary element method where the calculation of field point pressures often consumes the majority of the solution time.

1.3.5 Ritz vectors

In 1950 Lanczos proposed an algorithm for calculating the extreme eigenvalues and eigenvectors of a symmetric matrix [68]. This algorithm, called the Lanczos algorithm, could also be used to reduce a symmetric matrix to tridiagonal form, from which it was then a trivial matter to extract eigenvalues and eigenvectors.

However the Lanczos algorithm was greatly affected by round off error which manifested itself as a loss of orthogonality among the Lanczos vectors. The advent of Householders stable method of tridiagonalisation, combined with the orthogonality problem of the Lanczos algorithm lead to a decline in its use in the 1950's and 1960's. It was later revived because of the ability to generate a few eigenvalues of a matrix with a minimum of computational effort. This was especially useful for the large sparse matrices found in finite element problems. Various orthogonalisation schemes have been devised to minimise the loss of orthogonality of the Lanczos vectors, and the Kaniel-Paige theory [61, 78, 82] has been developed to provide a means of testing for convergence of the algorithm.

When care is taken the Lanczos algorithm will quickly and efficiently find a number of the largest and smallest eigenvalues and eigenvectors of the generalised eigenproblem.

Its speed of convergence is such that it is becoming the "eigensolver of choice" for finite element analyses [30, Appendix C.5], and is superior to most other methods for extracting a small number of eigenvectors and eigenvalues (in terms of the numerical effort required [75]). Guides to the theory and implementation of the Lanczos algorithm can be found in *The Finite Element Method* [51] and *Matrix Computations* [48].

At about the same time that the Lanczos method was rehabilitated, an algorithm was proposed by Wilson *et al.* [93] in 1982 to generate what they called *Ritz vectors*, with the aim of using these to solve dynamic response problems, avoiding the costly evaluation of eigenvalues and eigenvectors required in dynamic analyses based on modal expansions of the dynamic system. The Ritz vectors formed an alternative orthogonal set of vectors for use in a mode superposition analysis. It was also shown that using Ritz vectors for the mode superposition basis generated more accurate solutions, with fewer vectors, than if the exact eigenvectors had been used.

A subsequent paper [92] pointed out the similarly between the Ritz algorithm and the Lanczos algorithm. In fact, the recurrence part of the algorithms are identical except for the choice of starting vector. The Lanczos method uses an arbitrarily chosen vector, while the Ritz method uses a spatial load vector appropriate to the problem. This choice of a spatial load vector as the starting vector forces the Ritz algorithm to generate only vectors which are excited by the spatial load vector and therein lies the power of the Ritz method. When eigenvectors are used in a mode superposition analysis the eigenbasis can contain modes that cannot physically exist with the prescribed loading, causing some redundancy.

The original Ritz vector algorithm has been extended and applied to a variety of problem types. Bayo and Wilson have applied Ritz vectors to wave propagation and foundation response [17] and substructure analysis [91].

A paper by Léger and Wilson [69] brought together and clarified the relationship between the Lanczos and Ritz algorithms. It was mentioned in passing that the application of Ritz vectors to non-proportionally damped systems was possible. This was elaborated upon in the following year by a paper that compared the use of a real and a complex Ritz basis [52]. It was found that although the complex basis gave more accurate results, the increase in computation time over the real basis made the real basis the better choice. In the same year Coyette [32] applied the Ritz algorithm to damped, bounded acoustical finite element systems, using a complex Ritz basis.

Progress has been made by various researchers on developing truncation criteria for the Ritz vectors [53, 57]. The vectors have also been applied to non-linear systems [28, 54, 62], where the Ritz vectors have to be updated periodically.

Since the Ritz vectors are generated from the system loading vector, systems where the form of the loading vector changes with time or frequency are not immediately amenable to Ritz vector reduction. Some progress has been made in this area [94], using a combination of load dependent and frequency dependent vectors.

1.4 Scope of material covered in the remainder of the thesis: author's contribution

This thesis details two distinct areas of investigation. They are;

1. The implementation of higher order infinite, mapped, wave envelope elements for three-dimensional acoustical problems and testing of the resulting solutions against known solutions for radiation and scattering. The associated theory is covered in chapter 2, and the results are presented in chapter 4.

2. The investigation of the utility of mode superposition using Ritz vectors for multi-frequency calculations of radiation and scattering in infinite domains using the wave envelope formulation. The theory is covered in chapter 3 and the results presented in chapter 5.

All of the wave envelope results presented in this thesis were obtained from a computer program written by the author. This program implemented linear and quadratic, two- and three-dimensional wave envelope elements, as well as conventional acoustic finite elements. Solution of the resulting systems was performed via either a conventional LU decomposition or Ritz vector mode superposition method (the Ritz vector algorithm originally proposed by Wilson [93] was modified to allow for the unusual nature of the matrices found in the wave envelope element formulation).

Chapter 2

The application of finite element techniques to acoustical problems

2.1 Acoustics and sound propagation

The propagation of acoustic waves through a homogeneous, inviscid, compressible fluid is governed by the wave equation. For the purposes of this thesis it is assumed that only small disturbances to the equilibrium pressure occur, allowing one to neglect second order effects and giving a linear wave equation. Derivation of the wave equation from basic principles is covered in many books on acoustics and vibrations (for example *Fundamentals of Acoustics* [64]), and will not be covered here.

The linear wave equation is

$$\nabla^2 P = \frac{1}{c^2}\frac{\partial^2 P}{\partial t^2},$$

where ∇^2 is the Laplacian operator, P is the acoustical pressure, c is the speed of propagation of waves in the fluid, and t is time.

If only time-harmonic waves are permitted, one can define

$$P(\mathbf{x}, t) = p(\mathbf{x})e^{i\omega t},$$

where p is the time invariant amplitude of acoustical pressure, $\mathbf{x}$ is a spatial vector, i is equivalent to $\sqrt{-1}$ and ω is the circular frequency in radians/s.

Substituting this into the wave equation yields the Helmholtz equation,

$$\nabla^2 p + k^2 p = 0,$$

where $k = \omega/c$, is called the acoustical wavenumber and is inversely proportional to the wavelength of a plane wave. Subsequent sections will deal with the solution of the Helmholtz equation in arbitrary domains (including unbounded domains).

2.1.1 Boundary conditions

This section describes how various physical boundary conditions can be described mathematically.

Rigid surface

A rigid surface permits no motion of itself, and any sound field incident upon the surface will have a zero normal component of particle velocity on the surface. Using the expression developed in appendix D, the rigid surface boundary condition can be expressed as $U = 0$, and hence as

$$\nabla p \cdot \hat{\mathbf{n}} = 0, \tag{3}$$

where $\hat{\mathbf{n}}$ is the normal to the rigid surface.

Vibrating rigid surface

A vibrating rigid surface will drive the fluid adjacent to it at the same velocity as itself. This is expressed as (see appendix D)

$$\nabla p \cdot \hat{\mathbf{n}} = -ik\rho cU. \tag{4}$$

Scattering of an incident sound field

The sound field due to the scattering of an incident wave by a rigid object is given by the superposition of the incident and scattered waves,

$$P(x, y, z, t) = (p_i(x, y, z) + p_s(x, y, z))\, e^{i\omega t},$$

where p_i is the incident sound field and p_s the scattered sound field. Both p_i and p_s must satisfy the Helmholtz equation.

If p_i is known, the scattered field is found by solving the Helmholtz equation for an equivalent velocity distribution on the surface of the rigid scatterer, the total field being obtained by superposition.

The equivalent velocity distribution on the scattering surface is obtained in the following way.

Given that the normal velocity on the surface of the scatterer is zero, that is,

$$(\nabla p_i + \nabla p_s) \cdot \hat{\mathbf{n}} = 0.$$

The normal gradient of the scattered field must satisfy

$$\nabla p_s \cdot \hat{\mathbf{n}} = -\nabla p_i \cdot \hat{\mathbf{n}},$$

on the scattering boundary, which is equivalent to boundary condition 4 with p replaced by p_s and U given by

$$U = \frac{\nabla p_i \cdot \hat{\mathbf{n}}}{ik\rho c}.$$

To proceed further requires knowledge of the incident field. In the case of a plane wave travelling in the direction given by the vector wavenumber $\hat{\mathbf{k}}$ the pressure is

$$p = Ae^{-i\mathbf{k}\cdot\mathbf{x}},$$

where A is the amplitude of the wave (which can be complex), and $\mathbf{x}$ is the position vector of the point of interest. Hence

$$\nabla p_i \cdot \hat{\mathbf{n}} = -Ai\mathbf{k} \cdot \mathbf{n}e^{-i\mathbf{k}\cdot\mathbf{x}}$$

and then

$$U = \frac{-\hat{\mathbf{k}} \cdot \hat{\mathbf{n}}\, Ae^{-i\mathbf{k}\cdot\mathbf{x}}}{\rho c}.$$

2.2 Acoustic finite elements

This section summarises the development of a finite element formulation for the solution of the Helmholtz equation in bounded domains using the Galerkin method. Note that the theory is developed in three dimensions, but that the two-dimensional case is easily extracted.

2.2.1 General Galerkin formulation for solution of the Helmholtz equation in bounded regions

Consider the solution of the Helmholtz equation in a homogeneous region V bounded by a surface S with a unit outward normal $\hat{\mathbf{n}}$ (see figure 3).

The Helmholtz equation is

$$\nabla^2 p + k^2 p = 0,$$

and the associated residual is

$$R = \nabla^2 p' + k^2 p',$$

where p', an approximation to p, is termed the trial solution and is of the form

$$p'(x, y, z) = \sum_{j=1}^{n} q_j \phi_j(x, y, z). \tag{5}$$

Here ϕ_j are known basis functions and q_j are unknown coefficients. Integrated weighted residuals are equated to zero to give,

$$\int_V W_i R\, dV = \int_V W_i \left[\nabla^2 p' + k^2 p'\right] dV = 0;\ i = 1, \ldots, n,$$

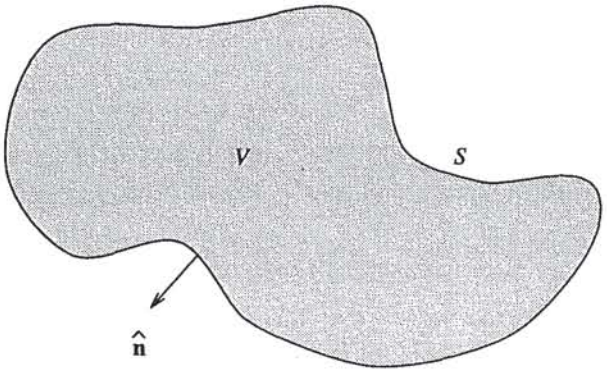

Figure 3: Domain of the bounded finite element Galerkin formulation.

where W_i are weighting functions, as yet undetermined. Applying the divergence theorem to the above equation transforms it to

$$\int_V \left(-\nabla W_i \cdot \nabla p' + k^2 W_i p'\right) dV + \int_S (W_i \nabla p') \cdot \hat{\mathbf{n}}\, dS = 0;\ i = 1, \ldots, n. \tag{6}$$

From the relationship developed in appendix D,

$$\nabla p \cdot \hat{\mathbf{n}} = -ik\rho cU,$$

where $\hat{\mathbf{n}}$ is the unit normal to the vibrating surface, U the normal velocity amplitude of any boundary excitation in the direction of $\hat{\mathbf{n}}$ and ρ the fluid density. The residual associated with the boundary S is

$$R_2 = \nabla p' \cdot \hat{\mathbf{n}} + ik\rho cU,$$

and the associated weighted residual, integrated over the surface and equated to zero, is then

$$\int_S W_i(\nabla p' \cdot \hat{\mathbf{n}} + ik\rho cU)\, dS = 0;\ i = 1, \ldots, n. \tag{7}$$

Subtracting expression 6 from 7 then gives

$$\int_V \left(\nabla W_i \cdot \nabla p' - k^2 W_i p'\right) dV + \int_S W_i ik\rho cU\, dS = 0;\ i = 1, \ldots, n,$$

and substitution of the trial solution (equation 5) results in

$$\left[\mathbf{k} - k^2\mathbf{m}\right] \mathbf{q} = \mathbf{f},$$

where

$$\begin{aligned} \mathbf{k}_{ij} &= \int_V \nabla W_i \cdot \nabla \phi_j\, dV, \\ \mathbf{m}_{ij} &= \int_V W_i \phi_j\, dV, \\ \mathbf{f}_i &= -ik\rho c \int_S W_i U\, dS, \end{aligned} \tag{8}$$

and

$$\mathbf{q} = [q_1, \ldots, q_n]^T,$$

where $i = 1, \ldots n$ and $j = 1, \ldots, n$.

Solving for $\mathbf{q}$ allows the calculation of p' in V from equation 5. If the weighting functions (W_i) are chosen to be identical to the basis functions, ϕ_j, symmetric $\mathbf{k}$ and $\mathbf{m}$ matrices result.

2.2.2 Conventional finite element method

In a Galerkin finite element formulation the domain of interest is divided into *elements*, typically rectangles or triangles in two dimensions, blocks, tetrahedra or prisms in three dimensions. If mapped elements are used, they are defined first in a 'parent' coordinate space and their size and orientation in the global coordinate system given by a mapping from the parent to global coordinate system. These mappings take the form

$$\begin{aligned} x &= \sum_{i=1}^{n} x_i M_i(\varepsilon, \eta, \psi), \\ y &= \sum_{i=1}^{n} y_i M_i(\varepsilon, \eta, \psi), \\ z &= \sum_{i=1}^{n} z_i M_i(\varepsilon, \eta, \psi), \end{aligned}$$

where x_i, y_i and z_i are the global coordinates of the node i, M_i the mapping function for node i, and ε, η and ψ are the parent coordinates.

Linear mapping functions give elements with straight sides and quadratic mapping functions give elements with quadratically curved sides—permitting more aesthetic and accurate modelling of curved geometries.

The case where the M_i are identical to the basis functions is common and the elements are then termed isoparametric. The mapping functions need not be identical to the basis functions, and can instead be chosen to satisfy other criteria. This is the case for wave envelope geometries.

Given the ability to distort the parent elements, the domain of interest can then be *meshed* with elements of arbitrary size, shape and orientation. An example is given in figure 4 where a two-dimensional model of a car interior has been meshed using isoparametric triangles and rectangles. The modelling of the acoustic behaviour of car interiors using models of this type was one of the early uses of acoustic finite elements [34, 81].

The basis functions of the Galerkin trial solution are taken to be interpolation or "shape" functions defined within each element, usually in the parent coordinate system. The weighting functions are chosen to be identical to the basis functions and equations 8

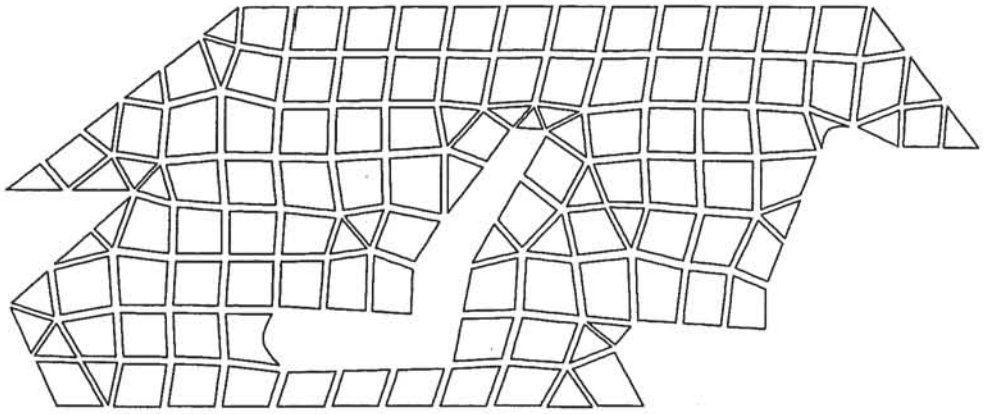

Figure 4: Two-dimensional mesh of a car interior.

can be restated as

$$\begin{aligned} \mathbf{k}_{ij} &= \int_V \nabla\phi_i \cdot \nabla\phi_j \, dV, \\ \mathbf{m}_{ij} &= \int_V \phi_i\phi_j \, dV, \\ \mathbf{f}_i &= -ik\rho c \int_S \phi_i U \, dS. \end{aligned}$$

By performing the integration over each element these become

$$\begin{aligned} \mathbf{k}_{ij} &= \sum^{e} \mathbf{k}^e_{ij}, \\ \mathbf{m}_{ij} &= \sum^{e} \mathbf{m}^e_{ij}, \\ \mathbf{f}_i &= \sum^{e} \mathbf{f}^e_i, \end{aligned}$$

where the superscript e indicates the contributions from a single element.

The mapping of the element from the parent to global space usually produces non-orthogonal elements, for which analytical integration becomes difficult. The remedy is to use numerical integration, and this involves two steps;

1. transformation of the integral from the global coordinates to the parent coordinates,
2. use of classical numerical integration techniques, most commonly Gaussian quadrature.

Converting to the parent coordinate system, the integrations become

$$\mathbf{k}^e_{ij} = \int_{-1}^{1}\int_{-1}^{1}\int_{-1}^{1} \left(\frac{\partial\phi_i}{\partial x}\frac{\partial\phi_j}{\partial x} + \frac{\partial\phi_i}{\partial y}\frac{\partial\phi_j}{\partial y} + \frac{\partial\phi_i}{\partial z}\frac{\partial\phi_j}{\partial z} \right) |J| \, d\varepsilon d\eta d\psi,$$

$$\begin{aligned} \mathbf{m}_{ij}^{e} &= \int_{-1}^{1}\int_{-1}^{1}\int_{-1}^{1} (\phi_i \phi_j \, |J|) \, d\varepsilon d\eta d\psi, \\ \mathbf{f}_{i}^{e} &= -ik\rho c \int\int_{S^e} \phi_i U \, |J| \, dS^e, \end{aligned} \tag{9}$$

where S^e is any portion of the surface of the parent element in which U is specified as per expression 4, and where $|J|$ represents the determinant of the Jacobian of the mapping functions and e represents the contribution from a single finite element. The derivative terms of the integral $\mathbf{k}_{ij}^{e}$ can be expanded to

$$\begin{aligned} \frac{\partial\phi}{\partial x} &= \frac{\partial\phi}{\partial\varepsilon}\frac{\partial\varepsilon}{\partial x} + \frac{\partial\phi}{\partial\eta}\frac{\partial\eta}{\partial x} + \frac{\partial\phi}{\partial\psi}\frac{\partial\psi}{\partial x}, \\ \frac{\partial\phi}{\partial y} &= \frac{\partial\phi}{\partial\varepsilon}\frac{\partial\varepsilon}{\partial y} + \frac{\partial\phi}{\partial\eta}\frac{\partial\eta}{\partial y} + \frac{\partial\phi}{\partial\psi}\frac{\partial\psi}{\partial y}, \\ \frac{\partial\phi}{\partial z} &= \frac{\partial\phi}{\partial\varepsilon}\frac{\partial\varepsilon}{\partial z} + \frac{\partial\phi}{\partial\eta}\frac{\partial\eta}{\partial z} + \frac{\partial\phi}{\partial\psi}\frac{\partial\psi}{\partial z}. \end{aligned}$$

The derivatives of ϕ with respect to the parent coordinates $(\varepsilon, \eta, \psi)$ are easily derived from the basis functions and the derivatives of ε, η, and ψ with respect to the global coordinates (x, y, z) can be found numerically from the inverse of the Jacobian. The Jacobian is defined as

$$J = \begin{bmatrix} \frac{\partial x}{\partial\varepsilon} & \frac{\partial y}{\partial\varepsilon} & \frac{\partial z}{\partial\varepsilon} \\ \frac{\partial x}{\partial\eta} & \frac{\partial y}{\partial\eta} & \frac{\partial z}{\partial\eta} \\ \frac{\partial x}{\partial\psi} & \frac{\partial y}{\partial\psi} & \frac{\partial z}{\partial\psi} \end{bmatrix},$$

and the inverse as

$$J^{-1} = \begin{bmatrix} \frac{\partial\varepsilon}{\partial x} & \frac{\partial\varepsilon}{\partial y} & \frac{\partial\varepsilon}{\partial z} \\ \frac{\partial\eta}{\partial x} & \frac{\partial\eta}{\partial y} & \frac{\partial\eta}{\partial z} \\ \frac{\partial\psi}{\partial x} & \frac{\partial\psi}{\partial y} & \frac{\partial\psi}{\partial z} \end{bmatrix}.$$

For two- and three-dimensional analyses the Jacobian is 2×2 or 3×3. The inverse of J is easily calculated to give the terms required to calculate the derivative expressions.

Applying Gaussian quadrature to equations 9 converts the integrals to summations of the form;

$$\begin{aligned} \mathbf{k}_{ij}^{e} &= \sum_{\alpha=1}^{l}\sum_{\beta=1}^{m}\sum_{\gamma=1}^{n} w_\alpha w_\beta w_\gamma \left(\frac{\partial\phi_i}{\partial x}\frac{\partial\phi_j}{\partial x} + \frac{\partial\phi_i}{\partial y}\frac{\partial\phi_j}{\partial y} + \frac{\partial\phi_i}{\partial z}\frac{\partial\phi_j}{\partial z} \right) |J|, \\ \mathbf{m}_{ij}^{e} &= \sum_{\alpha=1}^{l}\sum_{\beta=1}^{m}\sum_{\gamma=1}^{n} w_\alpha w_\beta w_\gamma \left(\phi_i \phi_j \, |J| \right), \end{aligned}$$

where w_α, w_β and w_γ are Gaussian weights and the integrals are evaluated at the Gauss points.

The number of Gaussian quadrature points required is determined by the polynomial order of the integrand in the parent coordinates. Gaussian quadrature with n integration

points, for example, will integrate exactly a polynomial of order $2n - 1$. The order of integration need not be the same in each dimension (that is, l, m and n need not be the same).

Summation or "assembly" of element contributions then yields all components of $\mathbf{k}$ and $\mathbf{m}$, giving the system equation

$$\left[\mathbf{k} - k^2\mathbf{m}\right] \mathbf{q} = \mathbf{f}.$$

This can be solved for explicit boundary excitation and frequencies. Alternatively, an eigenanalysis can be performed on

$$\left[\mathbf{k} - k^2\mathbf{m}\right] \mathbf{q} = 0,$$

to give the mode shapes and resonant frequencies of the system.

If the system is solved at a particular frequency the vector $\mathbf{q}$ will contain the acoustic pressure amplitudes at the nodes of the mesh. The pressure at any other point within the mesh can be found from interpolation within the appropriate element, via the trial functions.

2.3 Wave envelope elements

The wave envelope theory will be developed initially in terms of a one-dimensional model. This emphases the important aspects of wave envelope elements, without the unnecessary detail of higher dimensionality. Two- and three-dimensional theories will then be presented.

2.3.1 A one-dimensional model

A one-dimensional analogue for acoustic propagation in three dimensions is given by

$$\frac{1}{x^2}\left[\frac{\partial}{\partial x}\left\{x^2\frac{\partial P}{\partial x}\right\}\right] - \frac{1}{c^2}\frac{d^2P}{dt^2} = 0. \tag{10}$$

This governs acoustical propagation in a conically expanding horn where x is the distance from the origin (see figure 5). Solutions of the form $P(x,t) = p(x)e^{iwt}$ when substituted into equation 10 give

$$\frac{1}{x^2}\left[\frac{d}{dx}\left\{x^2\frac{dp}{dx}\right\}\right] + k^2p = 0. \tag{11}$$

This is Webster's horn equation for a duct where the cross-section $A(x)$ varies as x^2. It can also be regarded as a spherically symmetric form of the Helmholtz equation and has an analytic solution of the form

$$p(x) = \frac{\alpha}{x}e^{-ikx} + \frac{\beta}{x}e^{ikx}, \tag{12}$$

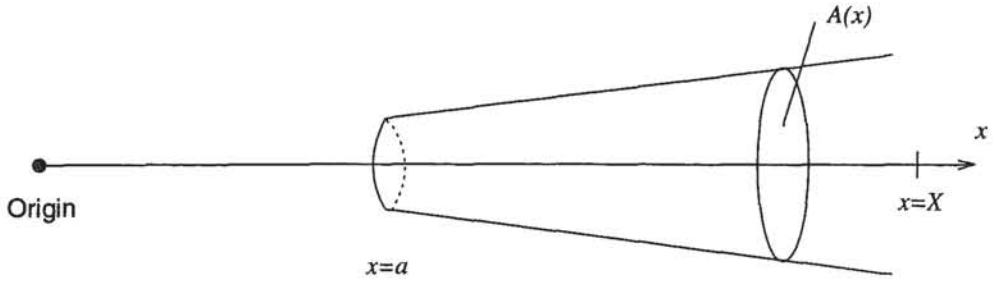

Figure 5: One-dimensional horn analogy

where α and β are constants. The two components represent outward and inward travelling waves that decay as $1/x$ with distance from the origin (at $x = 0$).

Boundary conditions appropriate for a horn are 1) a vibrating piston at the left hand end, and 2) an anechoic termination at the right hand end. With reference to figure 5, the piston boundary condition applied at $x = a$ with a velocity amplitude U is

$$\frac{dp}{dx} = -ik\rho cU \text{ at } x = a. \tag{13}$$

The anechoic termination to simulate an unbounded region is modelled using the Sommerfeld radiation condition [85]

$$x\left(\frac{dp}{dx} + ikp\right) \to 0 \text{ as } x \to \infty. \tag{14}$$

A solution to equation 11 in the form of equation 12, satisfying boundary conditions 13 and 14 is

$$p(x) = \frac{i\rho ckaU}{1 + ika}\left(\frac{a}{x}\right)e^{-ik(x-a)}. \tag{15}$$

The wave envelope concept will now be used to calculate a numerical solution to this problem.

Residual formulation

The wave envelope model will be initially developed on the interval from a to X. The unbounded solution will subsequently be found by taking the limit as $X \to \infty$.

Solution on the finite interval requires a modified Sommerfeld radiation condition. Equation 14 becomes

$$x\left(\frac{dp}{dx} + ikp\right) = 0 \text{ at } x = X. \tag{16}$$

The Galerkin procedure is now applied to the solution of the problem.

Assume a trial function of the form

$$p'(x) = \sum_{j=1}^{n} q_j \phi_j(x), \tag{17}$$

where $\phi_j(x)$ are known basis functions and q_j unknown coefficients.

Equation 17 is then substituted in place of p in equations 11, 13, and 16 and the following residuals are formed;

$$\begin{aligned} R_1(x) &= \frac{1}{x^2}\left[\frac{d}{dx}\left\{x^2\frac{dp'}{dx}\right\}\right] + k^2 p', \\ R_2 &= \left.\frac{dp'}{dx}\right|_{x=a} + ikpcU, \\ R_3 &= \left.\left(\frac{dp'}{dx} + ikp'\right)\right|_{x=X}. \end{aligned}$$

These are then multiplied by selected weighting functions and integrated over their respective domains. The domain of residual R_1 is the volume of the cone, that of residual R_2 the cross-sectional area of the piston end and that of residual R_3 the cone cross-section at $x = X$ (Let $A(x)$ be the cone cross-section, and define $A(x) = \gamma x^2$, where γ is a constant). Hence the weighted residual equations are

$$\int_a^X W_i(x) R_1(x) A(x) dx = \int_a^X W_i(x)\left(\frac{1}{x^2}\frac{d}{dx}\left\{x^2\frac{dp'}{dx}\right\} + k^2 p'\right) x^2 \gamma dx = 0, \tag{18}$$

$$W_i(a) R_2 A(a) = \left.\left(W_i(x)\left\{\frac{dp'}{dx} + ik\rho cU\right\}\gamma x^2\right)\right|_{x=a} = 0, \tag{19}$$

$$W_i(X) R_3 A(X) = \left.\left(W_i(x)\left\{\frac{dp'}{dx} + ikp'\right\}\gamma x^2\right)\right|_{x=X} = 0, \tag{20}$$

where $i = 1, \ldots, n$.

This set of $3n$ equations involves n unknowns and is therefore overdetermined. It is possible to reduce the number of equations to n by integrating equation 18 by parts, adding equation 19 and subtracting equation 20. This gives a new set of n equations of the form;

$$\int_a^X \left[-\left(\frac{dW_i}{dx}\right)\left(\frac{dp'}{dx}\right) + k^2 W_i p'\right] x^2 dx - ikX^2 W_i(X) p'(X) + ik\rho c a^2 W_i(a) U = 0. \tag{21}$$

Substitution of equation 17 for p' gives the system;

$$\left[\mathbf{k} + ik\mathbf{r} - k^2\mathbf{m}\right]\mathbf{q} = \mathbf{f}, \tag{22}$$

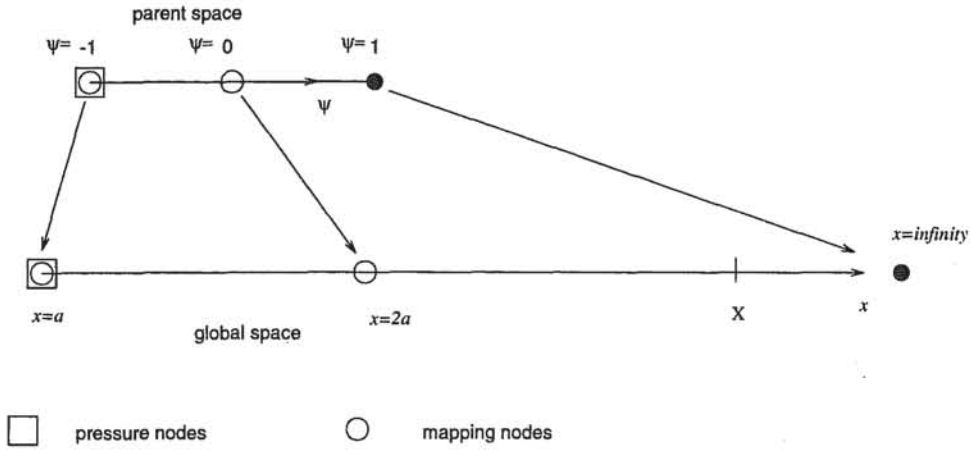

Figure 6: Wave envelope map from parent to global space

where

$$\mathbf{k}_{ij} = \int_a^X \frac{dW_i}{dx}\frac{d\phi_j}{dx}x^2 dx, \tag{23}$$

$$\mathbf{r}_{ij} = X^2 W_i(X)\phi_j(X), \tag{24}$$

$$\mathbf{m}_{ij} = \int_a^X W_i(x)\phi_j(x)x^2 dx, \tag{25}$$

$$\mathbf{f}_i = ik\rho c a^2 W_i(a)U, \tag{26}$$

$$\mathbf{q} = [q_1, \ldots, q_n]^T, \tag{27}$$

where $i = 1, \ldots, n$ and $j = 1, \ldots, n$. So far this is identical to a conventional Galerkin finite element development. The next step is to define the trial, mapping and weighting functions. In a conventional isoparametric finite element formulation they are chosen to be the same functions. For the wave envelope formulation all three are selected independently.

Element mesh and mappings

In the current example the horn is meshed with a single mapped wave envelope element extending over the interval $[a, X]$. The mapping is given by Zienkiewicz *et al.* [95] and is illustrated in figure 6. Two nodes are used to define the mapping and one node defines the pressure. Mathematically the mapping can be expressed as

$$x(\psi) = M_1(\psi)x_1 + M_2(\psi)x_2, \tag{28}$$

where $x_1 = a$, $x_2 = 2a$ and

$$M_1(\psi) = \frac{-2\psi}{1-\psi}, \tag{29}$$

$$M_2(\psi) = \frac{1+\psi}{1-\psi}. \tag{30}$$

To fully understand the nature of the mapping, consider the inverse of equation 28;

$$\psi = 1 - \frac{2a}{x}. \tag{31}$$

At $x = a$, $\psi = -1$, at $x = 2a$, $\psi = 0$ and as x approaches infinity ψ approaches 1. Consequently it can seen that the mapping transforms the parent region $[-1, 1]$ onto the global region $[a, \infty]$.

Basis and weight functions

The wave envelope concept uses basis functions that have a wave-like behaviour built into them, leaving the polynomial portion of the basis function to model the decay of the propagating wave as opposed to the actual wave behaviour. For the current model there is only one degree-of-freedom and hence only one basis function. This basis function is chosen so that it takes the value one at its own node and zero at infinity. A rate of decay of $1/x$ is required to match the correct asymptotic behaviour of a spherical wave. A suitable basis function is

$$\phi_1(x) = P_1(\psi)e^{-ik(x-a)}, \tag{32}$$

where $P_1(\psi) = (1-\psi)/2$ and ψ is given in terms of x by equation 31.

As ψ approaches 1 (and x approaches ∞), ϕ_1 approaches 0 as required, and at $\psi = -1$ ($x = a$), $\phi_1 = 1$. From equation 31, P_1 is given explicitly in terms of x by

$$P_1(\psi(x)) = \frac{a}{x}$$

and it is readily seen that the decay of $\phi(x)$ is as $1/x$ as $x \to \infty$.

It is also possible to express the basis function entirely in terms of the parent coordinates by substituting the mapping equation (28) into the harmonic factor of equation 32 to give

$$\phi_1(\psi) = P_1(\psi)e^{-ika\left(\frac{1+\psi}{1-\psi}\right)}.$$

This form is of more use for the multi-dimensional derivation.

A feature of previous finite element wave envelope formulations involving bounded rather than unbounded domains has been the use of the complex conjugates of the basis functions as the weighting functions. However this procedure results in unbounded terms in the integrals for $\mathbf{k}$ and $\mathbf{m}$ as the region of integration approaches infinity. To avoid this, the weighting functions will be further modified in the current model to remove these unbounded terms. To illustrate the need for this modification the wave envelope concept will initially be developed without them.

Selecting the weighting functions as the complex conjugates of the basis functions gives

$$W_1(\psi) = P_1(\psi(x))e^{ik(x-a)} = \frac{a}{x}e^{ik(x-a)}.$$

Substitution into equations 23–26 yields

$$\begin{aligned}
\mathbf{k}_{11} &= \int_a^X \left\{ \left(\frac{a}{x^2} + \frac{ika}{x} \right) e^{ik(x-a)} \left(\frac{a}{x^2} - \frac{ika}{x} \right) e^{-ik(x-a)} x^2 \right\} dx \\
&= a - \frac{a^2}{X} + (ka)^2 (X-a), \\
\mathbf{r}_{11} &= X^2 \left(\frac{a}{X} \right) e^{ik(x-a)} \left(\frac{a}{X} e^{-ik(x-a)} \right) = a^2, \\
\mathbf{m}_{11} &= \int_a^X \left\{ \frac{a}{x} e^{ik(x-a)} \frac{a}{x} e^{-ik(x-a)} x^2 \right\} dx = a^2 (X-a), \\
\mathbf{f}_1 &= ik\rho c a^2 U.
\end{aligned}$$

In the limit as $X \to \infty$, $\mathbf{k}_{11}$ and $\mathbf{m}_{11}$ have unbounded terms. Upon substitution into 22, these unbounded terms cancel leaving the bounded equation

$$\left(a - \frac{a^2}{X} + ika^2 \right) q_1 = ik\rho c a^2 U$$

and giving the solution

$$q_1 = \frac{ik\rho caU}{\left(1 - \frac{a}{X} + ika\right)}$$

and hence the trial solution (equation 17) becomes

$$p'(x) = q_1 \phi_1(x) = \frac{ik\rho caU}{1 - \frac{a}{X} + ika} \left(\frac{a}{x} \right) e^{-ik(x-a)}. \tag{33}$$

As $X \to \infty$, this expression converges to the analytic solution (equation 15). Extension of this method to two and three dimensions raises two potential difficulties:

- The unbounded terms in the mass and stiffness integrals cancel only when the coefficient matrix is assembled, introducing an undesirable complication to a multi-dimensional problem. That is, the unbounded terms must be segregated and considered separately in any numerical integration procedure.

- The $\mathbf{r}_{11}$ term is finite even as $X \to \infty$. Similar terms will arise in multi-dimensional cases. Practical difficulties arise when calculating the $\mathbf{r}_{11}$ term, as it involves evaluation of a surface integral over an unbounded surface at infinity.

Both of these difficulties can be removed if the weighting functions are multiplied by an additional factor $(a/x)^2$. $W_1(x)$ becomes

$$W_1(x) = \left(\frac{a}{x} \right)^2 P_1(x) e^{ik(x-a)} = \left(\frac{a}{x} \right)^3 e^{ik(x-a)}.$$

The choice of $(a/x)^2$ as a weighting factor is rather arbitrary. It is the lowest power of a/x that can achieve the desired removal of unbounded terms; however powers greater than two also work. The choice of a power of two can be justified as providing an intrinsic balance between near and far field weighted contributions: that is to say, given that the volume differential $A(x)\,dx$ is proportional to $x^2\,dx$, the inclusion of a compensatory factor $1/x^2$ within the weighted integral restores in some sense, equality of weighting between the near and far field effects. The same argument applies in three dimensions when x is replaced by the spherical radius r.

Repeating the procedure above, but now using the modified $W_1(x)$ gives

$$\begin{aligned}
\mathbf{k}_{11} &= \int_a^X \left\{ \left(\frac{-3a^3}{x^4} + \frac{ika^3}{x^3} \right) e^{ik(x-a)} \left(\frac{a}{x^2} + \frac{ika}{x} \right) e^{-ik(x-a)} x^2 \right\} dx \\
&= \left(a - \frac{a^4}{X^3} \right) + ik \left(a^2 - \frac{a^4}{X^2} \right) + k^2 \left(a^3 - \frac{a^4}{X} \right), \\
\mathbf{r}_{11} &= X^2 \left(\frac{a}{X} \right)^3 e^{ik(x-a)} \left(\frac{a}{X} \right) e^{-ik(x-a)} = \frac{a^4}{X^2}, \\
\mathbf{m}_{11} &= \int_a^X \left\{ \left(\frac{a}{x} \right)^3 e^{ik(x-a)} \left(\frac{a}{x} \right) e^{-ik(x-a)} x^2 \right\} dx = a^3 - \frac{a^4}{X}, \\
\mathbf{f}_1 &= i\rho ck a^2 U.
\end{aligned}$$

Unbounded terms no longer exist in any of the above expressions as $X \to \infty$. Substituting into 22 now gives

$$\begin{aligned}
\left\{ \left[\left(a - \frac{a^4}{X^3} \right) + ik \left(a^2 - \frac{a^4}{X^2} \right) + k^2 \left(a^3 - \frac{a^4}{X} \right) \right] \right. \\
\left. + ik \left[\frac{a^4}{X^2} \right] - k^2 \left[a^3 - \frac{a^4}{X} \right] \right\} q_1 = ik\rho ca^2 U.
\end{aligned}$$

The solution for q_1 is

$$q_1 = \frac{i\rho ckaU}{ika + 1 - \frac{a^3}{X^3}},$$

giving

$$p'(x) = \frac{i\rho ckaU}{ika + 1 - \frac{a^3}{X^3}} \left(\frac{a}{x} \right) e^{-ik(x-a)}.$$

This also converges to the analytical solution, with the denominator error decreasing as $1/X^3$, instead of $1/X^1$ (as in equation 33). Another attraction is the disappearance of the radiation term ($\mathbf{r}_{11}$) as $X \to \infty$, eliminating the need to calculate any integrals on infinite boundaries.

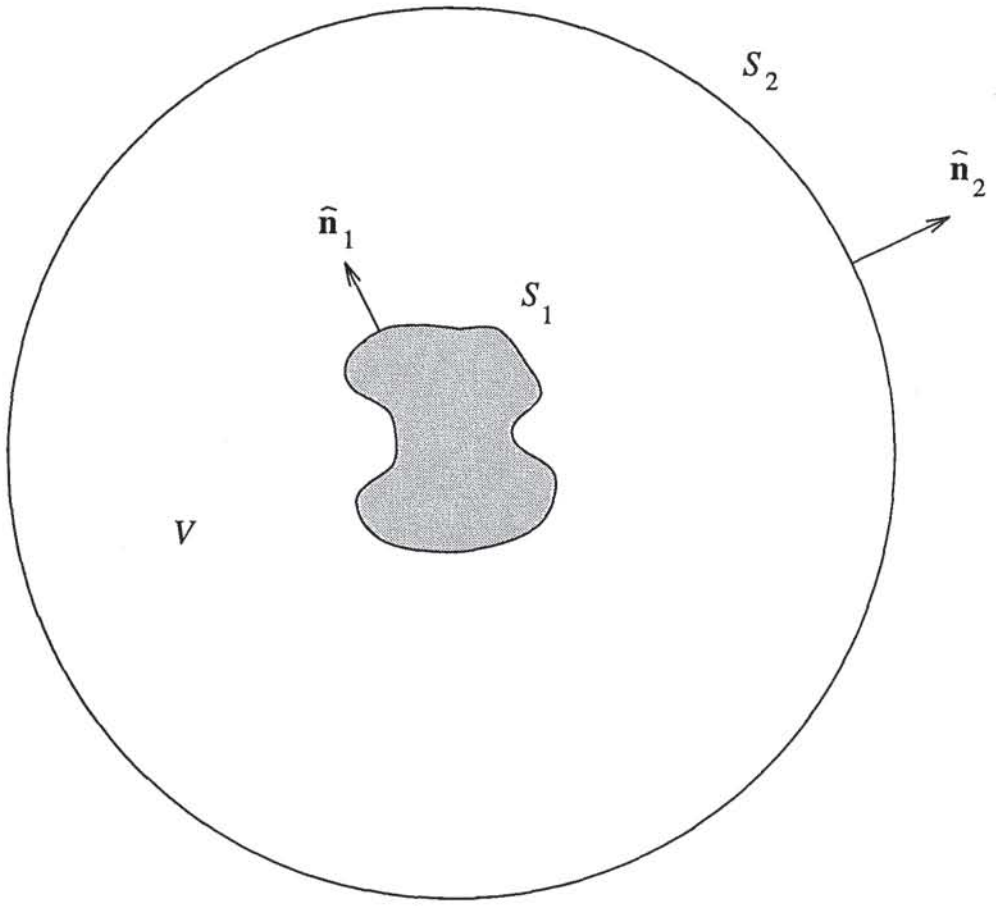

Figure 7: Multi dimensional domain

2.3.2 Wave envelope models in two and three dimensions

Residual formulation

The derivation proceeds in a similar manner to the one-dimensional case. The domain in which a solution is required now surrounds a body S_1, radiating or scattering sound waves into an unbounded region. There is also a second boundary S_2, at a large but finite distance from the body; figure 7 illustrates this geometry in a two-dimensional setting. In the limit as S_2 is extended to infinity, V will become unbounded. S_1 is analogous to the $x = a$ end of the one-dimensional horn, and S_2 is analogous to the $x = X$ end.

The vibrating body S_1 has the boundary condition

$$\nabla p \cdot \hat{\mathbf{n}}_1 = -ik\rho cU. \tag{34}$$

The far-field boundary condition is the Sommerfeld radiation condition [85]

$$r^{\frac{1}{2}}\left(\frac{\partial p}{\partial r}+ikp\right)\rightarrow 0 \text{ as } r\rightarrow\infty \quad \text{(for 2D)},$$
$$r\left(\frac{\partial p}{\partial r}+ikp\right)\rightarrow 0 \text{ as } r\rightarrow\infty \quad \text{(for 3D)}, \tag{35}$$

where r is the radius (cylindrical or polar).

When applied to the distant boundary S_2, the above equation becomes (see appendix D.2)

$$\nabla p\cdot\hat{\mathbf{n}}_2+ikp=0 \text{ on } S_2, \tag{36}$$

where $\hat{\mathbf{n}}_2$ is the unit normal to the boundary S_2.

Assume a trial function,

$$p'(x,y,z)=\sum_{j=1}^{n} q_j\phi_j(x,y,z), \tag{37}$$

where $\phi_j(x,y,z)$ are known basis functions and q_j unknown coefficients. Equation 37 is then substituted for p in the Helmholtz equation and in the two boundary conditions (34 and 36). Residuals are then formed;

$$R_1 = \nabla^2 p'+k^2p', \tag{38}$$
$$R_2 = \nabla p'\cdot\hat{\mathbf{n}}_1|_{S_1}+ik\rho cU, \tag{39}$$
$$R_3 = [\nabla p'\cdot\hat{\mathbf{n}}_2+ikp']|_{S_2}. \tag{40}$$

Weighted residuals are constructed with the use of weighting functions, W_i, giving

$$\int_V W_iR_1dV = \int_V W_i\left[\nabla^2p'+k^2p'\right]dV=0, \tag{41}$$
$$\int_{S_1} W_iR_2dS = \int_{S_1} W_i\left[\nabla p'\cdot\hat{\mathbf{n}}_1+ik\rho cU\right]dS=0, \tag{42}$$
$$\int_{S_2} W_iR_3dS = \int_{S_2} W_i\left[\nabla p'\cdot\hat{\mathbf{n}}_2+ikp'\right]dS=0, \tag{43}$$

where $i=1,\ldots,n$.

This set of $3n$ equations involves only n unknowns and is overdetermined. Reducing the number of equations to n can be achieved by taking equation 41;

$$\int_V\left(W_i\nabla^2p'+W_ik^2p'\right)dV=0, \tag{44}$$

and applying the divergence theorem. This gives

$$\int_V\left(-\nabla W_i\nabla p'+k^2W_ip'\right)dV+\int_S\left(W_i\nabla p'\right)\cdot\hat{\mathbf{n}}\,dS, \tag{45}$$

where

$$\int_S (W_i \nabla p') \cdot \hat{\mathbf{n}}\, dS = \int_{S_2} (W_i \nabla p') \cdot \hat{\mathbf{n}}_2\, dS - \int_{S_1} (W_i \nabla p') \cdot \hat{\mathbf{n}}_1\, dS. \tag{46}$$

Taking equation 45, adding 42 and subtracting 43 gives

$$\int_V \left[-\nabla W_i \cdot \nabla p' + k^2 W_i p' \right] dV + \int_{S_1} ik\rho c W_i U\, dS - \int_{S_2} ikW_i p'\, dS = 0, \tag{47}$$

which is analogous to equation 21 in the one-dimensional model. Substitution of the trial solution (equation 37) results in

$$\left[\mathbf{k} + ik\mathbf{c} - k^2 \mathbf{m} \right] \mathbf{q} = \mathbf{f}, \tag{48}$$

where

$$\mathbf{k}_{ij} = \int_V \nabla W_i \cdot \nabla \phi_j\, dV, \tag{49}$$

$$\mathbf{c}_{ij} = \int_{S_2} W_i \phi_j\, dS, \tag{50}$$

$$\mathbf{m}_{ij} = \int_V W_i \phi_j\, dV, \tag{51}$$

$$\mathbf{f}_j = ik\rho c \int_{S_1} W_i U\, dS, \tag{52}$$

$$\mathbf{q} = [q_1, \ldots, q_n]^T. \tag{53}$$

The unknown $\mathbf{q}$ coefficients are given by the solution of 48.

Element mesh and mapping

The division of the unbounded region into elements is accomplished in two parts—an inner mesh of conventional acoustic finite elements is generated in a region that extends out to an intermediate surface S_b. Matched to this mesh is a single layer of wave envelope elements extending to S_2 (see figure 8). Note that the inner conventional mesh is not always required, but is included here for generality. It is sometimes possible to completely eliminate the conventional mesh and match the wave envelope elements directly to the vibrating body and this is then the most economical way of meshing the unbounded region, especially for bodies that are completely convex in nature. The basis and weighting functions for the inner mesh are chosen in a manner identical to that employed in a conventional finite element formulation for a bounded region (see section 2.2.2). An isoparametric formulation is used in the current implementation, and hence the mapping functions are identical to the basis functions, giving symmetric element mass and stiffness matrices for the "conventional" elements.

The wave envelope elements are formed by using conventional interpolation functions in the non-infinite direction and hence match compatibility to the conventional finite element mesh at the inner boundary S_b if present. Lagrange polynomials of variable

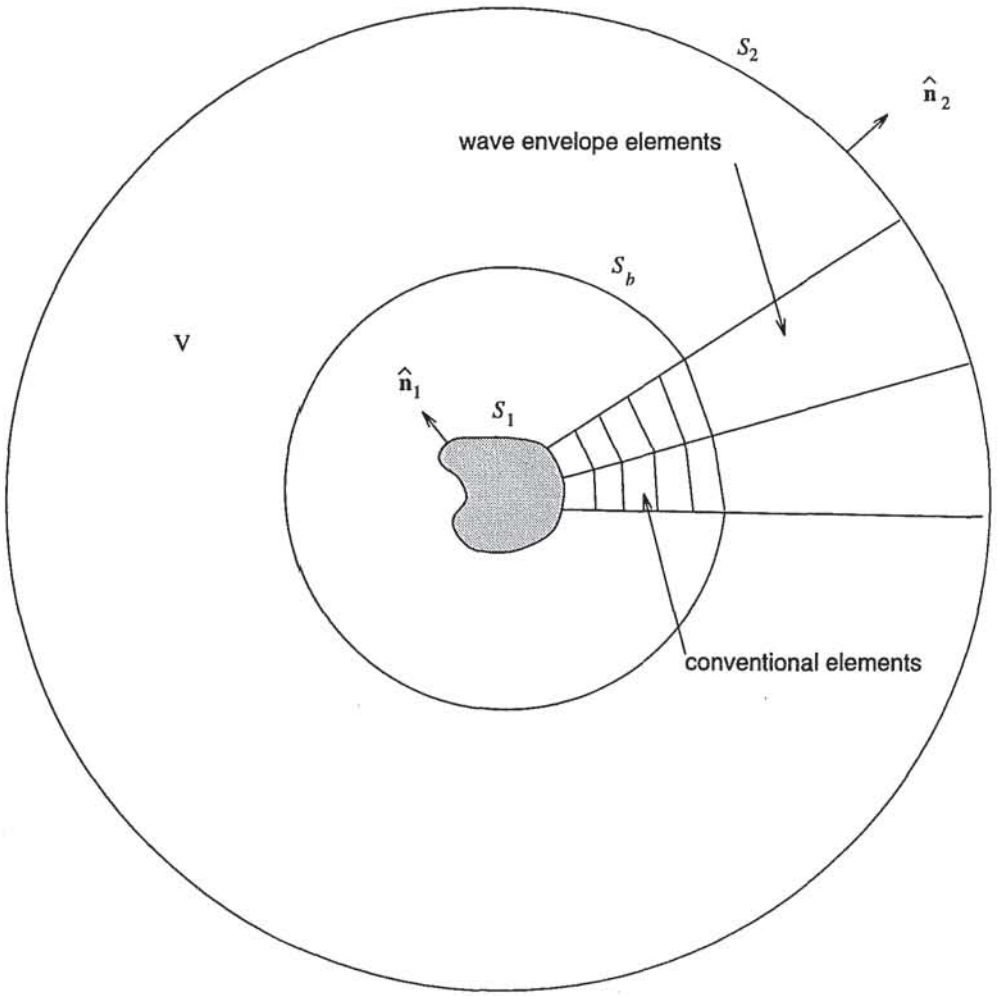

Figure 8: Model boundaries

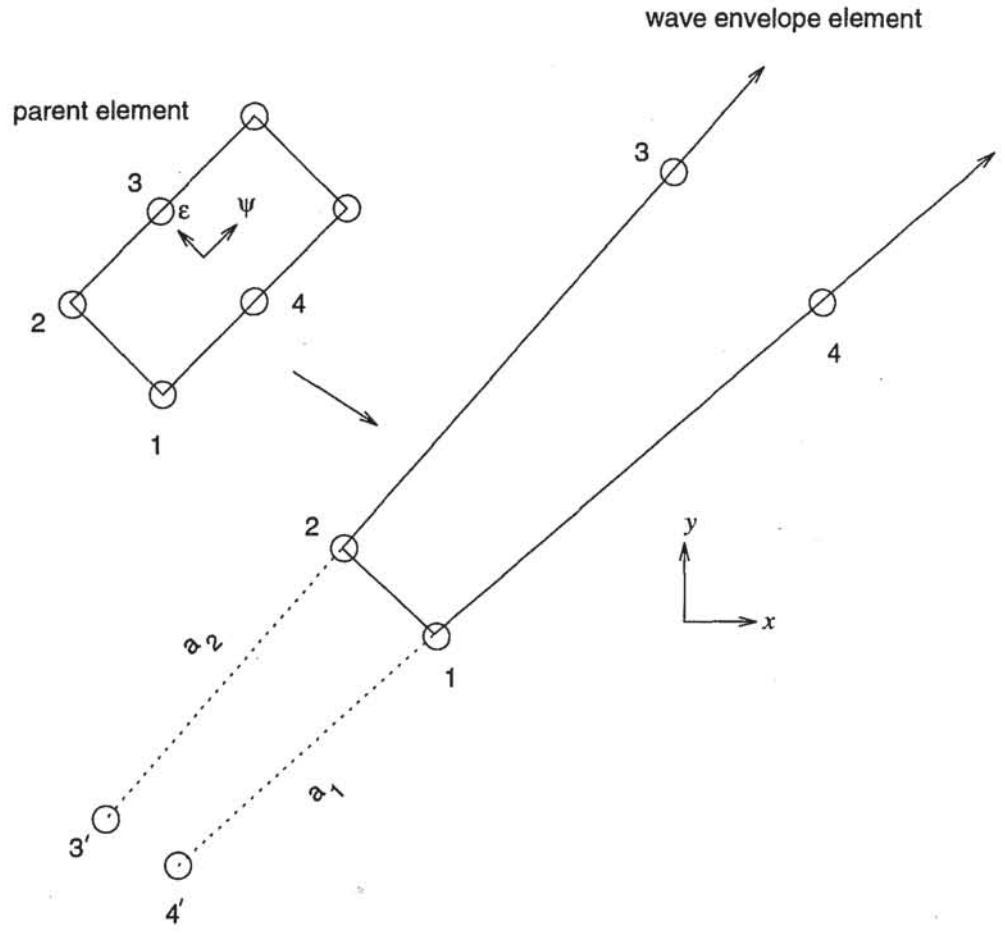

Figure 9: Mapping of a two-dimensional wave envelope element

order are used for interpolation in the infinite direction. The generation of the Lagrange polynomial interpolation is discussed in appendix A.2.

The mapping functions for the wave envelope elements are chosen to map the parent element onto the region extending from S_b to S_2. This mapping is the same as that used in the one-dimensional analogy, but also depends upon lateral coordinates in a conventional finite element fashion. As an example, the two-dimensional wave envelope element shown in figure 9 has a mapping defined by

$$\begin{aligned} x &= \sum_{i=1}^{4} M_i(\varepsilon, \psi) x_i, \\ y &= \sum_{i=1}^{4} M_i(\varepsilon, \psi) y_i, \end{aligned}$$

where

$$\begin{aligned} M_1 &= -(1-\varepsilon)\frac{\psi}{1-\psi}, \\ M_2 &= -(1+\varepsilon)\frac{\psi}{1-\psi}, \\ M_3 &= \frac{+(1+\varepsilon)}{2}\frac{(1+\psi)}{(1-\psi)}, \\ M_4 &= \frac{-(1-\varepsilon)}{2}\frac{(1+\psi)}{(1-\psi)}. \end{aligned}$$

Similar expressions are used for the three-dimensional mapping functions. Quadratic interpolation in the lateral directions can easily be incorporated by the use of second order polynomials in ε (and η for three dimensions). Mapping functions for two- and three-dimensional, linear and quadratic wave envelope elements are given in appendix B.

Wave envelope origin placement

The location of the mapping nodes along an infinite edge of a wave envelope element (at $r = a$ and $r = 2a$) implies a 'virtual' node at $r = 0$. Consider the 1–4 edge of the wave envelope element in figure 9. Here the mapping reduces to the one-dimensional form,

$$\psi = 1 - \frac{2a_1}{r},$$

where a_1 is the distance along the edge from node 1 to node 4, and r is measured outwards from virtual node 4′. The distance between node 4′ and 1 is also a_1. The wave-like behaviour which will subsequently be incorporated into the basis functions along this edge (see next section) is

$$e^{-ik(r-a_1)},$$

which can be thought of as a wave propagating along the edge, emanating from a source located at the virtual node 4′. Extending this to two dimensions, the virtual source becomes a series of sources emanating from a line between nodes 3′ and 4′. The distance a_1 in the above equation is then replaced by $a(\varepsilon)$ which is obtained by interpolating a_1 and a_2. The interpolation is identical to that used for nodal pressure along the 1–2 edge of the element. The distance $a(\varepsilon)$ becomes $a(\varepsilon, \eta)$ for a three-dimensional element, and is obtained from interpolation of a_1, a_2, a_3 and a_4 (see figure 10)) over the inner surface of the wave envelope element.

The location of the virtual sources can affect the solution accuracy (see [6] and [37]). When constructing a wave envelope mesh, careful placement of the wave envelope origins will give better solutions. For cylindrical and spherical radiating or scattering surfaces the optimum location is at the centre of the cylinder or sphere. In more realistic geometries the position of the wave envelope origins is less obvious, and the ability to cope with sub-optimal origin placement is desirable. In general a higher order element will cope with a less than ideal origin placement better than a low order element [6, 37].

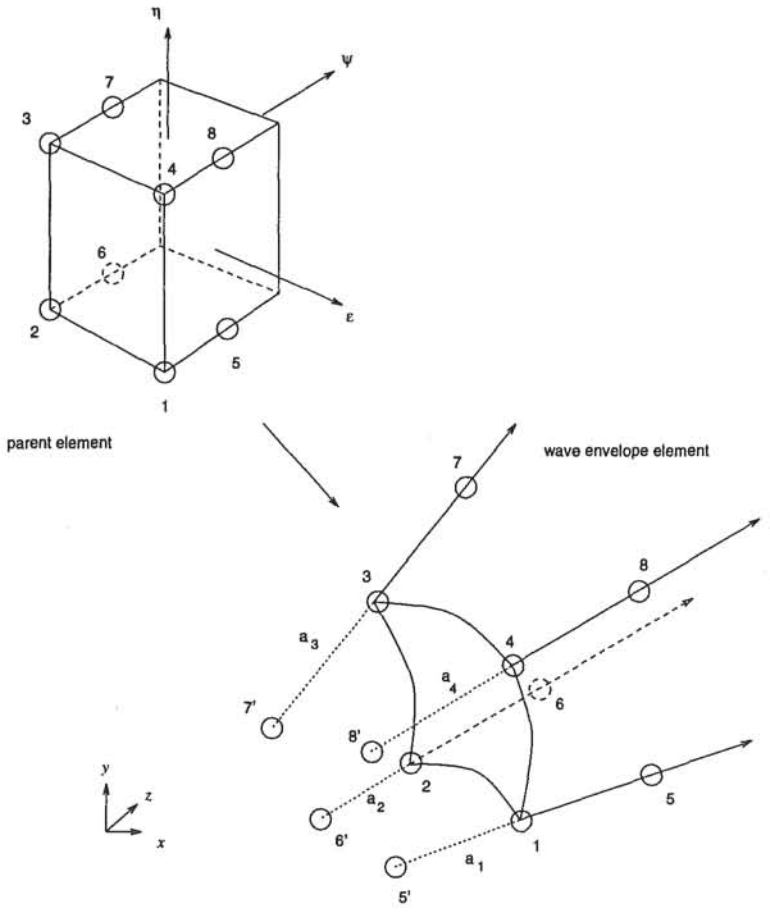

Figure 10: A three-dimensional wave envelope element

Basis and weighting functions

The basis and weight functions are selected so that integrals 49–52 are bounded as S_2 approaches infinity. As in conventional finite element formulations the pressure within the element is obtained from the interpolation of nodal pressure values. For wave envelope elements it is possible for any number of pressure nodes (>1) to be placed along an infinite edge. However, only two mapping nodes per infinite edge are required. The location of the pressure nodes is independent of the mapping nodes although it is convenient to use the mapping node positions as pressure nodes. There are numerical difficulties associated with edges which contain more than 11 nodes and this will be discussed in chapter 4.

The basis functions are constructed from two factors. The first is an interpolation function for the wave amplitude and angular dependence and the second a wave-like factor to model the wave detail.

The first function is closely related to that used in the one-dimensional theory. That is, a decay factor chosen to match the asymptotic behaviour of solutions to the wave equation in unbounded regions. Solutions for two-dimensional waves are given by cylindrical Hankel functions which decay asymptotically as $1/\sqrt{r}$. Three-dimensional solutions are given by spherical Hankel functions, and these decay as $1/r$.

Equation 31 when rearranged and with x replaced by r gives,

$$r \propto \frac{1}{1-\psi}.$$

Hence for two-dimensional basis functions the correct decay term is $\sqrt{1-\psi}$ and for three dimensions is $(1-\psi)$.

The first factor also requires an interpolation in the angular direction and this is provided by conventional finite element interpolation functions. As an example, consider the two-dimensional element shown in figure 9. This element has four mapping nodes and four pressure nodes. The wave amplitude and angular dependence of the basis functions are given by

$$\begin{aligned}
P_1(\varepsilon,\psi) &= \frac{-1}{\sqrt{8}}(1-\varepsilon)\psi\sqrt{1-\psi}, \\
P_2(\varepsilon,\psi) &= \frac{-1}{\sqrt{8}}(1+\varepsilon)\psi\sqrt{1-\psi}, \\
P_3(\varepsilon,\psi) &= \frac{1}{2}(1+\varepsilon)(1+\psi)\sqrt{1-\psi}, \\
P_4(\varepsilon,\psi) &= \frac{1}{2}(1-\varepsilon)(1+\psi)\sqrt{1-\psi}.
\end{aligned}$$

Note that the above definition ensures that P_1 takes the value 1.0 at node 1, P_2 takes the value 1.0 at node 2, et cetera. The interpolations in the finite (ε) direction are chosen so that they match the behaviour of the adjoining finite elements (if any) along the 1–2 side.

The second part of the basis function contains the required wave-like behaviour. An appropriate factor which asymptotically satisfies the radiation condition is

$$e^{-ik(r-a(\varepsilon))}, \tag{54}$$

where r is the radius from the virtual source. The quantity $a(\varepsilon)$ in the above equation is the distance from the virtual source to the inner edge of the wave envelope element and is found by interpolation of the a_1 and a_2 values along the 1–2 edge of the element. The $a(\varepsilon)$ term for the wave envelope element of figure 9 is given by

$$a(\varepsilon) = \frac{1}{2}(1-\varepsilon)a_1 + \frac{1}{2}(1+\varepsilon)a_2.$$

The relationship between the parent and global coordinates for the one-dimensional example (equation 31) can be written as

$$x = \frac{2a}{1-\psi}.$$

For two-dimensional wave envelope elements, this same behaviour holds for any value of ε and can be restated as

$$r = \frac{2a(\varepsilon)}{1-\psi},$$

where r is the radius from the virtual source as defined by ε, a_1 and a_2. Substituting this into the $(r - a(\varepsilon))$ part of equation 54 and rearranging gives

$$r - a(\varepsilon) = a(\varepsilon)\left(\frac{1+\psi}{1-\psi}\right).$$

Hence the required wave-like behaviour in parent coordinates is

$$e^{-ika(\varepsilon)\left(\frac{1+\psi}{1-\psi}\right)},$$

and the basis functions for two-dimensional wave envelope elements are given by

$$\phi_j(\varepsilon,\psi) = P_j(\varepsilon,\psi)e^{-ika(\varepsilon)\left(\frac{1+\psi}{1-\psi}\right)} \text{ for } j = 1,\ldots,n.$$

In three dimensions the basis functions take the form,

$$\phi_j(\varepsilon,\eta,\psi) = P_j(\varepsilon,\eta,\psi)e^{-ika(\varepsilon,\eta)\left(\frac{1+\psi}{1-\psi}\right)} \text{ for } j = 1,\ldots,n.$$

Note that at $\psi = -1$, the exponential term in both expressions equates to 1. This ensures that the wave envelope elements correctly match the basis functions for any adjacent conventional elements.

Behaviour of basis functions

To fully understand the behaviour of the basis functions consider the form of ϕ_j along a single infinite edge. The two-dimensional form of ϕ_j with two pressure nodes per edge (as in figure 9) is

$$\phi_j \sim \psi\sqrt{1-\psi}\, e^{-ika_j\left(\frac{1+\psi}{1-\psi}\right)};\ j = 1 \text{ or } 2$$

or

$$\phi_j \sim (1+\psi)\sqrt{1-\psi}\, e^{-ika_s\left(\frac{1+\psi}{1-\psi}\right)};\ j = 3 \text{ or } 4,$$

where $a_s = a_2$ for $j = 3$ and $a_s = a_1$ for $j = 4$. Conversion to global coordinates yields

$$\phi_j \sim \frac{1}{\sqrt{r}}\left(\alpha + \frac{\beta}{r}\right) e^{-ik(r-a)},$$

where α and β are constants. In the case of an element with three pressure nodes along each infinite edge,

$$\phi_j \sim \frac{1}{\sqrt{r}}\left(\alpha + \frac{\beta}{r} + \frac{\gamma}{r^2}\right) e^{-ik(r-a)}.$$

For the case of a single pressure node per infinite edge the form of the basis functions is

$$\phi_j \sim \frac{1}{\sqrt{r}} e^{-ik(r-a)}. \tag{55}$$

All of these expressions give the correct asymptotic behaviour with r as discussed on page 36.

Increasing the number of nodes on the infinite edge allows for a larger difference between asymptotic and actual behaviour, while still retaining the asymptotic behaviour as r becomes large. This allows the wave envelope elements to more accurately model the detailed sound field close to an object (where it does not necessarily exhibit the asymptotic behaviour present in the far-field) and to dispense therefore with more of the conventional acoustic mesh. Results will be presented in chapter 4 to illustrate this behaviour. The three-dimensional basis functions are similar to the two-dimensional functions except that the $1/\sqrt{r}$ factor is replaced by $1/r$ and two local coordinates are required in the finite directions. Further details are given in appendix A.

Wave envelope element order classification

Throughout this thesis wave envelope elements are classified according to their interpolation order in the infinite direction. An element with one pressure node along an infinite edge is classed as having linear interpolation (order 1). Two pressure nodes give quadratic interpolation (order 2), et cetera. The observant reader will note that the wave envelope element in figure 9 has three nodes per infinite edge, yet only two of these were used as pressure nodes. This is because the third node on each edge (at $\psi = 1$) is mapped to infinity where the nodal value of pressure is prescribed to be zero.

Choice of weighting functions

Following the reasoning of the one-dimensional examples, the weighting functions for the two- and three-dimensional wave envelope elements are selected as the complex conjugates of the basis functions, multiplied by an additional factor $(a/r)^2$. It is more convenient to express the two- and three-dimensional equations completely in terms of parent coordinates and hence the additional factor becomes

$$\left(\frac{1-\psi}{2}\right)^2.$$

The weighting functions are then

$$W_i = DP_i e^{ik\mu},$$

where

$$D = \left(\frac{1-\psi}{2}\right)^2$$

and

$$\mu = a(\varepsilon)\frac{(1+\psi)}{(1-\psi)}$$

for two-dimensional wave envelope elements, and

$$\mu = a(\varepsilon,\eta)\frac{(1+\psi)}{(1-\psi)}$$

for three-dimensional wave envelope elements.

After substitution of these relations into expressions 49–52 and summation of the integrals over each elements, the exponential terms $e^{\pm ik\mu}$ cancel within each integral to yield

$$\mathbf{k}_{ij} = \sum_e \int_{V^e} (D\nabla P_i + P_i\nabla D + ikDP_i\nabla\mu)\cdot(\nabla P_j - ikP_j\nabla\mu)dV, \quad (56)$$

$$\mathbf{c}_{ij} = \sum_e \int_{S_2^e} DP_iP_j\,dS, \quad (57)$$

$$\mathbf{m}_{ij} = \sum_e \int_{V^e} DP_iP_j dV, \quad (58)$$

$$\mathbf{f}_j = ik\rho c\sum_e \int_{S_1^e} DP_i e^{ik\mu}U\,dS, \quad (59)$$

where V^e is the volume of the element and S_1^e and S_2^e are portions of the boundaries S_1 and S_2 bounding the element. The D term in the integral for $\mathbf{c}_{ij}$ expands to give

$$\mathbf{c}_{ij} = \int_{S_2^e}\left(\frac{1-\psi}{2}\right)^2 P_iP_j\,dS$$

and in the limit as S_2^e approaches infinity, $((1-\psi)/2)^2$ behaves as $1/r^2$ and P_iP_j behaves as $1/r$ or $1/r^2$ for two or three dimensions respectively, causing the $\mathbf{c}_{ij}$ integral to equate to zero.

Final system

Integrals 56–59 are bounded as V^e becomes infinite and can therefore be mapped to a finite parent region and integrated using standard Gauss-Lengendre techniques. From the form of the integrands of equations 56–59, equation 48 can be rearranged to give

$$\left[\mathbf{K} + ik\mathbf{C} - k^2\mathbf{M}\right]\mathbf{q} = \mathbf{f}, \tag{60}$$

where $\mathbf{K}$, $\mathbf{C}$, $\mathbf{M}$ and $\mathbf{f}$ are assembled from element contributions;

$$\begin{aligned}
\mathbf{K}^e_{ij} &= \int_{V^e} \nabla(DP_i)\cdot\nabla P_j \, dV, \\
\mathbf{C}^e_{ij} &= \int_{V^e} \nabla\mu\cdot(DP_i\nabla P_j - P_j\nabla(DP_i)) \, dV, \\
\mathbf{M}^e_{ij} &= \int_{V^e} DP_iP_j(1-\nabla\mu\cdot\nabla\mu) \, dV, \\
\mathbf{f}^e_j &= ik\rho c\int_{S^e_1} DP_j e^{ik\mu}U \, dS,
\end{aligned}$$

where $i = 1,\ldots,n$ and $j = 1,\ldots,n$. Note that $\psi = -1$ on the inner edge of the wave envelope element gives $D = 1$ and $\mu = 0$. Consequently $\mathbf{f}^e_j$ becomes

$$\mathbf{f}^e_j = ik\rho c\int_{S^e_1} P_jU \, dS,$$

when the inner boundary of the wave envelope mesh coincides with the boundary S_1. An important feature of the above form of these equations is the frequency independence of the component matrices, $\mathbf{K}$, $\mathbf{C}$ and $\mathbf{M}$. This means that they need only be calculated once for an entire frequency range.

The $\mathbf{K}$ and $\mathbf{C}$ matrices are non-symmetric, unlike those found in conventional finite element formulations. This arises because the weighting functions are different from the basis functions. Non-symmetry is the price that one must pay to remove the wave-like components from the integrals, which would result from identical basis and weighting functions. The price paid is a doubling of the matrix storage requirements and an associated increase in solution times, although sparsity of the matrices is preserved.

The $\nabla\mu\cdot\nabla\mu$ term

For certain geometries the $\nabla\mu\cdot\nabla\mu$ term in the integral for $\mathbf{M}^e_{ij}$ can be very close to 1, giving an $\mathbf{M}$ matrix which has terms that are close to zero. This has significance when using Ritz vectors to solve the system.

To understand how $\nabla\mu\cdot\nabla\mu$ can take the value 1 consider the physical interpretation of μ as the distance between the point D and point A as shown in figure 11. Points 1, 2, 3 and 4 define a wave envelope element, and points 4′ and 3′ define the wave envelope element origins. Consider the point Q which is on the curve 4′–3′, and express the distance from

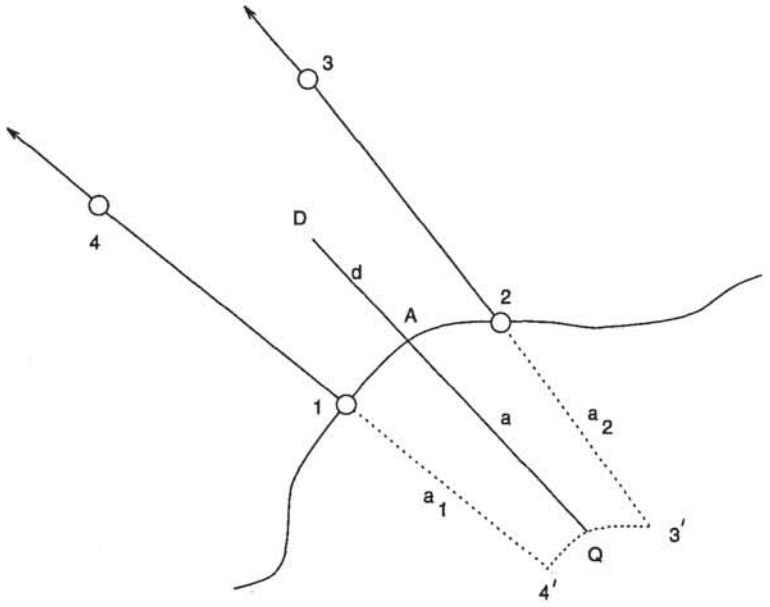

Figure 11: Physical interpretation of μ.

$4'$ to Q as a proportion of the distance from $4'$ to $3'$. The point A is defined by the same proportion along the curve 1–2. By defining a to be the distance from point Q to point A and defining d to be the distance from point Q to point D, the distance μ is given by

$$\mu = d - a.$$

As A and Q travel along 1–2 and $4'$–$3'$ respectively, they define a series of diverging, or possibly parallel lines and corresponding distances μ.

For the special case where points $4'$ and $3'$ are coincident and the curve 1–2 is circular with its origin at $4'$ (or $3'$), μ can be expressed as

$$\mu = r - a,$$

where r is the distance from the origin ($4'$ or $3'$) to point D, and a is the distance from $4'$ (or $3'$) to A. They are both are invariant with θ, as can be seen in figure 12. The gradient of μ then becomes

$$\nabla\mu = \frac{\partial\mu}{\partial r}\hat{\mathbf{r}} + \frac{1}{r}\frac{\partial\mu}{\partial\theta}\hat{\boldsymbol{\theta}} \tag{61}$$

$$= \hat{\mathbf{r}} \tag{62}$$

and hence $\nabla\mu \cdot \nabla\mu = 1$. However, the finite element approximation to the circular arc 1–2 never results in a being perfectly constant for varying θ. In practice, for circular geometries represented by a finite element mesh with the wave envelope origins at a single point, $\nabla\mu \cdot \nabla\mu$ is close to 1 over the entire element. For all other geometries and for multiple wave envelope origins, $\nabla\mu \cdot \nabla\mu$ varies over the element.

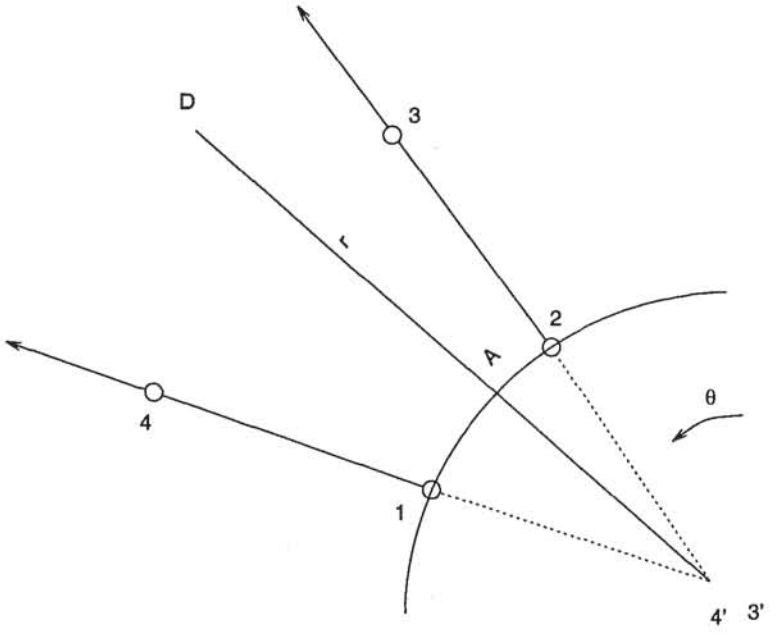

Figure 12: μ for circular geometries

2.3.3 Meshing objects with wave envelope elements

Wave envelope elements, like conventional finite elements give better results if they are not excessively distorted, however they also have the requirement that their infinite edges be either parallel or diverging. This has interesting implications for objects that possess some form of concavity.

The two-dimensional object depicted in figure 13 is completely convex and location of wave envelope elements is straightforward. An object that contains a mild indentation is shown in figure 14, along with a possible wave envelope mesh of the surrounding region. Note how the wave envelope elements in the indentation have near parallel sides. A more severe indentation is shown in figure 15, for which it is impossible to mesh the surrounding region solely with wave envelope elements. The obvious solution (as illustrated) is to fill in the indentation with conventional elements and then place wave envelope elements around the resulting shape.

To explain the difference between the indentation in figure 14 and the one in figure 15 a definition is necessary:

- the *local region* is the region of the curve that contains the indentation and extends out to some local maximum on both sides of the indentation

To determine if a region can be meshed with only wave envelope elements;

1. consider the local region that includes the indentation

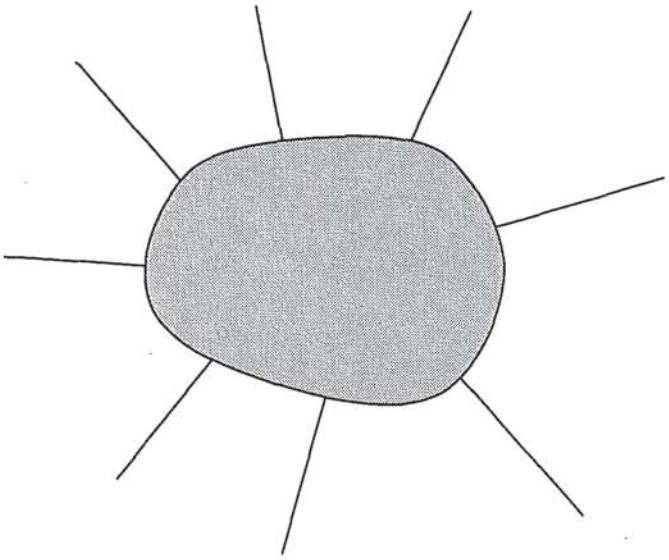

Figure 13: A completely convex object.

2. consider the tangents to the curve in the local region

3. if any two tangents can be found that are parallel, then the indentation requires conventional elements.

Figure 16 illustrates the two possible situations. Note that restraints on distortion of the wave envelope elements will require the use of conventional elements even when the above definition suggests otherwise. In most situations it will be advantageous to fill in an indentation even if it is not strictly necessary. This makes the wave envelope elements easier to place, and will give a better solution. If more than one body exists in the domain it will be necessary to use conventional elements to fill in the spaces between the objects, and create a shape that wave envelope elements can mesh.

Similar comments apply to three-dimensional objects, with the proviso that the above reasoning then applies to any slice of the solid object or objects.

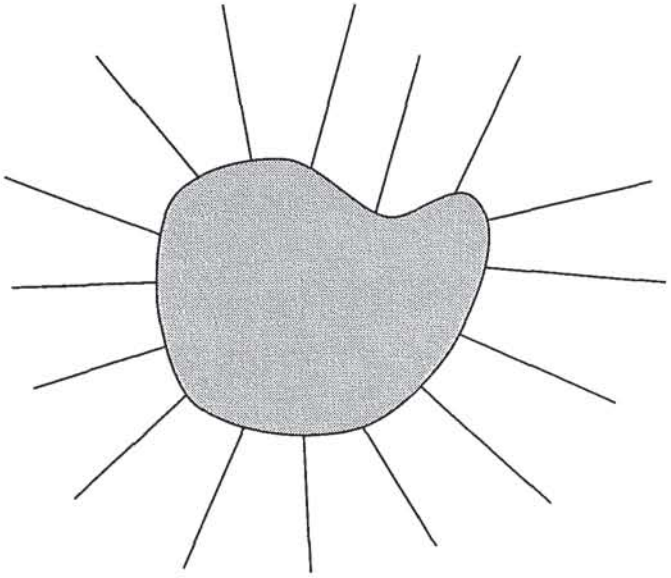

Figure 14: An object with a mild indentation.

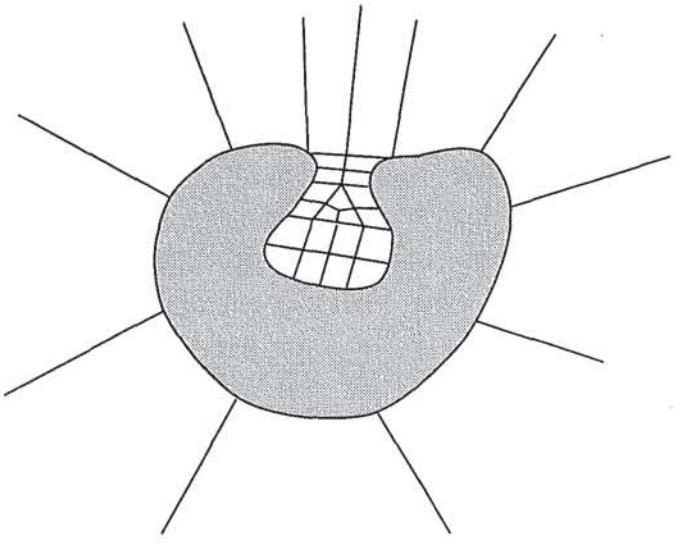

Figure 15: An object with a severe indentation.

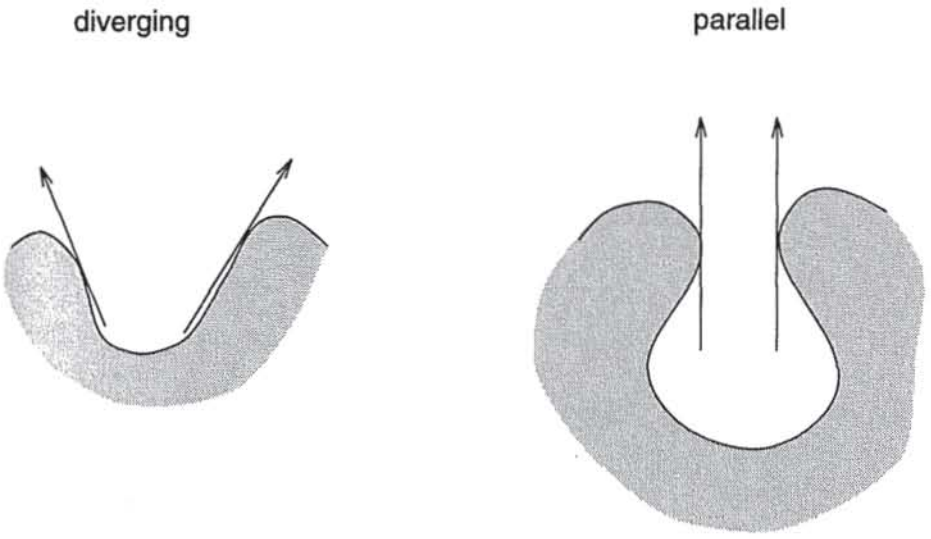

Figure 16: The two indentation types.

Chapter 3

Ritz vectors

3.1 Introduction

A frequency response curve is a useful output from an acoustical analysis. Calculating one such curve involves the solution of the acoustical system at many separate frequencies and can become very time consuming. However, Ritz vectors provide a means of significantly reducing the time spent on solving the system at each frequency. Ritz vectors are similar in concept to frequency eigenvectors, and can be thought of as mode shapes of the system, but are easily and quickly generated (unlike eigenvectors). The generation of Ritz vectors is driven by the excitation applied to the model, and as such, all the Ritz vectors generated will participate in the solution. All of the eigenvectors calculated will not necessarily participate in the solution.

The Ritz algorithm developed by Wilson [93] for generating Ritz vectors is presented, along with a modified algorithm that is applicable to acoustical wave envelope finite element systems.

3.2 The mode superposition method

The dynamic equilibrium equation for a system modelled by a finite number of discrete members and lumped masses is

$$\mathbf{Ku}(s,t) + \mathbf{Cv}(s,t) + \mathbf{Ma}(s,t) = \mathbf{r}(s,t), \tag{63}$$

where $\mathbf{K}$, $\mathbf{C}$ and $\mathbf{M}$ are constant $n \times n$ stiffness, damping and mass matrices respectively and the vectors $\mathbf{u}$, $\mathbf{v}$, and $\mathbf{a}$ are time-dependent displacements, velocities, and accelerations respectively. For many structural loadings the time dependent load ($\mathbf{r}(s,t)$) can be represented as a product of a space vector and a time function,

$$\mathbf{r}(s,t) = \mathbf{f}(s)\mathbf{g}(t), \tag{64}$$

where $\mathbf{f}(s)$ is the spatial component of the loading and $\mathbf{g}(t)$ the time dependent component of the loading. The mode superposition method introduces a set of mode shapes in the form of a matrix, $\mathbf{P}$ of size $n \times m$, with the modes as columns. This matrix is used in the transformation

$$\mathbf{u}(s,t) = \mathbf{P}(s)\mathbf{u}_x(t) \text{ or } \mathbf{u} = \mathbf{P}\mathbf{u}_x, \tag{65}$$

where $\mathbf{u}_x$ is a vector of m unknown time functions. Similar transformations are defined for the velocity, acceleration and loading vectors. Substitution of these transformations into equation 63 and premultiplication by $\mathbf{P}^T$ gives

$$\hat{\mathbf{K}}\mathbf{u}_x + \hat{\mathbf{C}}\mathbf{v}_x + \hat{\mathbf{M}}\mathbf{a}_x = \hat{\mathbf{f}}(s)\mathbf{g}(t), \tag{66}$$

in which

$$\begin{aligned} \hat{\mathbf{K}} &= \mathbf{P}^T\mathbf{K}\mathbf{P}, \\ \hat{\mathbf{C}} &= \mathbf{P}^T\mathbf{C}\mathbf{P}, \\ \hat{\mathbf{M}} &= \mathbf{P}^T\mathbf{M}\mathbf{P}, \\ \hat{\mathbf{f}} &= \mathbf{P}^T\mathbf{f}. \end{aligned}$$

Note that $\hat{\mathbf{K}}, \hat{\mathbf{C}}$, and $\hat{\mathbf{M}}$ are of size $m \times m$. If the columns of $\mathbf{P}$ are chosen to be the m lowest eigenvectors of the generalised eigenproblem

$$(\mathbf{K} - \lambda\mathbf{M})\,\psi = 0,$$

$\hat{\mathbf{K}}$ and $\hat{\mathbf{M}}$ are diagonal. If modal damping is assumed, $\hat{\mathbf{C}}$ will also be diagonal, reducing equation 66 to a set of uncoupled, linear, second-order, ordinary differential equations. Solution of this system is possible via standard analytic or numerical techniques.

If $\mathbf{P}$ consists of Ritz vectors, the $\hat{\mathbf{K}}$ and $\hat{\mathbf{M}}$ matrices are no longer diagonal (modal damping cannot be assumed for wave envelope systems) and one is left with a full system similar to the original system (63). The mitigating difference is the reduction in size of the matrices; typically m is much smaller than n. The eigenvectors of this reduced system can be found and the reduced system decoupled and then solved, or the reduced system can be solved using a step-by-step integration method. The solution to the original system can be extracted from the solution to the reduced system by applying the original transformation (expression 65).

3.2.1 Wilson's Ritz vector algorithm

The first Ritz vector is generated from the solution of

$$\mathbf{K}\mathbf{x}_1' = \mathbf{f}$$

and normalised so that

$$\mathbf{x}_1^T\mathbf{M}\mathbf{x}_1 = 1.$$

Subsequent vectors are generated via the recurrence relationship

$$\mathbf{K}\mathbf{x}_i' = \mathbf{M}\mathbf{x}_{i-1}\,, i = 2, \ldots, m,$$

and each newly created vector is orthogonalised using

$$\mathbf{x}_i = \mathbf{x}_i' - \sum_{j=1}^{i-1} c_j \mathbf{x}_j,$$

where

$$c_j = \mathbf{x}_j^T \mathbf{M}\mathbf{x}_i', \tag{67}$$

and then normalised with respect to $\mathbf{M}$ by imposing the condition,

$$\mathbf{x}_i^T \mathbf{M}\mathbf{x}_i = 1.$$

This recurrence relationship proceeds until sufficient vectors have been found. Note that only vectors which are excited by the initial loading ($\mathbf{f}$) are generated, and this is the main advantage of the Ritz method. The orthogonalisation procedure is the Gram-Schmidt process with expression 67 as the inner product. Hence c_j must satisfy all the requirements of inner products (which are given in appendix C).

If eigenvectors of the reduced system are to be used, the eigensystem

$$\left[\hat{\mathbf{K}} - \omega_i^2 \hat{\mathbf{M}}\right] \mathbf{z}_i = 0$$

is solved and the eigenvectors normalised with respect to $\hat{\mathbf{M}}$. These reduced eigenvectors are then premultiplied by $\mathbf{P}$ to give a set of vectors $\mathbf{X}$ which are orthogonal to both the stiffness and mass matrices of the original system. These vectors can be good approximations to the eigenvectors of the original system. The degree of accuracy is dependent upon the number of Ritz vectors used, in the sense that more Ritz vectors will give a better approximation to the exact eigenvectors.

Wilson and many others [2, 28, 56] have presented results which show that fewer Ritz vectors are required than eigenvectors to generate results of similar accuracy. Computational savings are made because significantly less effort is required to generate the Ritz vectors, compared to generating eigenvectors.

3.3 Ritz vectors for damped systems

The above algorithm was developed by Wilson for applications in structural systems with proportional (modal) damping. The application to non-proportionally damped systems was by Ibrahimbegovic *et al.* [52] and Coyette [32] for structural and acoustic systems respectively. The technique used in both methods was to convert the second order differential equation into a first order system and then apply the Ritz vector algorithm.

The second order differential equation for damped acoustical systems is

$$\mathbf{K}\mathbf{p} + \mathbf{C}\dot{\mathbf{p}} + \mathbf{M}\ddot{\mathbf{p}} = \mathbf{f}, \tag{68}$$

where $\mathbf{p}$, $\dot{\mathbf{p}}$, and $\ddot{\mathbf{p}}$ are the acoustical pressure, the first derivative, and the second derivative of the pressure with respect to time respectively. This system can be transformed to a first order system by adding the identity

$$\mathbf{M}\dot{\mathbf{p}} - \mathbf{M}\dot{\mathbf{p}} = 0$$

to give a system twice the original size,

$$\mathbf{A}\dot{\mathbf{z}} - \mathbf{B}\mathbf{z} = \mathbf{y}, \tag{69}$$

where

$$\mathbf{A} = \begin{bmatrix} \mathbf{C} & \mathbf{M} \\ \mathbf{M} & 0 \end{bmatrix}, \mathbf{B} = \begin{bmatrix} -\mathbf{K} & 0 \\ 0 & \mathbf{M} \end{bmatrix},$$
$$\mathbf{z} = \begin{pmatrix} \mathbf{p} \\ \dot{\mathbf{p}} \end{pmatrix}, \mathbf{y} = \begin{pmatrix} \mathbf{f} \\ 0 \end{pmatrix}, \dot{\mathbf{z}} = \begin{pmatrix} \dot{\mathbf{p}} \\ \ddot{\mathbf{p}} \end{pmatrix}.$$

Wilson's Ritz algorithm was then applied to the above system with $\mathbf{M}$, $\mathbf{K}$, $\mathbf{x}$, and $\mathbf{f}$ replaced by $\mathbf{A}$, $\mathbf{B}$, $\mathbf{z}$ and $\mathbf{y}$ respectively.

3.3.1 Ritz algorithm for acoustical wave envelope systems

To apply the Ritz algorithm to acoustical wave envelope systems consideration must be given to the non-symmetry of the $\mathbf{K}$ and $\mathbf{C}$ matrices and the possibility of a near-zero $\mathbf{M}$ matrix. The non-symmetry of the $\mathbf{K}$ matrix is of little consequence, but the $\mathbf{C}$ matrix causes problems with the inner product used in the orthogonalisation and normalisation.

The Ritz algorithm for wave envelope systems is presented in two parts; the first part sets out the main details of the algorithm, and the second considers in detail the consequences of having a near-zero mass matrix.

The inner product used in Wilson's algorithm to both normalise and orthogonalise $\mathbf{z}$ involves the $\mathbf{A}$ matrix. As an inner product it must satisfy the axioms of appendix C, one of which is a symmetry condition. In the context of the damped acoustical system, this can be stated as a requirement that

$$\bar{\mathbf{x}}^T\mathbf{A}\mathbf{y} = \overline{\bar{\mathbf{y}}^T\mathbf{A}\mathbf{x}}, \tag{70}$$
$$= \mathbf{y}^T\mathbf{A}\bar{\mathbf{x}} \tag{71}$$

where $\mathbf{x}$ and $\mathbf{y}$ are any two complex valued vectors and an overline indicates the complex conjugate. This expression requires that $\mathbf{A}$ be symmetric. Recalling the contents of $\mathbf{A}$,

$$\mathbf{A} = \begin{bmatrix} \mathbf{C} & \mathbf{M} \\ \mathbf{M} & 0 \end{bmatrix},$$

it is obvious that $\mathbf{C}$ must be symmetric for $\mathbf{A}$ to be symmetric ($\mathbf{M}$ is already symmetric). This is not the case. A possible solution is to use the symmetric portion of $\mathbf{A}$, that is, $\mathbf{A}_s$, where

$$\mathbf{A}_s = \begin{bmatrix} \frac{1}{2}(\mathbf{C} + \mathbf{C}^T) & \mathbf{M} \\ \mathbf{M} & 0 \end{bmatrix}$$

for the purposes of orthogonalising the Ritz vectors. However, the positivity axiom of inner products requires that this modified matrix be not only symmetric, but also positive-definite and this cannot be guaranteed. A more satisfactory solution is to replace the inner product by the simple dot product between $\mathbf{x}$ and $\mathbf{y}$. That is, to define $\langle \mathbf{x}, \mathbf{y} \rangle = \overline{\mathbf{x}}^T \cdot \mathbf{y}$. The generation of Ritz vectors then proceeds as follows;

The first vector is obtained by solving

$$-\mathbf{B}\mathbf{z}_1' = \mathbf{y}, \tag{72}$$

and then normalising $\mathbf{z}_1'$ to give a scaled version $\mathbf{z}_1$ with the property that

$$\langle \mathbf{z}_1, \mathbf{z}_1 \rangle = 1.$$

Subsequent vectors (that is to say, for $i = 2, \ldots, n$) are found from the solution of

$$\mathbf{B}\mathbf{z}_i' = \mathbf{A}\mathbf{z}_{i-1}. \tag{73}$$

The result ($\mathbf{z}_i'$) is then made orthogonal to all existing vectors by defining

$$\mathbf{z}_i = \mathbf{z}_i' - \sum_{j=1}^{i-1} c_j \mathbf{z}_j, \tag{74}$$

where

$$c_j = \langle \mathbf{z}_j', \mathbf{z}_i \rangle \ , j = 1, \ldots, i-1. \tag{75}$$

Finally $\mathbf{z}_i$ is normalised so that

$$\langle \mathbf{z}_i, \mathbf{z}_i \rangle = 1. \tag{76}$$

The procedure given by equations 73 to 76 is then repeated for $i = 2, \ldots, n$ to generate n Ritz vectors.

Recalling that

$$\mathbf{z}_i = \begin{pmatrix} \mathbf{p}_i \\ \dot{\mathbf{p}}_i \end{pmatrix},$$

the set of Ritz vectors can be assembled into a matrix $\mathbf{P}$ via

$$\mathbf{P} = [\mathbf{p}_1, \mathbf{p}_2, \ldots, \mathbf{p}_n].$$

The reduced system can then be formed;

$$\left[\hat{\mathbf{K}} + ik\hat{\mathbf{C}} - k^2\hat{\mathbf{M}}\right] \hat{\mathbf{q}} = \hat{\mathbf{f}},$$

where

$$\begin{aligned}\hat{\mathbf{K}} &= \mathbf{P}^T\mathbf{K}\mathbf{P},\\ \hat{\mathbf{C}} &= \mathbf{P}^T\mathbf{C}\mathbf{P},\\ \hat{\mathbf{M}} &= \mathbf{P}^T\mathbf{M}\mathbf{P},\\ \hat{\mathbf{q}} &= \mathbf{P}^T\mathbf{q},\\ \hat{\mathbf{f}} &= \mathbf{P}^T\mathbf{f}.\end{aligned}$$

Solving this reduced system to give $\hat{\mathbf{q}}$ allows one to regenerate the full solution via

$$\mathbf{q} = \mathbf{P}\hat{\mathbf{q}}.$$

The nature of $\mathbf{A}$ and $\mathbf{B}$ allow some simplifications to be made when implementing the Ritz algorithm. Equation 72 expands to

$$\begin{bmatrix}\mathbf{K} & 0\\ 0 & -\mathbf{M}\end{bmatrix}\begin{pmatrix}\mathbf{p}_1'\\ \dot{\mathbf{p}}_1'\end{pmatrix} = \begin{pmatrix}\mathbf{f}\\ 0\end{pmatrix}$$

and this becomes

$$\begin{aligned}\mathbf{K}\mathbf{p}_1' &= \mathbf{f},\\ -\mathbf{M}\dot{\mathbf{p}}_1' &= 0.\end{aligned}$$

The calculation of $\mathbf{p}_1'$ is straightforward, and involves a decomposition of $\mathbf{K}$ and a back substitution, and as long as $\mathbf{M}$ is non-singular, $\dot{\mathbf{p}}_1' = 0$.

Equation 73 expands to

$$\begin{bmatrix}-\mathbf{K} & 0\\ 0 & \mathbf{M}\end{bmatrix}\begin{pmatrix}\mathbf{p}_i'\\ \dot{\mathbf{p}}_i'\end{pmatrix} = \begin{bmatrix}\mathbf{C} & \mathbf{M}\\ \mathbf{M} & 0\end{bmatrix}\begin{pmatrix}\mathbf{p}_{i-1}\\ \dot{\mathbf{p}}_{i-1}\end{pmatrix}, \tag{77}$$

which becomes

$$\begin{aligned}-\mathbf{K}\mathbf{p}_i' &= \mathbf{C}\mathbf{p}_{i-1} + \mathbf{M}\dot{\mathbf{p}}_{i-1},\\ \mathbf{M}\dot{\mathbf{p}}_i' &= \mathbf{M}\mathbf{p}_{i-1}.\end{aligned}$$

The second line simplifies to

$$\dot{\mathbf{p}}_i' = \mathbf{p}_{i-1}'$$

for a non-singular $\mathbf{M}$. The $\mathbf{K}$ matrix has already been decomposed, hence obtaining $\mathbf{p}_i'$ requires two matrix-vector multiplications, a vector addition and a back substitution.

3.3.2 Consideration of near zero mass matrices

As discussed in section 2.3.2, wave envelope elements may have near-zero mass terms, leading to near-zero terms in the global mass matrix. This raises the possibility of numerical difficulties in the Ritz vector algorithm due to the assumed non-singularity of the mass matrix. Particular attention will now be paid to the situation where the mass matrix may have zero terms on the diagonal.

Consider the simple conventional/wave envelope element mesh in figure 17 which shows one conventional element joined to one wave envelope element. If all the nodes on the conventional elements are numbered first, as in the figure, a mass matrix of the form shown in figure 18 results. A 'c' represents contributions from the conventional element, a 'w' represents contributions from the wave envelope element, and '0' represents a zero term. However, if all contributions from the wave envelope element are zero the matrix can be partitioned into four sub-matrices, $\mathbf{M}_1$, $\mathbf{M}_2$, $\mathbf{M}_3$, and $\mathbf{M}_4$, with $\mathbf{M}_1$ the only non-zero sub-matrix. A mixed conventional/wave envelope mesh will always be able to be numbered in this manner.

An identical partitioning is used on the other matrices and vectors in equation 69. In particular the vectors are partitioned into two sections denoted by the subscripts 'c' and 'w'. The subscript 'c' denotes those nodal quantities that receive contributions from the conventional element region, including points on the interface between the conventional and wave envelope regions. The subscript 'w' denotes those nodal quantities which receive contributions from the wave envelope region only. That is to say, the nodal pressure vector $\mathbf{z}$ is partitioned as

$$\mathbf{z} = \begin{pmatrix} \mathbf{p}_c \\ \mathbf{p}_w \end{pmatrix}.$$

The first Ritz vector is calculated from

$$-\mathbf{B}\mathbf{z}_1' = \mathbf{y},$$

which becomes

$$\begin{bmatrix} \mathbf{K} & 0 \\ 0 & -\mathbf{M} \end{bmatrix} \begin{pmatrix} \mathbf{p}_1' \\ \dot{\mathbf{p}}_1' \end{pmatrix} = \begin{pmatrix} \mathbf{f} \\ 0 \end{pmatrix},$$

or

$$\underset{\text{(a)}}{\mathbf{K}\mathbf{p}_1' = \mathbf{f}} \quad , \quad \underset{\text{(b)}}{-\mathbf{M}\dot{\mathbf{p}}_1' = 0.}$$

Consider part (a). When expressed in partitioned form this can be written as

$$\begin{bmatrix} -\mathbf{K}_1 & -\mathbf{K}_2 \\ -\mathbf{K}_3 & -\mathbf{K}_4 \end{bmatrix} \begin{pmatrix} \mathbf{p}_{1c}' \\ \mathbf{p}_{1w}' \end{pmatrix} = \begin{pmatrix} \mathbf{f}_c \\ \mathbf{f}_w \end{pmatrix},$$

Solution of this system causes no difficulties. Consider part (b). This becomes

$$\begin{bmatrix} -\mathbf{M}_1 & -\mathbf{M}_2 \\ -\mathbf{M}_3 & -\mathbf{M}_4 \end{bmatrix} \begin{pmatrix} \dot{\mathbf{p}}_{1c}' \\ \dot{\mathbf{p}}_{1w}' \end{pmatrix} = \begin{pmatrix} 0 \\ 0 \end{pmatrix},$$

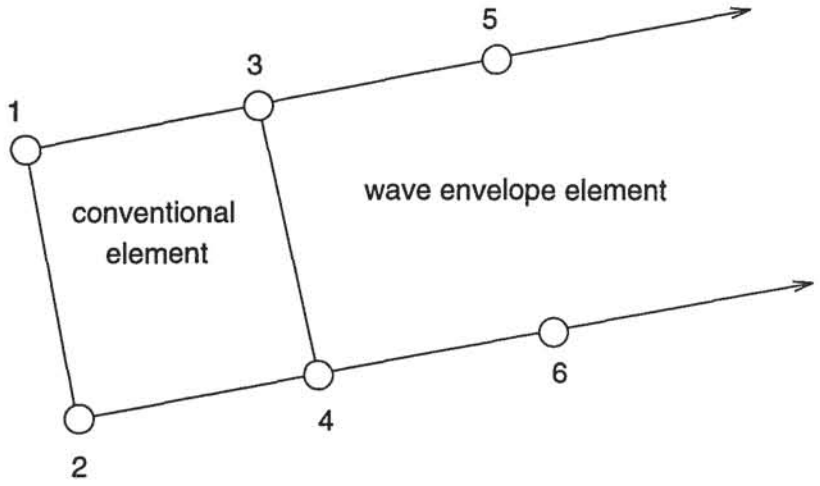

Figure 17: Simple wave envelope mesh

	1	2	3	4	5	6
1	c	c	c	c	0	0
2	c	c	c	c	0	0
3	c	c	c+w	c+w	w	w
4	c	c	c+w	c+w	w	w
5	0	0	w	w	w	w
6	0	0	w	w	w	w

$$\begin{bmatrix} \mathbf{M}_1 & \mathbf{M}_2 \\ \mathbf{M}_3 & \mathbf{M}_4 \end{bmatrix}$$

Figure 18: Mass matrix for mesh in figure 17

which expands to give

$$\begin{aligned} \mathbf{M}_1\dot{\mathbf{p}}'_{1c} + \mathbf{M}_2\dot{\mathbf{p}}'_{1w} &= 0, \\ \mathbf{M}_3\dot{\mathbf{p}}'_{1c} + \mathbf{M}_4\dot{\mathbf{p}}'_{1w} &= 0. \end{aligned}$$

However, $\mathbf{M}_2 = \mathbf{M}_3 = \mathbf{M}_4 = 0$ and hence

$$\dot{\mathbf{p}}'_{1c} = 0, \tag{78}$$

provided that $\mathbf{M}_1$ is not singular. Note that $\dot{\mathbf{p}}'_{1w}$ is arbitrary and can be chosen to be zero without loss of generality.

The normalisation of $\mathbf{z}'_1$ is given by

$$\mathbf{z}_1 = \frac{\mathbf{z}'_1}{\langle \mathbf{z}'_1, \mathbf{z}'_1 \rangle^{1/2}},$$

where

$$\langle \mathbf{z}'_1, \mathbf{z}'_1 \rangle = \overline{\left(\mathbf{p}'^T_{1c}\, \mathbf{p}'^T_{1w}\, \dot{\mathbf{p}}'^T_{1c}\, \dot{\mathbf{p}}'^T_{1w}\right)} \cdot \begin{pmatrix} \mathbf{p}'_{1c} \\ \mathbf{p}'_{1w} \\ \dot{\mathbf{p}}'_{1c} \\ \dot{\mathbf{p}}'_{1w} \end{pmatrix}.$$

If the $\dot{\mathbf{p}}'_{1w}$ term is set to zero as suggested above, the normalisation of $\mathbf{z}_1$ is clearly defined.

Additional vectors are obtained by solving

$$\mathbf{B}\mathbf{z}'_i = \mathbf{A}\mathbf{z}_{i-1},$$

which expands to

$$\begin{bmatrix} -\mathbf{K} & 0 \\ 0 & \mathbf{M} \end{bmatrix} \begin{pmatrix} \mathbf{p}'_i \\ \dot{\mathbf{p}}'_i \end{pmatrix} = \begin{bmatrix} \mathbf{C} & \mathbf{M} \\ \mathbf{M} & 0 \end{bmatrix} \begin{pmatrix} \mathbf{p}_{i-1} \\ \dot{\mathbf{p}}_{i-1} \end{pmatrix},$$

or

$$\underset{\text{(a)}}{-\mathbf{K}\mathbf{p}'_i = \mathbf{C}\mathbf{p}_{i-1} + \mathbf{M}\dot{\mathbf{p}}_{i-1}} \quad , \quad \underset{\text{(b)}}{\mathbf{M}\dot{\mathbf{p}}'_i = \mathbf{M}\mathbf{p}_{i-1}}.$$

For part (a) the only critical term is the one containing M. The M term expands to

$$\begin{bmatrix} \mathbf{M}_1 & 0 \\ 0 & 0 \end{bmatrix} \begin{pmatrix} \dot{\mathbf{p}}_{(i-1)c} \\ \dot{\mathbf{p}}_{(i-1)w} \end{pmatrix} = \begin{pmatrix} \mathbf{M}_1\dot{\mathbf{p}}_{(i-1)c} \\ 0 \end{pmatrix}$$

and the arbitrarily chosen $\dot{\mathbf{p}}_{(i-1)w}$ is not involved in the calculation. Part (b) expands to

$$\begin{bmatrix} \mathbf{M}_1 & 0 \\ 0 & 0 \end{bmatrix} \begin{pmatrix} \dot{\mathbf{p}}'_{ic} \\ \dot{\mathbf{p}}'_{iw} \end{pmatrix} = \begin{bmatrix} \mathbf{M}_1 & 0 \\ 0 & 0 \end{bmatrix} \begin{pmatrix} \mathbf{p}_{(i-1)c} \\ \mathbf{p}_{(i-1)w} \end{pmatrix} \tag{79}$$

and yields

$$\dot{\mathbf{p}}'_{ic} = \mathbf{p}_{(i-1)c}$$

provided $\mathbf{M}_1$ is non-singular.

The normalisation of $\mathbf{z}'_i$ to give $\mathbf{z}_i$ proceeds as for $\mathbf{z}'_1$. Note, however, that $\dot{\mathbf{p}}'_{iw}$ is used in the normalisation, but is not defined in expression 79. It is convenient to specify

$$\dot{\mathbf{p}}'_{iw} = \mathbf{p}_{(i-1)w}$$

to provide a value for $\dot{\mathbf{p}}'_{iw}$. For the purposes of constructing a Ritz basis to solve acoustical wave envelope systems only the $\mathbf{p}_i$ component of $\mathbf{z}$ is used in the Ritz basis, and the $\dot{\mathbf{p}}_i$ component is discarded.

3.4 Form of the forcing vector

The Ritz algorithm originally proposed by Wilson has the requirement that the forcing vector be able to be expressed as a product of space vectors and time functions (see section 64). The analogous statement for acoustical systems is that the forcing vector be able to be written as a product of space vectors and frequency functions, that is,

$$\mathbf{f} = \mathbf{g}(s)\mathbf{h}(k), \tag{80}$$

where $\mathbf{g}(s)$ is the spacial component and $\mathbf{h}(k)$ the frequency component. In wave envelope finite element analyses the $\mathbf{f}$ vector is generated from

$$\mathbf{f} = ik\rho c \int_{S_1} P_j U \, dS,$$

of which U is the only component in the integral that can depend upon k. Hence the requirement that $\mathbf{f}$ take the form of 80 above reduces to a requirement that U be able to be written as

$$U = g(s)h(k).$$

With reference to section 2.1.1, it can be seen that the rigid surface and vibrating rigid surface boundary conditions satisfy this requirement, while the scattering boundary condition does not.

To apply Ritz vectors to scattering type excitations requires the periodic recalculation of the Ritz basis. This is discussed in the subsequent section.

3.5 Frequency interpolation of the Ritz bases

When applying Ritz vectors to scattering type boundary conditions, the vector $\mathbf{f}$ cannot be expressed as a product of a spatial vector and a frequency vector, implying that a new

Ritz basis has to be calculated for every frequency of interest. This is clearly a waste of effort as solving the full system would use less CPU time. However, if the change in Ritz bases is well-behaved as the frequency is varied, it is possible to calculate widely spaced Ritz bases and for each frequency of interest to generate an interpolated Ritz basis. Linear interpolation is described below.

3.5.1 Linear interpolation

Two Ritz bases are generated, at frequencies ω_l and ω_u. An interpolated Ritz basis at ω is defined by

$$\begin{aligned}\mathbf{P}_\omega &= \mathbf{P}_l + \left(\frac{\omega-\omega_l}{\omega_u-\omega_l}\right)[\mathbf{P}_u - \mathbf{P}_l] \\ &= \left(1-\frac{\omega-\omega_l}{\omega_u-\omega_l}\right)\mathbf{P}_i + \left(\frac{\omega-\omega_l}{\omega_u-\omega_l}\right)\mathbf{P}_u \\ &= \alpha\mathbf{P}_l + \beta\mathbf{P}_u,\end{aligned}$$

where l indicates lower, u upper and $\omega_l \leq \omega \leq \omega_u$.

The reduced matrices are defined as

$$\begin{aligned}\hat{\mathbf{K}} &= \mathbf{P}^T\mathbf{K}\mathbf{P}, \\ \hat{\mathbf{C}} &= \mathbf{P}^T\mathbf{C}\mathbf{P}, \\ \hat{\mathbf{M}} &= \mathbf{P}^T\mathbf{M}\mathbf{P},\end{aligned}$$

and substitution of the interpolated Ritz basis results in

$$\begin{aligned}\hat{\mathbf{K}} &= \left(\alpha\mathbf{P}_l^T + \beta\mathbf{P}_u^T\right)\mathbf{K}\left(\alpha\mathbf{P}_l + \beta\mathbf{P}_u\right) \\ &= \alpha^2\mathbf{P}_l^T\mathbf{K}\mathbf{P}_l + \beta^2\mathbf{P}_u^T\mathbf{K}\mathbf{P}_u + \alpha\beta\left[\mathbf{P}_l^T\mathbf{K}\mathbf{P}_u + \mathbf{P}_u^T\mathbf{K}\mathbf{P}_l\right].\end{aligned}$$

Likewise for $\hat{\mathbf{C}}$ and $\hat{\mathbf{M}}$.

Also required is $\hat{\mathbf{f}}$ and the form for recovering $\mathbf{q}$ from $\hat{\mathbf{q}}$,

$$\begin{aligned}\hat{\mathbf{f}} &= \left(\alpha\mathbf{P}_l^T + \beta\mathbf{P}_u^T\right)\mathbf{f}, \\ \mathbf{q} &= \left(\alpha\mathbf{P}_l + \beta\mathbf{P}_u\right)\hat{\mathbf{q}}.\end{aligned}$$

Note that $\left(\alpha\mathbf{P}_l^T + \beta\mathbf{P}_u^T\right) = \left(\alpha\mathbf{P}_l + \beta\mathbf{P}_u\right)^T$.

Each frequency range that a basis set applies to requires the calculation and storage of one new Ritz basis and the pre- and post-multiplications of $\mathbf{K}$, $\mathbf{C}$ and $\mathbf{M}$. For each frequency at which one wishes to calculate the solution it is necessary to calculate the $\hat{\mathbf{K}}$, $\hat{\mathbf{C}}$, $\hat{\mathbf{M}}$ and $\hat{\mathbf{f}}$ matrices, assemble the reduced system, solve and then regenerate the full solution vector, $\mathbf{q}$.

For subsequent frequency ranges savings in computation can be made by re-using some of the matrices from the previous frequency range. The Ritz basis $\mathbf{P}_u$ becomes $\mathbf{P}_l$ and also

$$\begin{aligned} \mathbf{P}_l^T \mathbf{K} \mathbf{P}_l &= \left(\mathbf{P}_u^T \mathbf{K} \mathbf{P}_u\right)^*, \\ \mathbf{P}_u^T (\mathbf{K} \mathbf{P}_l) &= \mathbf{P}_u^T (\mathbf{K} \mathbf{P}_u)^*, \end{aligned}$$

where $*$ indicates from the previous iteration. Likewise for the C and M matrices.

Obviously if $\alpha = 1$ or $\beta = 1$, the calculation of the reduced matrices becomes

$$\begin{aligned} \hat{\mathbf{K}} &= \mathbf{P}_l^T \mathbf{K} \mathbf{P}_l \text{ for } \alpha = 1, \\ \hat{\mathbf{K}} &= \mathbf{P}_u^T \mathbf{K} \mathbf{P}_u \text{ for } \beta = 1. \end{aligned}$$

Likewise for $\hat{\mathbf{C}}$ and $\hat{\mathbf{M}}$.

Chapter 4

Wave envelope results

4.1 Introduction

This chapter presents results that illustrate the performance of wave envelope elements.

In the same manner as for conventional finite element methods, linear, quadratic or higher order interpolations are possible in the non-infinite directions of the wave envelope elements. All results presented here are obtained by using quadratic interpolation elements with the exception of an initial example that compares linear and quadratic elements.

As discussed earlier, the basis functions of the wave envelope elements approximate the amplitude of outwardly propagating waves with inverse polynomials. The form of these waves are described by Hankel functions (of integer order for two-dimensional radiation and fractional order for three-dimensional radiation), and the accuracy of these wave envelope elements is determined by the ability of the polynomial to represent the Hankel functions. This is demonstrated on three models; axi-symmetric multi-pole radiation from a three-dimensional sphere, scattering of an incident plane wave by a sphere (both with a radius of 100mm), and radiation from a vibrating angled block.

Appendix E contains results for the two-dimensional analogy of the sphere, an infinitely long cylinder. Similar trends are observed as for the three-dimensional sphere.

4.2 Angular interpolation comparison

Wave envelope elements possess conventional interpolation functions in the non-infinite directions, posing the question of what order interpolation to use. Typically the choice is between linear or quadratic interpolation—the latter having several advantages over the former. These include better matching of the mesh to the geometry, requiring fewer nodes and giving better solutions—all of which apply to wave envelope elements.

The improvement which is of most interest is the increase in accuracy of the wave envelope solution, which is achieved with fewer degrees-of-freedom and consequently less CPU time.

The wave envelope program developed by the author allows both linear and quadratic interpolation in the non-infinite directions, and an example is presented that illustrates the increase in accuracy obtained by moving from a linear to a quadratic mesh. The comparison was performed on a mesh of the unbounded domain surrounding a sphere of radius 0.1m, with two symmetry planes utilised to reduce the size of the problem. A slice of the linear and quadratic wave envelope meshes is shown in figure 19. The linear mesh contains 384 wave envelope elements and 3753 degrees-of-freedom; the quadratic mesh contains 96 wave envelope elements and 2889 degrees-of-freedom (both meshes use order nine wave envelope elements). An isometric view of the quadratic mesh is given in a later section as figure 23. All subsequent illustrations of wave envelope meshes omit the nodes, and represent the infinite wave envelope elements with finite elements.

The sphere was placed in the path of a plane wave and the resulting pressure field calculated. A plot of the scattered pressure field for linear and quadratic meshes, compared against the analytical solution is given in figure 20 for $ka = 10$, where $a = 0.1$m. Although it is difficult to discern, the quadratic wave envelope elements give a better solution, especially in the low to medium pressure regions to the left of the sphere.

The scattering excitation was chosen for this example because it exhibited noticeable differences in solution between the linear and quadratic meshes. The multi-pole excitation did not clearly show any difference in the accuracy of linear and quadratic wave envelope elements, due to the less complicated pressure field.

A more quantitative comparison of the improvement in accuracy is given in figure 21, where the percentage error (at the point marked with a cross in figure 20) is plotted for the linear and quadratic meshes over a frequency range. The quadratic mesh has considerably better accuracy than the linear mesh. Beyond the ka value of approximately 12, the solution accuracy for the quadratic wave envelope mesh becomes unacceptably high, and the reasons for this are discussed in subsequent sections. Note that the improvement in accuracy was achieved with fewer degrees-of-freedom (3753 reduced to 2889) and hence with less CPU time (62 seconds down to 57 seconds). All subsequent models use wave envelope elements with quadratic interpolation in the transverse directions unless mentioned otherwise.

4.3 Multi-pole radiation

Consider a sphere with the surface vibrating in the axi-symmetric form

$$U(\theta) = U_0 P_n(\cos\theta),$$

where the angle θ is measured as shown in figure 23, $U(\theta)$ is the normal surface velocity at angle θ, U_0 the maximum velocity amplitude, and P_n a Legendre polynomial of order n. The radiated sound field from this excitation is given by Skudrzyk [84], which after

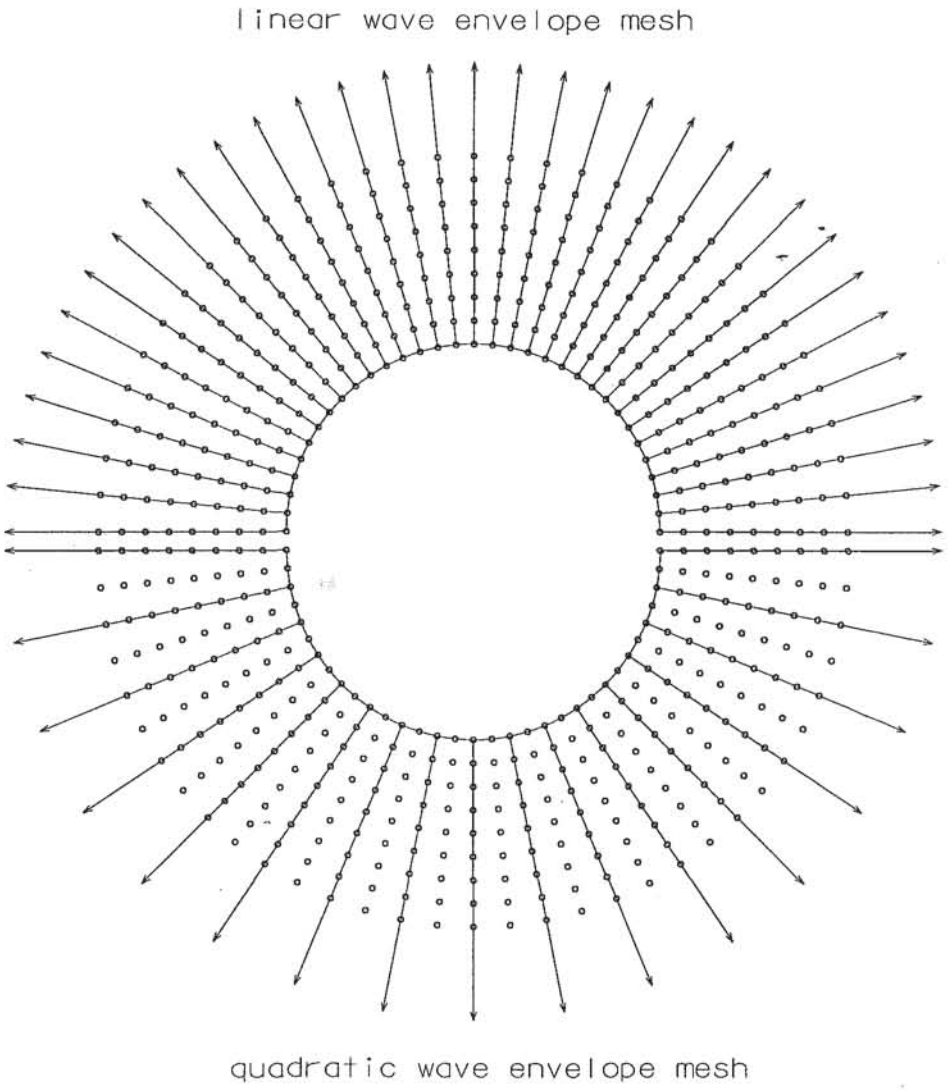

Figure 19: Slice of the wave envelope meshes used to compare linear and quadratic wave envelope elements. The linear wave envelope mesh (top half) has 384 elements and 3753 degrees-of-freedom, while the quadratic wave envelope mesh (bottom half) has 96 elements and 2889 degrees-of-freedom.

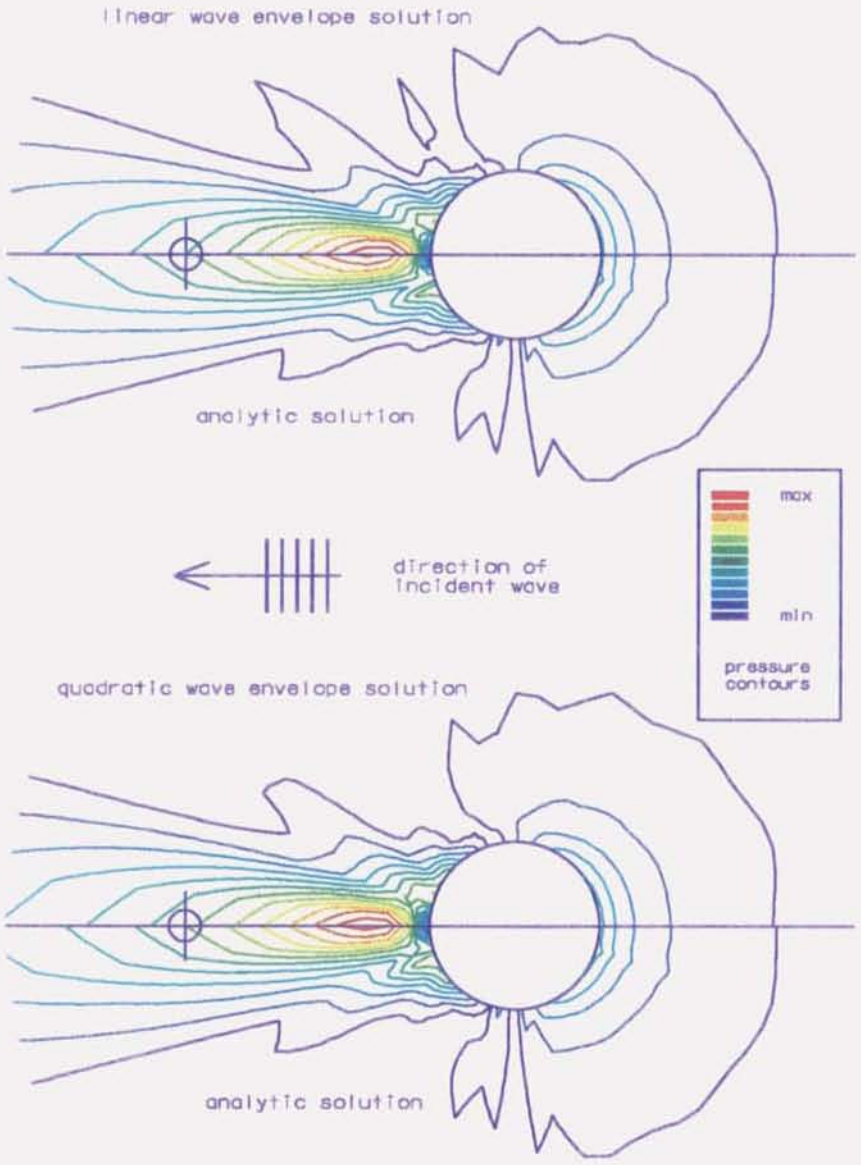

Figure 20: Pressure contours comparing linear and quadratic wave envelope element solutions of the scattering of a plane wave by a rigid sphere to the analytical solutions. Order nine wave envelope elements are used in both meshes, and the solution is calculated at $ka = 10$. Contours are plotted on a plane passing through the origin of the sphere.

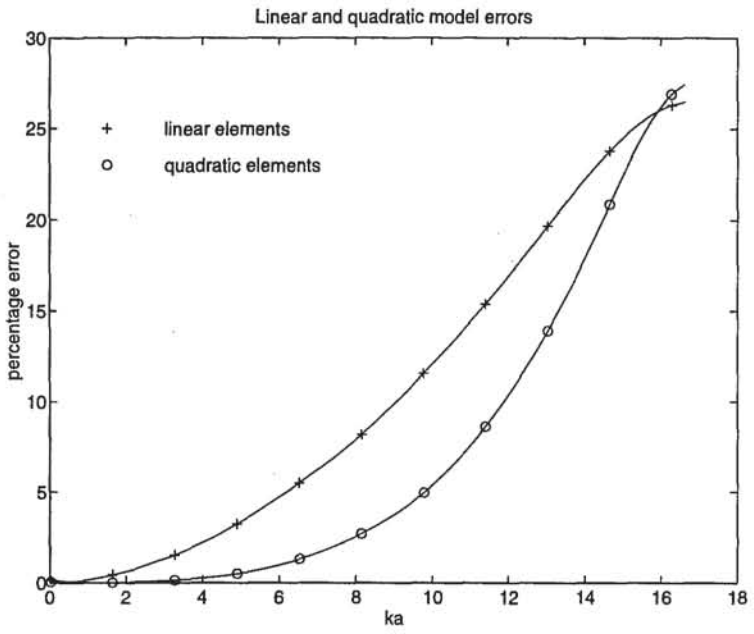

Figure 21: Percentage error of wave envelope solution compared to analytic solution at $(-5a, 0, 0)$ for an order nine wave envelope element. Models is a 3D sphere with 96 quadratic or 384 linear elements.

some simplification becomes

$$p(r,\theta) = -i\rho c U_0 P_n(\cos\theta)\frac{h_n^{(2)}(kr)}{h_n^{(2)\prime}(ka)}, \tag{81}$$

where $h_n^{(2)}(z)$ is a spherical Hankel function of the second kind, $h_n^{(2)\prime}(z)$ is the derivative of $h_n^{(2)}(z)$ with respect to z, k the wavenumber, r the distance from the sphere centre and a the sphere radius.

The angular and radial dependence of the sound field are separable and their effect on the solution is considered independently.

4.3.1 Radial behaviour

The radially varying factor of equation 81 is

$$h_n^{(2)}(kr),$$

which for large kr becomes

$$h_n^{(2)}(kr) \sim \frac{1}{kr} e^{-ikr + i\frac{\pi}{2}(n+1)}.$$

For constant n, and large kr this reduces to

$$h_n^{(2)}(kr) \sim \frac{\text{const}}{r} e^{-ikr}.$$

This matches exactly the basis function behaviour of an order 1 wave envelope element (compare to equation 55). At lower values of kr (lower wavenumbers and/or smaller radii) the deviation of the Hankel functions from the asymptotic form discussed above can be modelled by the higher order interpolation incorporated into the high order wave envelope elements.

4.3.2 Angular behaviour

The angular behaviour is governed by the Legendre polynomials, $P_n(\cos\theta)$, which have a wave-like behaviour for varying θ and constant n. Polar plots of Legendre polynomials of order 1 to 6 are given in figure 22. Note how a polynomial of order n gives $n/2$ waves around half the circumference. The 10 nodes per wavelength 'rule of thumb' can be used here, where for example, the order 6 Legendre polynomial requires 30 nodes in half the circumference to adequately resolve the wave pattern. For quadratic elements the nodes per wavelength can be reduced to 5, and hence only 15 nodes would be necessary. For a given mesh density this sets the maximum order multi-pole that can be modelled.

4.3.3 Multi-pole radiation results

Frequency response plots for various multi-pole excitations of a sphere of radius 0.1m are presented and the effect of radial interpolation order is discussed. The mesh consists entirely of wave envelope elements with quadratic interpolation in the transverse (angular)directions, and is shown in figure 23. It contains 96 quadratic wave envelope elements; the number of degrees-of-freedom for varying wave envelope radial interpolation order is given in table 1.

Pressure contours that indicate the form and overall accuracy of order 2, 10 and 15 multi-poles are shown in figure 24, for ka values of 25, 20 and 20 respectively. (The order two multi-pole solution is obtained by using order three wave envelope elements, the order 10 multi-pole solution by using order six wave envelope elements and the order 15 multi-pole solution by using order eight wave envelope elements). Frequency response curves for order 2, 10, 15 and 20 multi-poles for varying wave envelope orders are given in figures 25, 26, 27 and 28 respectively. The point used for the frequency response curves is marked on figure 24 with a cross and is at the position $(5a, 0, 0)$.

Several conclusions can be drawn from these results:

- At high ka values the wave envelope solutions converge to the analytical solution. This is due to the asymptotic behaviour of the analytical solution matching the wave envelope asymptotic element behaviour. Because of this, even low order wave envelope elements can yield good solutions at high ka values.

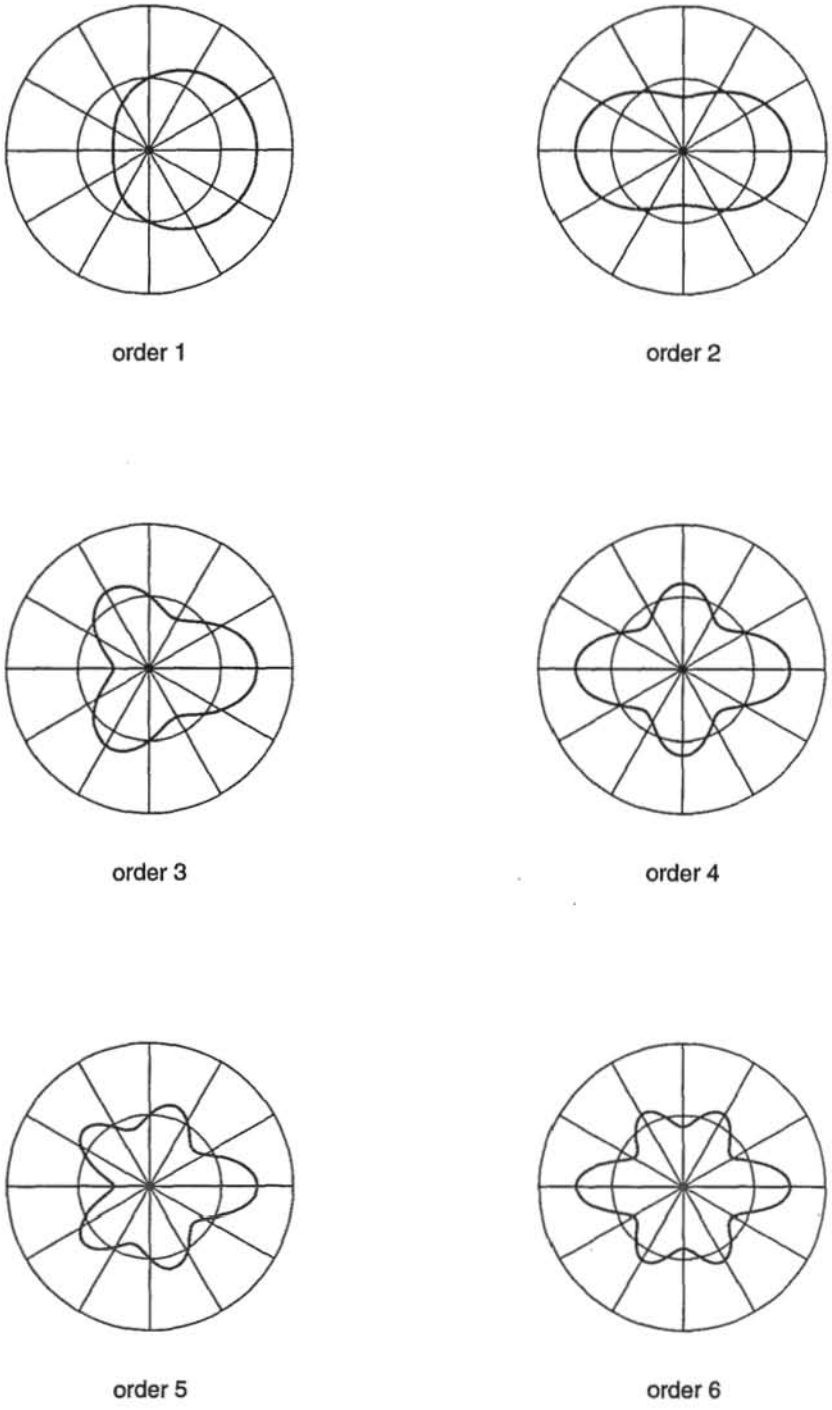

Figure 22: Legendre polynomials of order 1 to 6, representing the axi-symmetric vibration of a sphere.

wave envelope order	degrees of freedom
2	642
3	963
4	1284
5	1605
6	1926
7	2247
8	2568
9	2889

Table 1: Degrees of freedom for various wave envelope orders.

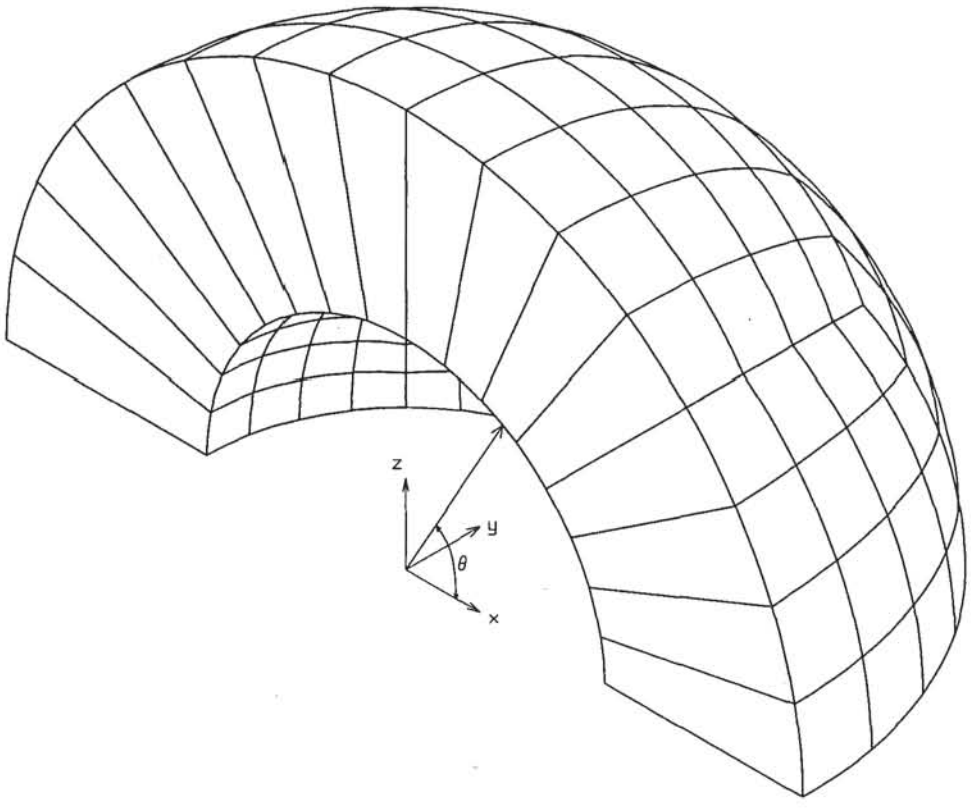

Figure 23: Quadratic wave envelope mesh surrounding a three-dimensional sphere of radius 0.1 m (two symmetry planes have been used to reduce the mesh size).

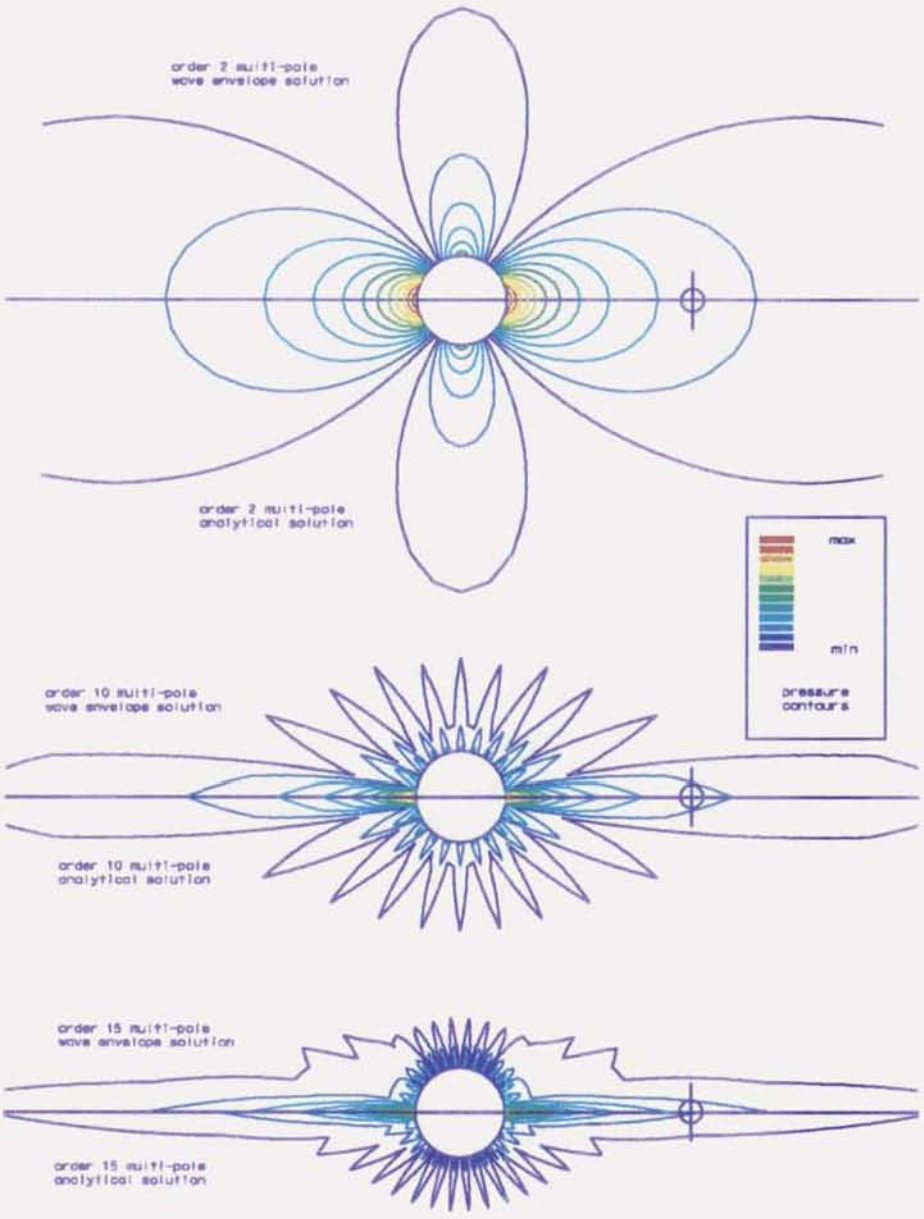

Figure 24: Pressure contours for order 2, 10 and 15 multi-poles compared to analytical solutions. The order two multi-pole was calculated at $ka = 25$ with an order three wave envelope element; the order 10 multi-pole is calculated at $ka = 20$ and uses an order six wave envelope element. The order 15 multi-pole is calculated at $ka = 20$ and uses an order eight wave envelope element.

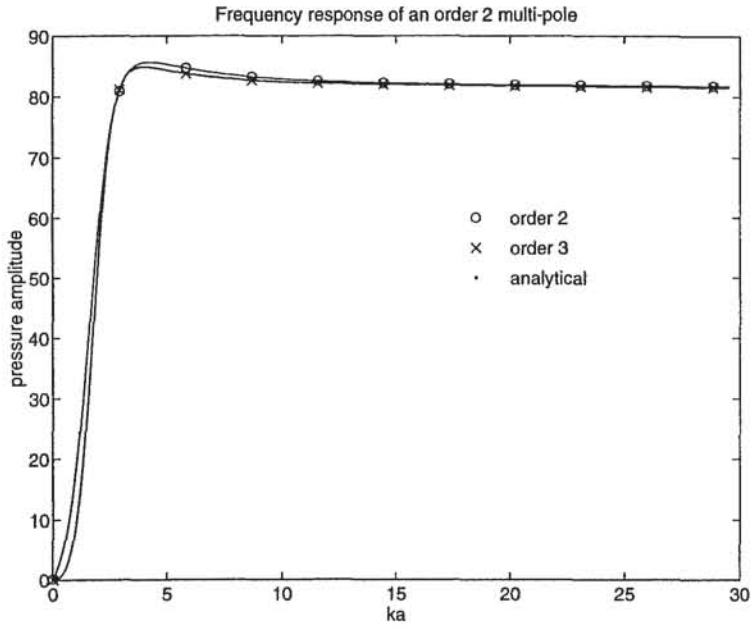

Figure 25: Radiated pressure at $(5a, 0, 0)$ for varying wave envelope interpolation orders. Model is a 3D sphere with 96 quadratic wave envelope elements.

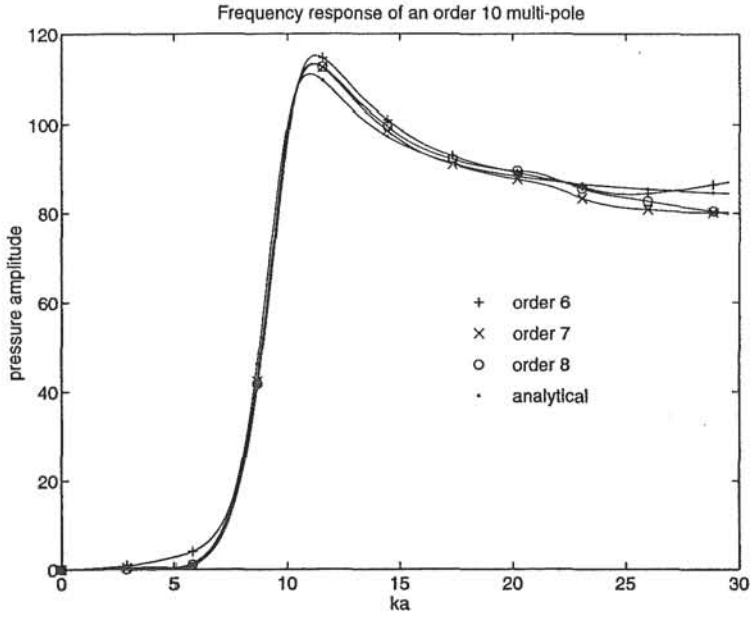

Figure 26: Radiated pressure at $(5a, 0, 0)$ for varying wave envelope interpolation orders. Model is a 3D sphere with 96 quadratic wave envelope elements.

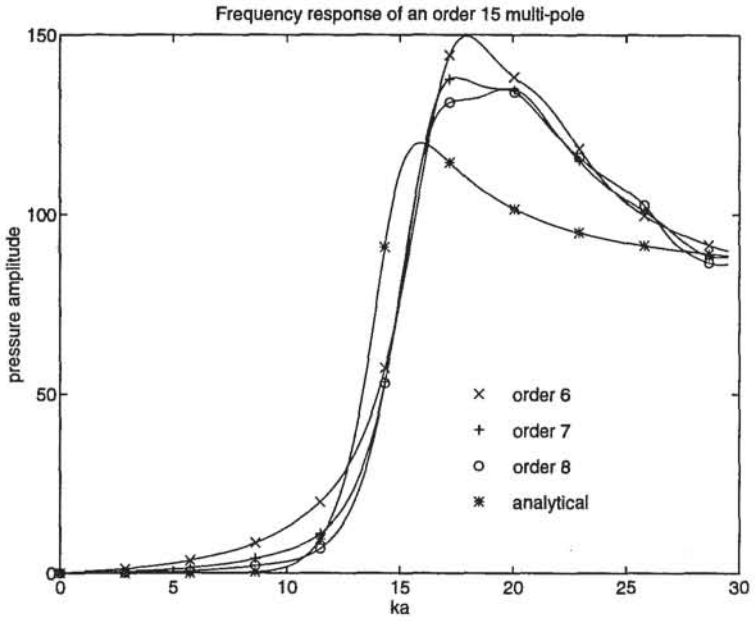

Figure 27: Radiated pressure at $(5a, 0, 0)$ for varying wave envelope interpolation orders. Model is a 3D sphere with 96 quadratic wave envelope elements.

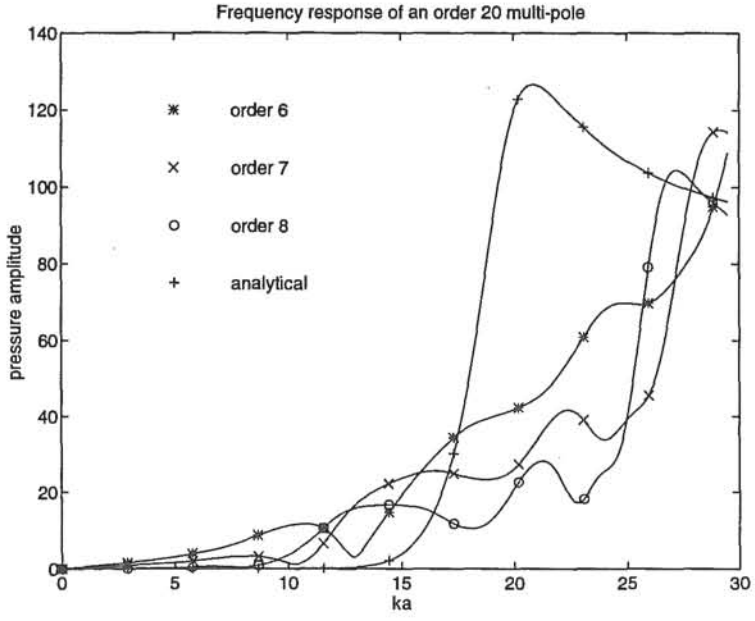

Figure 28: Radiated pressure at $(5a, 0, 0)$ for varying wave envelope interpolation orders. Model is a 3D sphere with 96 quadratic wave envelope elements.

- Some wave envelope solutions lose accuracy at high ka, occurring mainly with high interpolation elements and high order multi-poles. This occurs in figure 26 at $ka \approx 22$ and in figure 27 at $ka \approx 17$, but does not occur for the order two multi-pole (figure 25), even at extremely high values of ka (the order two multi-pole solution has been calculated up to $ka = 200$, with no sign of any loss of accuracy). This behaviour is of minor concern because the frequencies at which it occurs are well within the region where high ka approximation techniques are applicable (for example, acoustical ray theory). An explanation was not found for this loss of accuracy, although the ill-conditioned matrices (section 4.6) probably make some contribution.

- Better solutions were obtained for lower ka values by using higher order wave envelope interpolations. This occurs because the higher order elements are able to model more accurately the near-field behaviour of the Hankel functions, which differ from the asymptotic form.

- The mesh used for all of the solutions presented has sufficient nodes in the angular direction to cope with Legendre polynomials up to order 15, but can be expected to lose accuracy for higher orders. This is illustrated in figure 28 which shows an order 20 multi-pole excitation. It is obvious that increasing the wave envelope order does not improve the solution which is limited in this case by the angular rather than radial resolution of the mesh.

- As discussed in section 4.3.1, the asymptotic behaviour of spherical Hankel functions for large kr is

$$h_n^{(2)}(kr) \sim \frac{\text{const}}{kr} e^{-ikr}. \tag{82}$$

  However, the value of ka at which the behaviour given by expression 82 dominates increases with n. Hence to maintain accuracy at low ka values in high order multi-poles it is necessary to use higher order wave envelope elements.

- Wave envelope elements with interpolation orders of more that 10 result in ill-conditioned matrices. This places an upper limit of approximately 10 on the order of Hankel function that these elements can accurately represent. See section 4.6 for a discussion of this ill-conditioning.

Due to the orthogonal nature of the Legendre polynomials any axi-symmetric vibration of a sphere can be represented by a linear combination of Lengendre polynomials. Consequently, the radiated field for any form of axi-symmetric surface excitation becomes a linear combination of Legendre polynomials and Hankel functions. The next form of excitation, scattering, is of this type.

4.4 Scattering of a plane wave by a rigid sphere

The scattering of a plane wave by a rigid sphere is a more complicated problem than the multi-pole radiation, although it is still axi-symmetric. The implementation of the scattering excitation is discussed in section 2.1.1, and the analytic solution is given by Junger and Feit [58],

$$p_s(r,\theta) = -P_i \sum_{n=0}^{\infty} (2n+1) i^n P_n(\cos\theta) \frac{j_n'(ka)}{h_n^{(2)\prime}(ka)} h_n^{(2)}(kr). \tag{83}$$

The form is similar to the multi-pole solution, the main difference being the summation over a range of orders of Legendre polynomials, Hankel functions and Bessel functions.

When calculating the analytical solution using expression 83, the series is truncated at some value of n, say m. This truncation occurs when the addition of more terms alters the solution by less than some specified tolerance level. The value of m varies with k. The results from the multi-pole models showed that an order nine wave envelope element gave acceptable results for up to order 10 Hankel functions. Order 10 Hankel functions become significant in the above summation for kr values greater than 45.0. For the r value used in the results produced here (0.5 m), this is equivalent to a restriction on ka to nine or less ($ka = kr/r \times a$). This is confirmed in figure 29 where the order nine curve loses accuracy beyond $ka \approx 9$. (The frequency response curves in figure 29 were obtained from the scattering of a plane wave by a rigid sphere with order 2, 5 and 9 wave envelope elements and illustrate the same improvement in accuracy as seen in the multi-pole results).

To show that the angular node density is not the cause of this loss of accuracy, the same excitation was applied to a much finer mesh (600 wave envelope elements). As can be seen in figure 30, the loss of accuracy occurs at a similar ka value (it was not possible to calculate an order nine curve for the fine mesh due to computer memory restrictions).

The form of the scattered field has already been shown in figure 20 of section 4.2. Of practical interest is the form of the total pressure field, and this is shown in figure 31, for $ka = 10$. Note how standing waves form from the interference of the reflected and incident waves to the right of the sphere. The correspondence between the wave envelope solution and the analytical solution is good.

4.5 Use of conventional acoustic finite elements

In this section, a model is presented that benefits from the addition of conventional acoustic finite elements (multi-pole radiation and plane wave scattering by a sphere gain little from the use of conventional finite elements, and is discussed later).

The addition of layers of conventional elements around the object of interest moves the wave envelope elements further from the near-field. The further out that the wave envelope elements are, the more asymptotic is the behaviour of the analytic solution in the

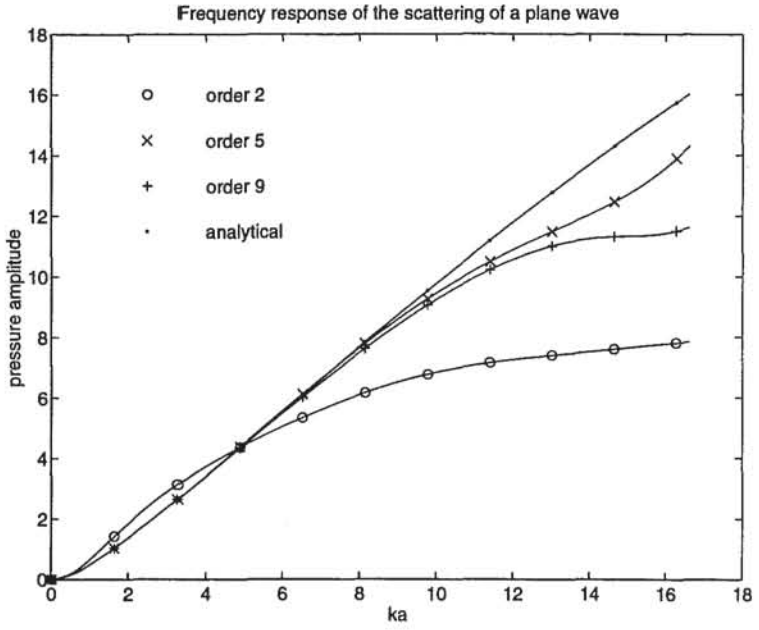

Figure 29: Radiated pressure at $(-5a, 0, 0)$ for varying wave envelope interpolation orders. Model is a 3D sphere with 96 quadratic wave envelope elements.

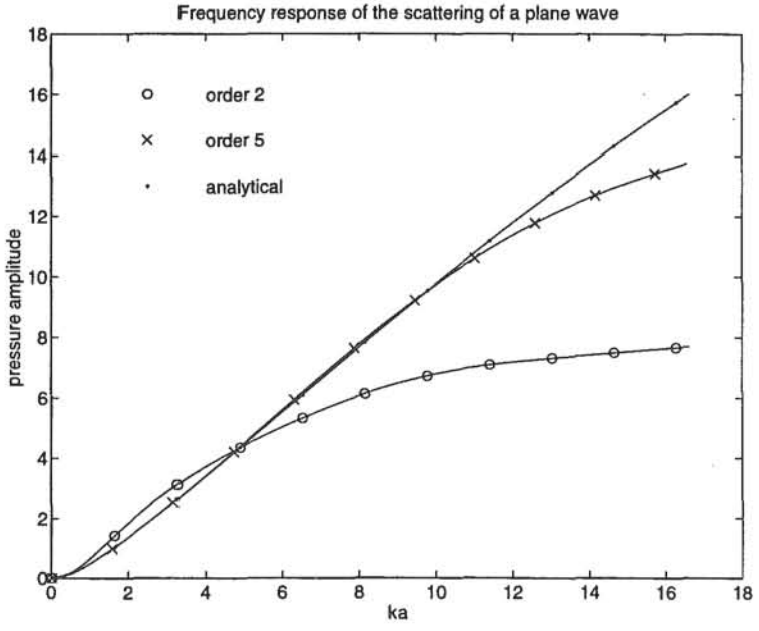

Figure 30: Radiated pressure at $(-5a, 0, 0)$ for varying wave envelope interpolation orders. Model is a 3D sphere with 600 quadratic wave envelope elements.

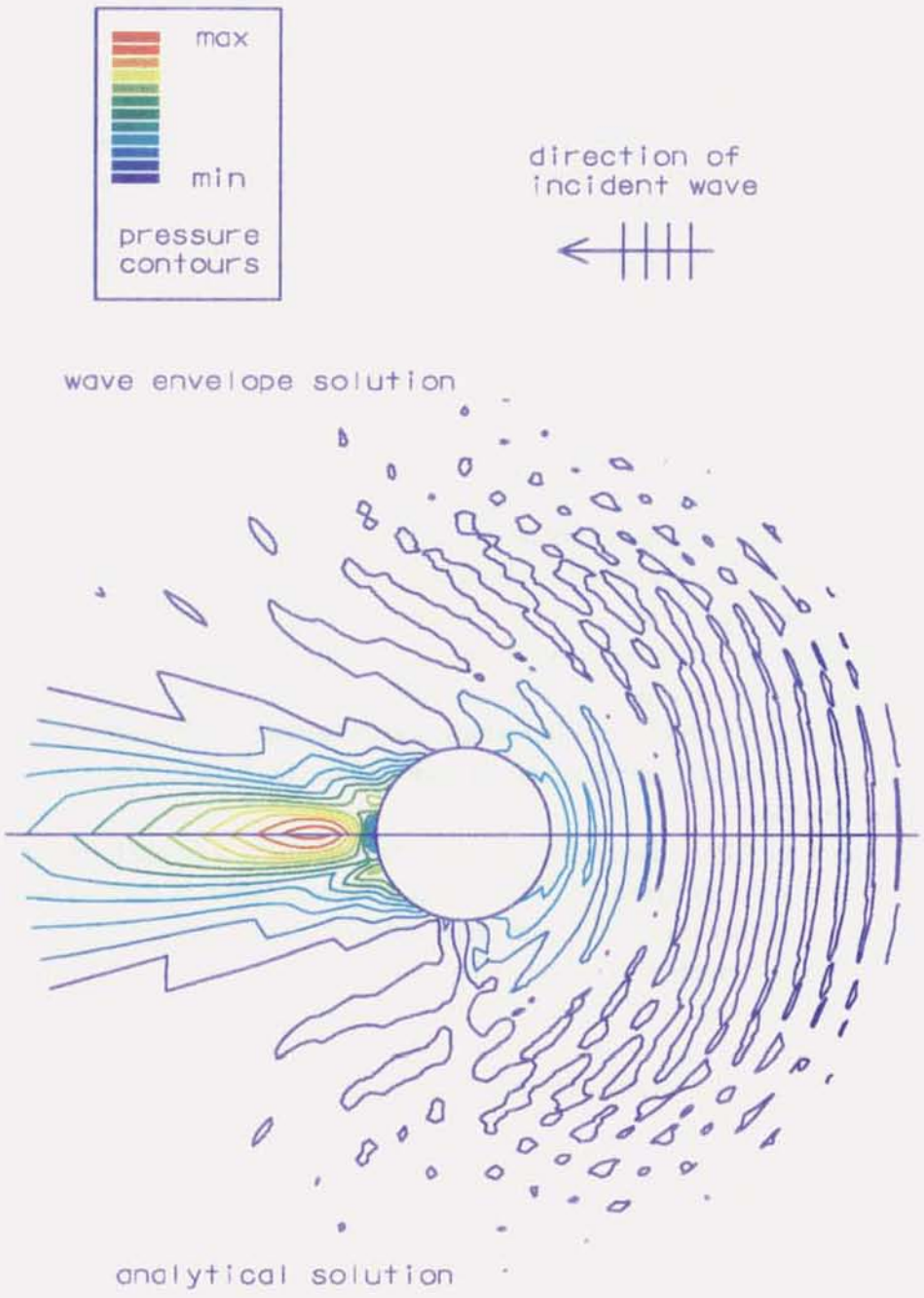

Figure 31: Pressure contours of the total field from the scattering of plane wave by a rigid sphere. Calculated at $ka = 10$ using order nine wave envelope elements. Contours are plotted on a plane passing through the origin of the sphere.

region modelled by the wave envelope elements. This allows the use of lower order wave envelope elements and/or the modelling of higher frequencies.

This reasoning will only apply if the conventional mesh extends far enough to significantly change the acoustic field that the wave envelope elements are required to represent. The question of how far is far enough is dependent upon the maximum frequency desired and the complexity of the near-field. A complicated near-field benefits more from a conventional mesh than does a simple near-field.

The effect on solution accuracy from using layers of conventional elements for the scattering of a plane wave by a sphere (at $ka = 10$) is shown in figure 33, and the mesh used is shown in figure 32 (for the model with three conventional layers). Each conventional layer has a thickness of approximately one tenth of a wavelength at $ka = 10$. The lines on the graph (figure 33) represent solution accuracy for constant number of conventional layers. The use of more conventional layers gives marginally better accuracy for models with wave envelope element orders of up to four. This occurs because the portion of the domain that the wave envelope elements are covering is being extended further into the far-field, and hence the pressure field is behaving more like the asymptotic form that the low order wave envelope elements can model intrinsically. For orders greater than or equal to five, the accuracy remains relatively constant for varying numbers of conventional layers. This occurs because an order five wave envelope element is sufficient to accurately represent the entire scattered field at this frequency, and the addition of conventional layers do not move the wave envelope elements far enough into the far-field to allow the use of lower interpolation order.

A comparison of the CPU time used to calculate the solution at a single frequency for the above model are given in figure 34. This graph illustrates that it is computationally advantageous to use higher order wave envelope elements, as opposed to using more layers of conventional elements—the use of an additional conventional element layer increases the number of degrees-of-freedom by more than an increase of one in the wave envelope interpolation order (see table 2, where the number of degrees-of-freedom for each conventional layer/wave envelope order combination used in figure 34 are tabulated).

4.5.1 The angled block

A two-dimensional model which gives a more complicated near-field is shown in figure 35. The mesh at the top is a boundary element model of the object, which rests on a infinite rigid baffle. The width of the base is 100mm, the height 200mm and the sloping face is at an angle of 45° to the vertical. The other two meshes are formed from wave envelope elements, one without and one with a conventional inner region. The boundary element mesh contained 64 degrees of freedom, the wave envelope element mesh 496 degrees of freedom and the conventional and wave envelope element mesh 540 degrees of freedom (both wave envelope models used order eight wave envelope elements). The sloping side and left hand vertical side are excited in a harmonic manner, with a maximum velocity

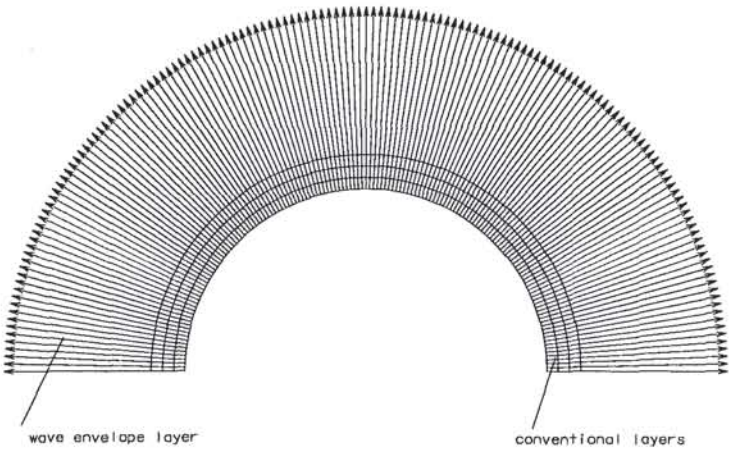

Figure 32: Two-dimensional mesh of the region surrounding an infinitely long cylinder, using conventional and wave envelope elements. Only one half is shown, and indeed modelled, due to the symmetry about the horizontal.

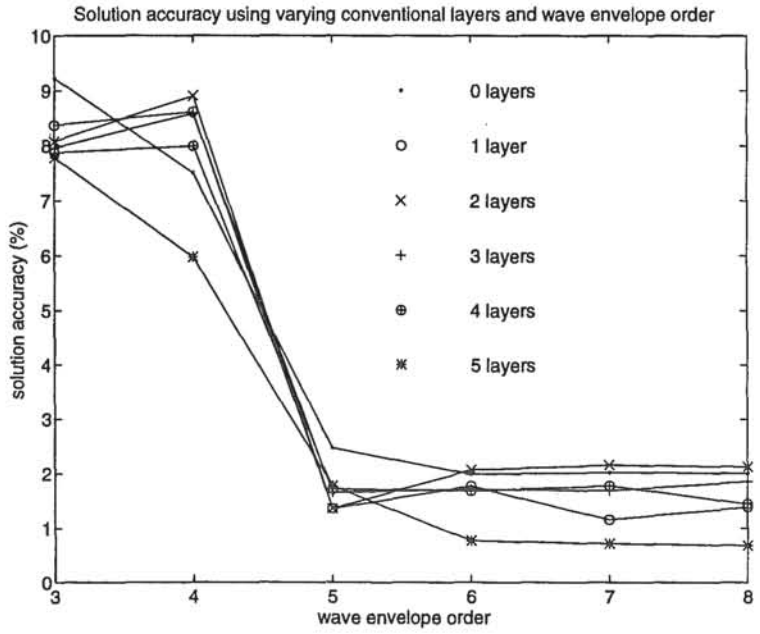

Figure 33: Effect on solution accuracy of varying the number of layers of conventional elements and the order of the wave envelope element interpolation.

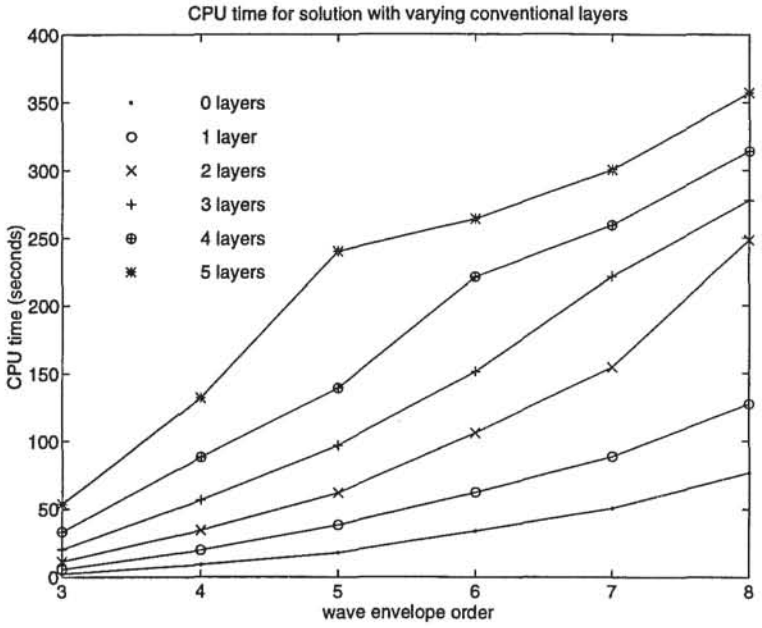

Figure 34: CPU times for solution at a single frequency. Model is a 3D sphere with 96 quadratic wave envelope elements

number of conventional layers	wave envelope order					
	3	4	5	6	7	8
0	642	963	1284	1605	1926	2247
1	1076	1397	1718	2039	2360	2681
2	1510	1831	2152	2473	2794	3115
3	1944	2265	2586	2907	3228	3549
4	2378	2699	3020	3341	3662	3983
5	2812	3133	3454	3775	4096	4417

Table 2: Number of degrees-of-freedom for the three-dimensional sphere model with varying numbers of conventional layers and wave envelope orders.

amplitude of 1.0 m/s normal to the appropriate surface. The complicated near-field is caused by the constructive and destructive interference of the waves propagating from the two vibrating sides.

Pressure contours at $ka = 1.0$ ($a = 100$mm) and $ka = 3.0$ were calculated using the three models and are shown in figure 36 and 37 respectively. The boundary element solution was calculated by the SYSNOISE [76] boundary/finite element acoustic analysis program and is compared to the wave envelope model with and without conventional elements. The boundary element model shown in figure 35 has been refined from the original mesh, which contained the same angular resolution as the wave envelope models in figure 35. This was necessary to obtain convergence of the boundary element results (finer wave envelope models did not significantly change the wave envelope results). The collocation boundary element method was used in the generation of the boundary element results, and required the placement of 'collocation points' in the interior of the vibrating object. The object of these points was to remove internal resonances of the object from the exterior solution. Selection of the location and number of points is arbitrary, although more points are required for accurate solution at higher frequencies. Increasing the number of randomly placed collocation points in the initial coarse boundary element model did not consistently improve the solution—very confusing behaviour. However, the accuracy of the refined boundary element model did improve consistently with the use of increasing numbers of randomly placed collocation points.

It is clear from figure 37 that the wave envelope mesh, when coupled with conventional finite elements, gives better agreement with the SYSNOISE contours (the SYSNOISE contours do not extend onto the boundary of the object because the postprocessor in SYSNOISE gives erroneous results for points on or close to the boundary). A frequency response curve is given in figure 38 for the point marked with a cross in figure 37. The model that uses conventional elements gives better agreement with the SYSNOISE curve than does the model with only wave envelope elements—especially at higher frequencies. The close agreement between all three curves at low frequencies occurs because the pressure field is not particularly complicated, and this is illustrated in figure 36 where the general form of the solution at $ka = 1.0$ is a shown. The two wave envelope curves begin to differ at $ka \approx 1.2$, at which point the near-field has become more complicated than the wave envelope elements can handle on their own.

This object is indicative of the geometries where conventional elements improve the wave envelope solution. All objects that have some form of concavity will benefit from the use of conventional elements. These will a) improve the solution accuracy in the near field and b) by filling in the concave regions make the wave envelope elements easier to place and less distorted.

A comparison of solution times between the boundary element and wave envelope method was not possible because the SYSNOISE code and the wave envelope code ran on different computers. However, comparison of computation times for two- and three-dimensional spherical models was performed by Astley *et al.* [6] and led to the conclusion

that the wave envelope method is less computationally demanding than the boundary element method. The wave envelope method has the added advantage that pressures at any point in the acoustical domain (including the wave envelope region) can be calculated quickly and easily by interpolation of nodal pressures (using the element basis functions). The boundary element method requires further integrations to calculate pressures in the acoustical domain.

4.6 Ill-conditioned systems

The assembled system matrix can become ill-conditioned for high-order wave envelope interpolations, leading to erratic solutions. Table 3 lists the reciprocal condition numbers of various matrices used to generate the assembled system matrix for the two-dimensional order 2 multi-pole radiation model used in appendix E (this model consists of 150 order 11 linear wave envelope elements, with the assembled matrices calculated at $ka = 1.85$). The reciprocal condition number is the reciprocal of the condition of a matrix in the 1-norm as obtained by the LINPACK condition estimator, where a result near 1.0 indicates a well-conditioned matrix, and a result near 0.0 indicates a poorly conditioned matrix. The condition numbers where calculated by the Matlab `rcond` function.

The reciprocal condition for the assembled system matrix of an order 11 wave envelope mesh is approximately 10^{-17}, and since all the calculations were performed in 32 bit real arithmetic (giving 16–17 significant figures), this was insufficient to cope with the condition of 10^{-17}. The poorly conditioned assembled system matrix is caused by the poorly conditioned assembled stiffness, damping and mass matrices, which in turn are caused by the poorly conditioned element stiffness, damping and mass matrices. It is not clear why the element matrices become poorly conditioned.

The result of the ill-conditioned matrices is shown in figure 39 (for an order 2 two-dimensional multi-pole and using the mesh detailed in appendix E). Unfortunately, the figure is not particularly clear; the order 10 curve labelled with the '+' symbol and the analytical curve labelled with the 'o' symbol are identical over the entire frequency range. The order 11 curve, labelled with the '×' symbol exhibits the erratic behaviour. Lower order wave envelope elements give progressively better conditioned matrices, as seen in table 3.

The addition of conventional elements to the mesh used for the results presented in table 3 was found to improve the matrix condition numbers by a factor of at least 100 in all cases (the order 11 curve in figure 39 no longer exhibited the erratic behaviour and was indistinguishable from the order 10 curve and analytic curve). Table 4 presents reciprocal condition numbers for the assembled $\mathbf{K}$ matrix for a series of two-dimensional meshes, analogous to that discussed above, but with varying layers of conventional elements surrounding the cylinder. The wave envelope elements are attached to the outer boundary of the conventional elements. Condition numbers for the mass matrix and assembled

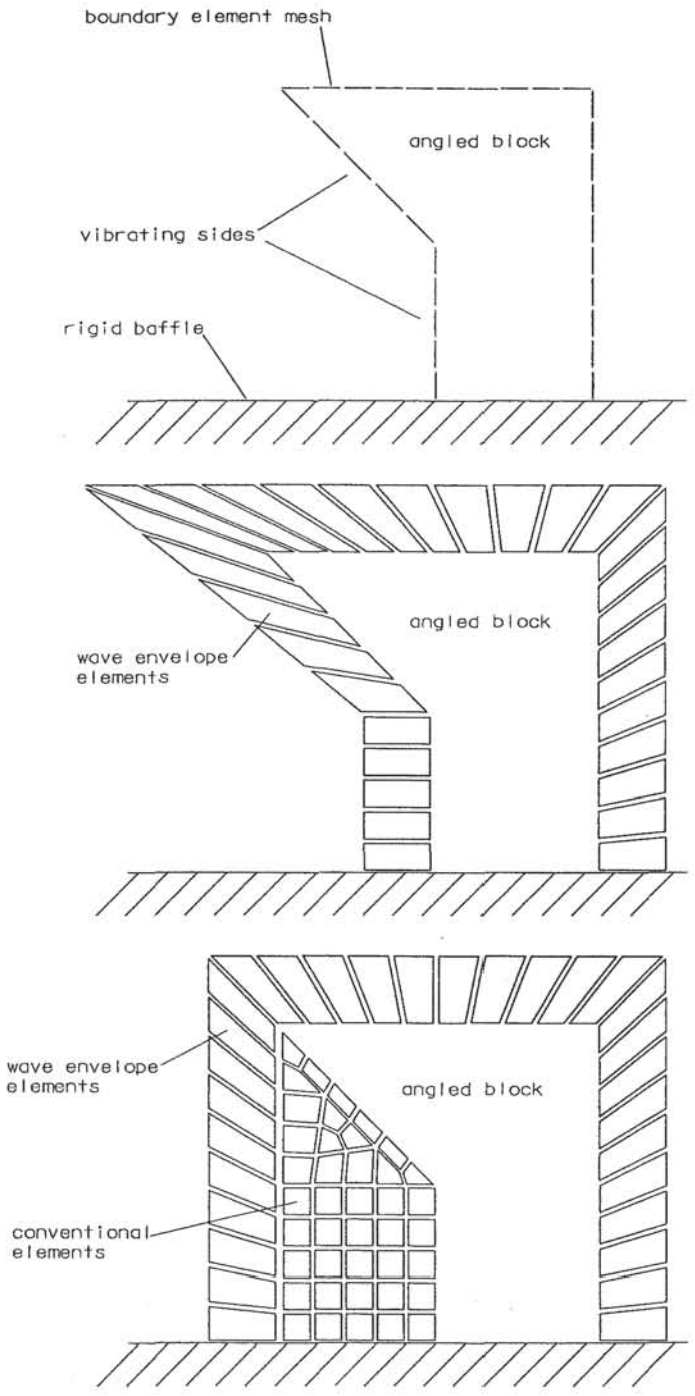

Figure 35: Boundary element and wave envelope meshes used for the angled block. The top mesh consists of 60 linear boundary elements, the middle of 30 linear wave envelope elements and the bottom mesh of 41 linear conventional and 30 linear wave envelope elements.

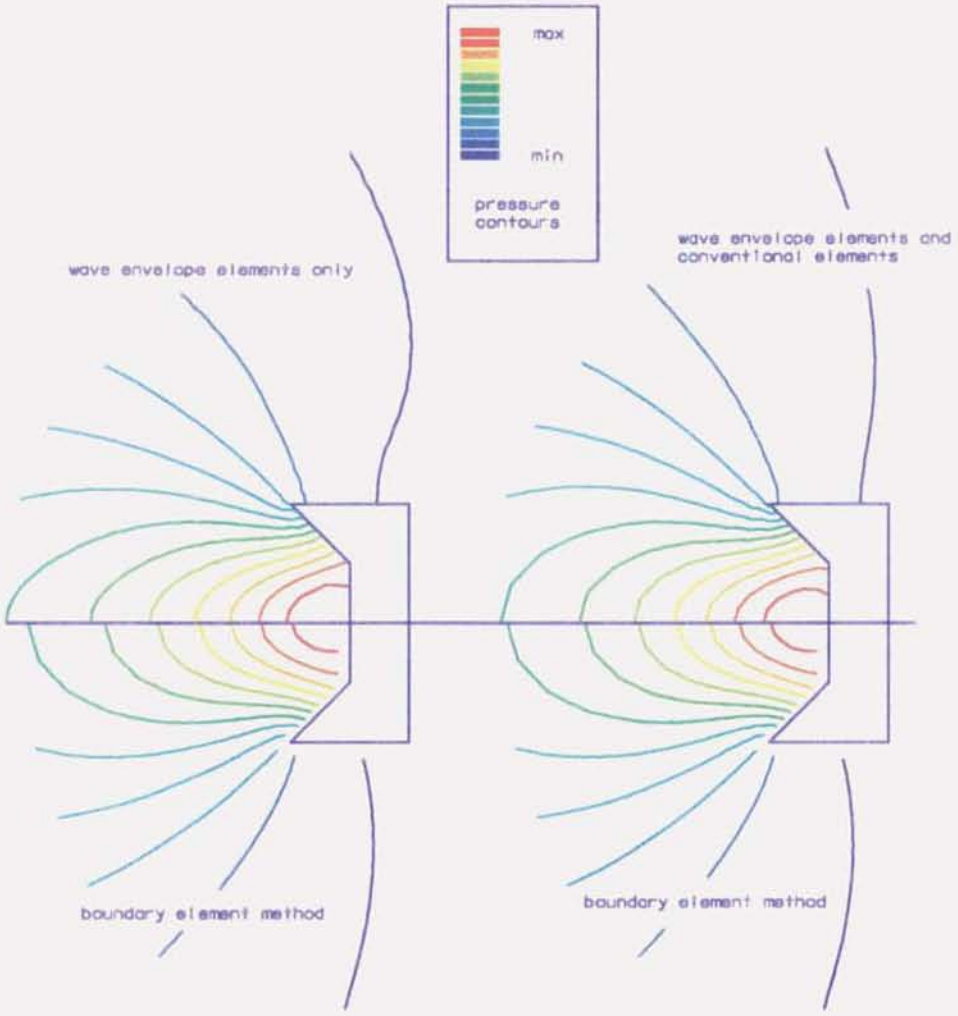

Figure 36: Pressure contours from the vibrating angled block, calculated by wave envelope/conventional elements and boundary elements at $ka = 1.0$

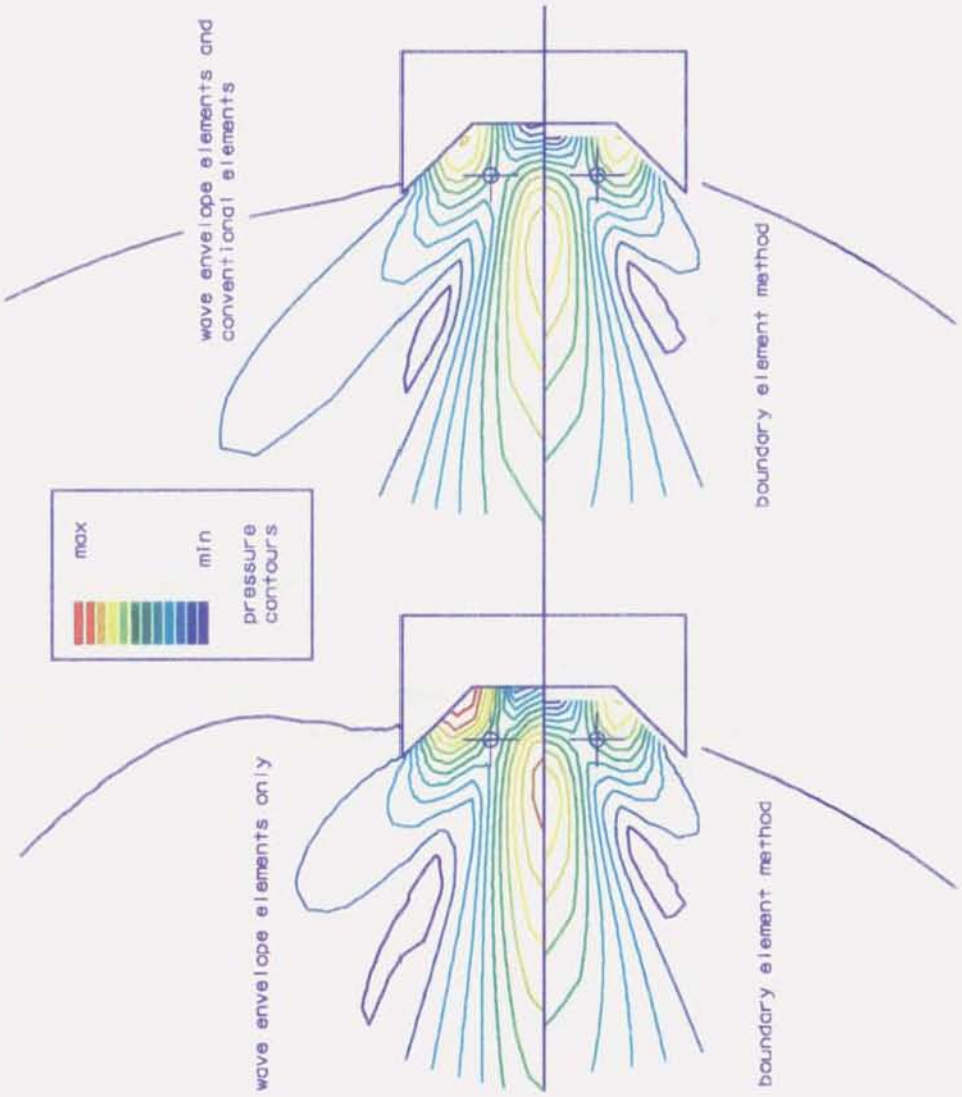

Figure 37: Pressure contours from the vibrating angled block, calculated by wave envelope/conventional elements and boundary elements at $ka = 3.0$

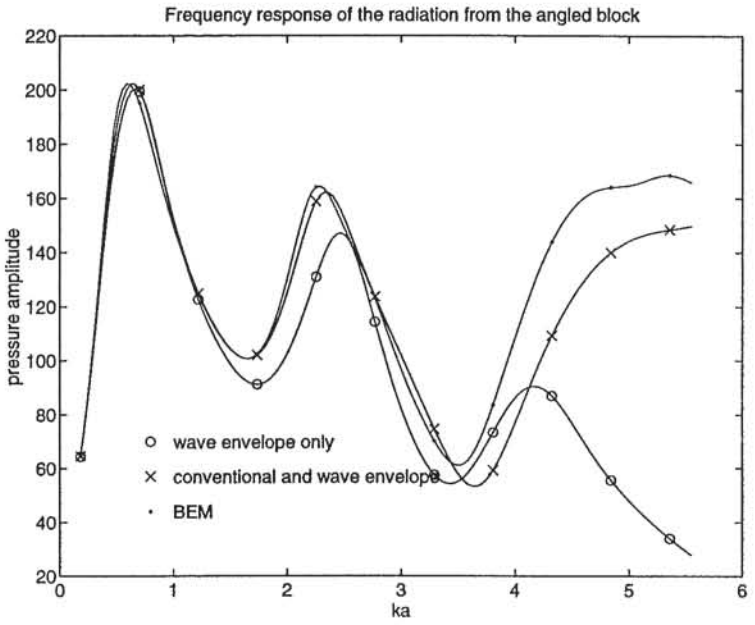

Figure 38: Radiated pressure at (-0.75,0.75) using order 8 wave envelope elements. Three different meshes were used.

system matrix exhibit a similar behaviour to the K matrix (the C matrix condition numbers are zero, due to a number of zero terms on the diagonal which occur because conventional elements do not contribute to the C matrix).

	wave envelope interpolation order				
	2	3	4–9	10	11
element **K**	$2.4 \cdot 10^{-5}$	$3.7 \cdot 10^{-6}$	...	$1.0 \cdot 10^{-14}$	$9.7 \cdot 10^{-16}$
element **C**	$1.0 \cdot 10^{-1}$	$3.6 \cdot 10^{-2}$	...	$2.7 \cdot 10^{-13}$	$2.8 \cdot 10^{-15}$
element **M**	$2.7 \cdot 10^{-2}$	$1.3 \cdot 10^{-3}$	...	$1.4 \cdot 10^{-15}$	$2.0 \cdot 10^{-17}$
assembled **K**	$2.9 \cdot 10^{-5}$	$5.4 \cdot 10^{-6}$	...	$9.3 \cdot 10^{-17}$	$4.3 \cdot 10^{-17}$
assembled **C**	$9.9 \cdot 10^{-2}$	$3.6 \cdot 10^{-2}$	...	$4.8 \cdot 10^{-13}$	$8.4 \cdot 10^{-15}$
assembled **M**	$2.5 \cdot 10^{-2}$	$1.2 \cdot 10^{-3}$	...	$1.0 \cdot 10^{-15}$	$1.2 \cdot 10^{-18}$
assembled system	$3.3 \cdot 10^{-4}$	$9.6 \cdot 10^{-5}$	...	$1.7 \cdot 10^{-15}$	$2.1 \cdot 10^{-17}$

Table 3: Matrix condition numbers for a mesh consisting solely of wave envelope elements

conventional layers	wave envelope interpolation order			
	2	3	10	11
1	$1.3 \cdot 10^{-3}$	$6.1 \cdot 10^{-4}$	$1.5 \cdot 10^{-11}$	$3.6 \cdot 10^{-13}$
2	$7.9 \cdot 10^{-4}$	$1.4 \cdot 10^{-3}$	$1.3 \cdot 10^{-11}$	$3.3 \cdot 10^{-13}$
3	$6.9 \cdot 10^{-4}$	$6.7 \cdot 10^{-4}$	$6.9 \cdot 10^{-12}$	$1.7 \cdot 10^{-13}$
4	$1.4 \cdot 10^{-4}$	$1.9 \cdot 10^{-4}$	$2.3 \cdot 10^{-12}$	$5.6 \cdot 10^{-14}$
5	$3.2 \cdot 10^{-5}$	$6.5 \cdot 10^{-4}$	$3.8 \cdot 10^{-13}$	$9.2 \cdot 10^{-15}$

Table 4: **K** matrix condition numbers for meshes with conventional finite elements as well as wave envelope elements

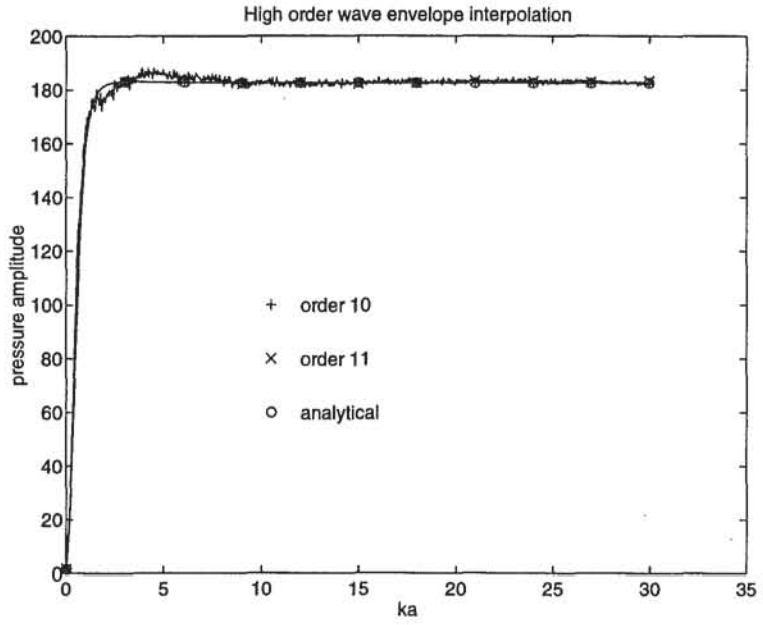

Figure 39: Radiated pressure at $(5a, 0)$ for an order 2 multi-pole with high order wave envelope interpolations. Model is a 2D cylinder with 150 linear wave envelope elements.

Chapter 5

Ritz vector results

In this chapter results are presented that illustrate the behaviour and performance of a Ritz vector condensation which can be used to reduce the size of the set of simultaneous equations that result from the wave envelope finite element formulation.

The form of the prescribed normal velocity U on the radiating or scattering surface influences the effectiveness of a Ritz vector condensation. In many radiation problems the form of the prescribed velocity (if not its magnitude) is independent of frequency, and for these situations the Ritz vector scheme is shown to be effective in reducing the computational effort required for multi-frequency calculations. In scattering problems the form of the equivalent prescribed velocity is frequency dependent and this reduces the effectiveness of the Ritz vector scheme.

5.1 Application to radiation problems

5.1.1 Multi-pole excitation

The form of the prescribed velocity for multi-pole excitation is frequency independent—consequently Ritz vectors produce good results. To illustrate the behaviour of Ritz vector solutions for this class of problem, two examples have been chosen from the preceding chapter; an order two multi-pole and an order ten multi-pole, for which frequency response curves are given in figures 40 and 41 respectively. These show the accuracy of various Ritz basis solutions by comparing them to the full (non Ritz vector) solution.

The multi-pole models used are identical to those of section 4.3, namely a three-dimensional sphere meshed with 96 quadratic wave envelope elements. The wave envelope interpolation order has been chosen so that the full solution gives a good approximation to the analytical solution over the full frequency range shown. Note that the Ritz vector solutions are compared (in figure 40 and 41) to the full solution, and not the analytical solution. This is because the errors that the Ritz procedure introduces are relative to the full solution and not to the analytical solution.

A characteristic of the frequency response curves shown in figures 40 and 41 is that the Ritz solution converges to the full solution as the size of the Ritz basis is increased. The number of Ritz vectors required to give an acceptable solution is dependent upon the complexity of the solution—an order two multi-pole requires only three vectors, while the order ten multi-pole requires in excess of 30 vectors to give an acceptable solution. If insufficient vectors are used, completely erroneous solutions are obtained. This behaviour can be used to determine if sufficient Ritz vectors have indeed been calculated, via the following procedure;

- calculate a Ritz basis of m vectors
- use this basis to produce a frequency response curve
- generate more Ritz vectors, continuing on from the first m vectors
- produce a second frequency response curve and compare to the first
- continue generating larger Ritz bases until the frequency response curves converge to within some tolerance level

The attractive feature of this procedure is that the existing Ritz vectors are used to generate more vectors. That is, if a basis of ten vectors was initially calculated, a basis of twenty of vectors can be found by the generation of just ten more vectors. Typically, the time to generate a frequency response curve is much less than the time to generate additional Ritz vectors.

5.1.2 Solution efficiencies

Any savings in CPU time gained by using Ritz vectors are dependent upon the number of Ritz vectors used, the sparsity and size of the system matrix and the number of frequencies at which the solution is calculated. A comparison of CPU times for the results produced in figures 40 and 41 are given in table 5, where CPU time for various parts of the solution process are given.

The order two multi-pole was reduced from a 963 degree-of-freedom system to a 3 degree-of-freedom system, with the total CPU time decreasing by a factor of approximately 90. Note that the 963 degree-of-freedom system is sparse, while the 3 degree-of-freedom system is fully populated. This effect becomes more significant as the Ritz basis contains more vectors, as occurs with the order ten multi-pole. As an example, the time to generate the Ritz basis for the order two multi-pole was twice the time to solve the full solution, while for the order ten multi-pole the ratio was 4.5 (that is, if the solution is needed at more than five frequencies, the Ritz method would be quicker).

By using eigenvectors in place of the Ritz vectors, similar reductions in problem size could be achieved, however the CPU time required to generate eigenvectors is much longer

	Order 2 multi-pole		Order 10 multi-pole	
	full soln	3 Ritz vectors	full soln	30 Ritz vectors
element assembly	2.44	2.44	34	34
generate Ritz basis	-	4.22	-	186
solve system	2.0	< 0.01	41	0.07
CPU time for 400 freqs	903	10.9	16539	254
DOF in system	963	3	2568	30

Table 5: Comparison of solution times with and without Ritz vectors. Model is a 3D sphere with 96 quadratic wave envelope elements with order 3 radial interpolation for the order 2 multi-pole and order 8 radial interpolation for the order 10 multi-pole. All times are in seconds with a clock resolution of 0.01 seconds.

that the time to generate Ritz vectors (see Wilson [93]) and such an approach would be much less effective.

The loss of accuracy of the full wave envelope solution that was discussed in section 4.3.3 is seen again in the full solution curve of figure 41 (the kink in the full solution curve near $ka = 22$). It is interesting that the Ritz solution does not exhibit the same behaviour, but instead appears to behave more like the analytical solution. This is illustrated in figure 42 which shows a comparison of full, Ritz and analytical frequency response curves for the order ten multi-pole.

A second situation in which the use of Ritz vectors gave a better approximation to the analytic result than the full solution is shown in figure 43 (the model used to generate figure 43 is identical to that used to generate the results for figure 39, that is, order two multi-pole radiation from a two-dimensional cylinder with the surrounding region meshed with 150 linear wave envelope elements of order 11). The erratic behaviour displayed by the full solution (the noisy curve) and which is thought to be caused by ill-conditioned element matrices (and consequently the assembled matrices), is not present in the Ritz vector curve. The three curves in figure 43 are difficult to distinguish—the analytical and Ritz solution are smooth and coincident, while the full solution curve is not smooth.

The improvement in accuracy of the Ritz solution over the full solution is thought to occur because the reduced stiffness, damping and mass matrices do not have the same degree of ill-conditioning that the full matrices have. In effect, the Ritz basis is acting as a kind of filtering process that removes insignificant components of the full system.

5.1.3 The angled block

The angled block discussed in section 4.5 has also been solved using Ritz vectors. The form of the boundary excitation is independent of frequency, and hence Ritz vectors work well. Results are presented in figures 44 and 45 and show frequency response curves for selected Ritz basis sizes, for the angled block without and with conventional elements

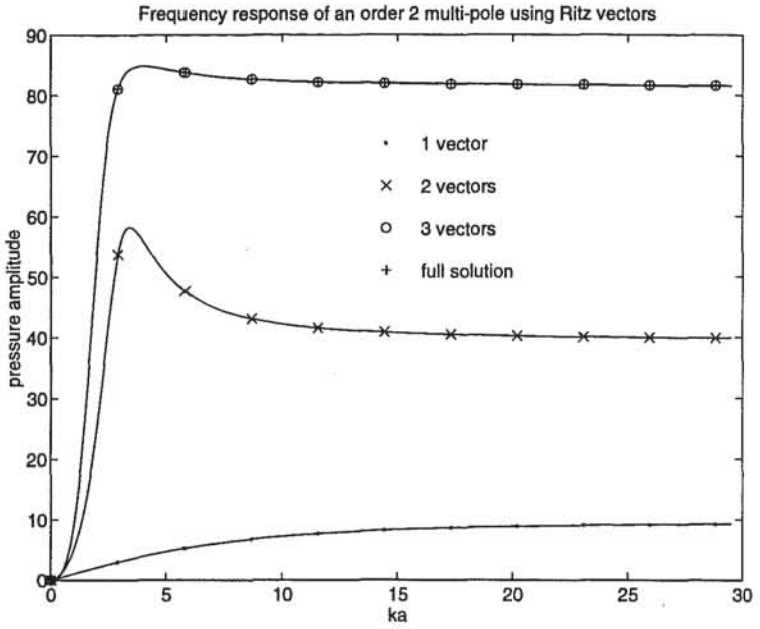

Figure 40: Radiated pressure at $(5a, 0, 0)$ for varying numbers of Ritz vectors. Model is a 3D sphere with 96 quadratic wave envelope elements with order 3 radial interpolation.

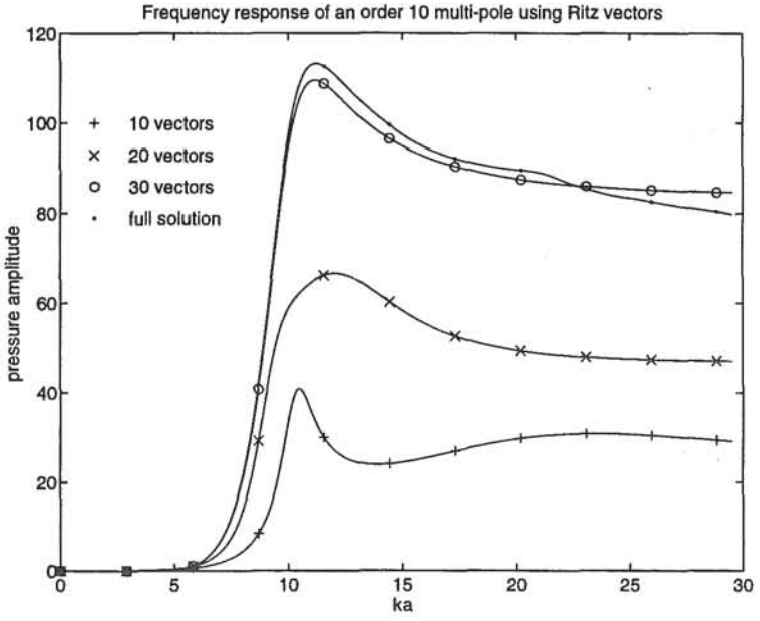

Figure 41: Radiated pressure at $(5a, 0, 0)$ for varying numbers of Ritz vectors. Model is a 3D sphere with 96 quadratic wave envelope elements with order 8 radial interpolation.

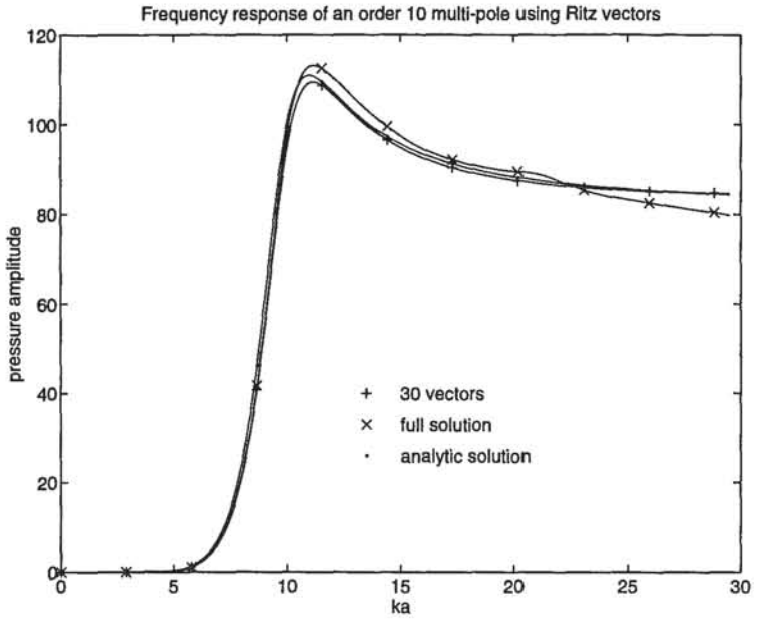

Figure 42: Radiated pressure at $(5a, 0, 0)$. Curves are calculated with the analytic solution, the full wave envelope solution and also with 30 Ritz vectors. Model is a 3D sphere with 96 quadratic order 8 wave envelope elements.

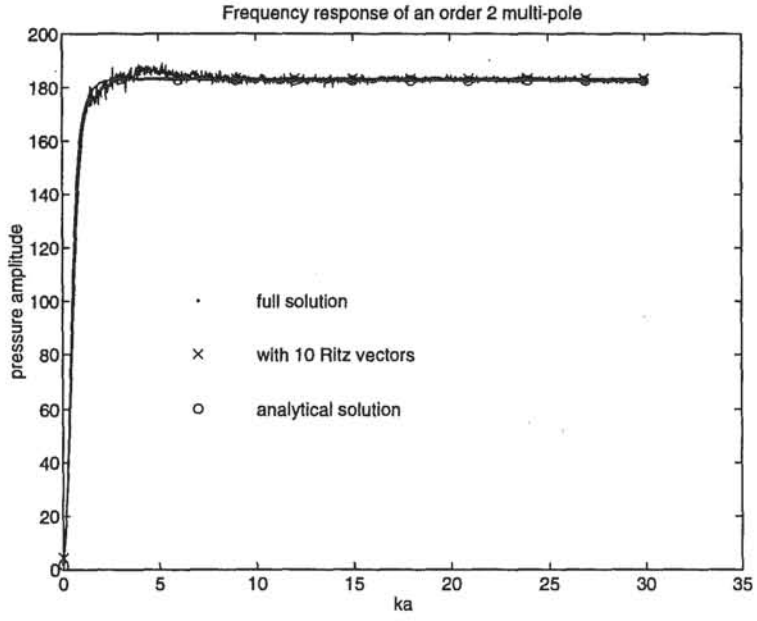

Figure 43: Radiated pressure at $(5a, 0)$. Model is a 2D cylinder with 150 order 11 wave envelope elements.

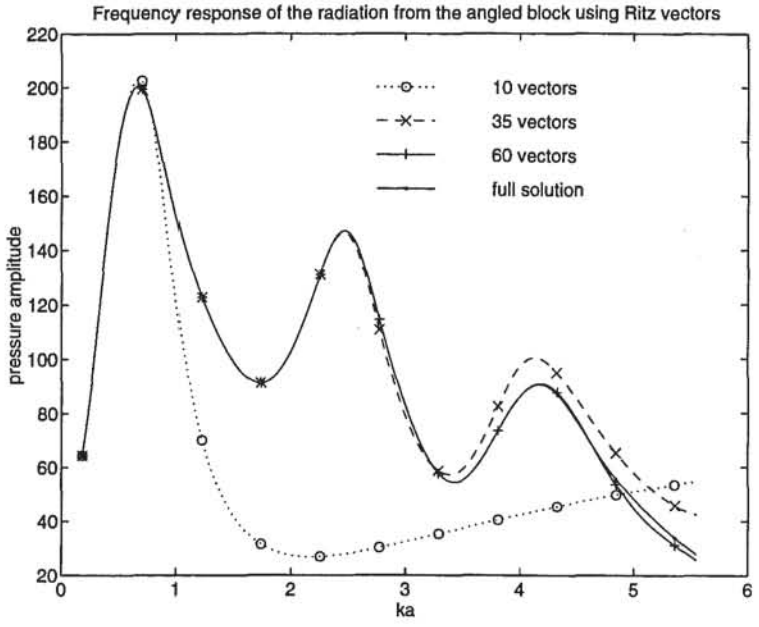

Figure 44: Radiated pressure at $(-0.75, 0.75)$ using order eight wave envelope elements. Mesh consists solely of wave envelope elements.

respectively (the full solution is included in both figures to indicate the ka values for which the Ritz solutions are valid).

The results presented in figures 44 and 45 exhibit the same behaviour as the Ritz solutions presented in previous sections, that is, the use of Ritz bases of larger sizes increases the ka value at which the Ritz solution is valid to. It is concluded that Ritz vectors work irrespective of whether the mesh consists solely of wave envelope elements, or includes conventional elements.

5.2 Application to scattering problems

The form of the boundary conditions required to model the scattering of sound waves are dependent upon the frequency of the incident wave. This means that a single Ritz basis will not suffice for an entire frequency range. Several more or less useful options exist that allow the use of Ritz vectors. These are;

1. The Ritz basis can be calculated at each frequency for which a solution is desired. This is pointless in terms of computational efficiency because the time to generate a Ritz basis will always be greater than the time to solve the full system (a system equivalent in size to the full system is solved for each new Ritz vector).

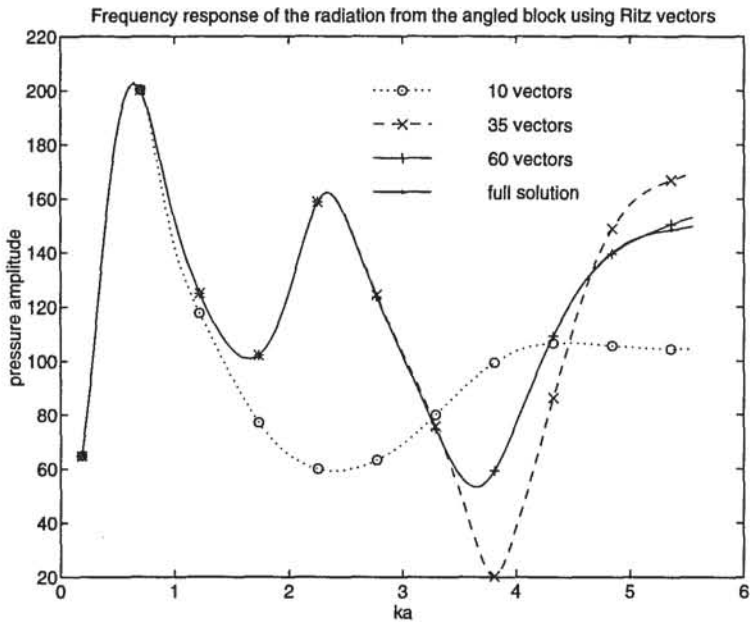

Figure 45: Radiated pressure at $(-0.75, 0.75)$ using order eight wave envelope elements. Mesh also contains conventional elements.

2. A single basis calculated at some mid-frequency can be used over the entire frequency range. Provided that many frequency steps can be accurately represented by a single Ritz basis the solution accuracy will be acceptable. This appears not generally to hold. This method will yield similar CPU savings as those discussed for radiation problems in the previous section.

3. Ritz bases can be generated at regular intervals over the frequency range and each basis used for solutions at frequencies close to the frequency for which it was generated. This method falls somewhere between the first two options, and its success depends on the spacing of the Ritz bases, and on how rapidly the Ritz bases change with frequency.

4. Ritz bases can be generated at regular frequency intervals, and the Ritz basis for each frequency at which a solution is required obtained by interpolation of the surrounding Ritz bases. This method requires more CPU time than the non-interpolation method (option 3) if the same frequency intervals are used.

5.2.1 Number of Ritz vectors required to approximate the full solution

To provide a means for comparison of later Ritz results, the scattering problem of previous sections (that is, scattering of a plane wave by a rigid sphere) was solved with a range of

Ritz basis sizes. Initially the Ritz basis was recalculated at every frequency step (option 1). These results are shown in figures 46 and 47. The field point at which the pressures are given is $(5a, 0, 0)$. Note that this is different from the point used in previous scattering examples (which was $(-5a, 0, 0)$) and this new point was chosen to give a greater variation of pressure with frequency than the original point, providing a better test of the Ritz basis. The results are presented in two separate graphs to more clearly show individual lines.

It is clear from figures 46 and 47 that a larger Ritz basis extends the region of acceptable results to higher frequencies. This occurs because at higher values of ka the solution contains higher order Hankel functions and additional Ritz vectors are required to represent these.

A Ritz basis of 70 vectors is required to achieve acceptable solutions up to $ka \approx 9$. This value of ka is significant also as the point where the wave envelope solution begins to depart from the analytical solution (see figure 29 in section 4.4). The results in figures 46 and 47 show that given sufficient Ritz vectors, acceptable accuracy can be obtained for any frequency at which the full solution is valid. When the Ritz solution loses accuracy, it does so extremely rapidly, a property which can be utilised to determine if the Ritz basis is too small for the frequency at which it is being used.

The rate at which increasing the Ritz basis size increases the value of ka that the Ritz solution is valid to is shown in figure 48. The points on the graph represent the ka value at which the Ritz solution first exceeds 5% relative error (compared to the full solution) for various basis sizes. A reasonably monotonic increase in ka for increasing Ritz basis size can be seen in the figure.

It is interesting to note the component times involved in generating the reduced order system. Table 6 contains CPU times in seconds for various parts of the Ritz procedure. A Ritz vector *scattering* analysis requires assembly of the K, C and M matrices, the generation of the Ritz vectors, the subsequent use of the vectors in generating the reduced order system, and the solution of this reduced order system. A non-Ritz vector analysis requires the assembly of the K, C and M matrices, and combination together as per equation 2. The resulting system is then solved. Note that the time to generate the Ritz vectors is comparable to the time to generate the reduced system (this holds true for any number of Ritz vectors or system size), and that the time to solve the reduced system is comparatively small. Contrast those times to the 12.0 seconds required to solve the full, non-Ritz vector, system. For this particular model, if a single Ritz basis can be used at more than 14 $((84.0 + 81.6 + 0.36)/12.0)$ solution frequencies, CPU savings will be obtained when compared to the full solution method. This is discussed in the next section.

5.2.2 Spacing of Ritz bases

In the results presented so far, the Ritz vector procedure does not give any CPU time savings over the full solution when the Ritz basis is recalculated at every frequency for

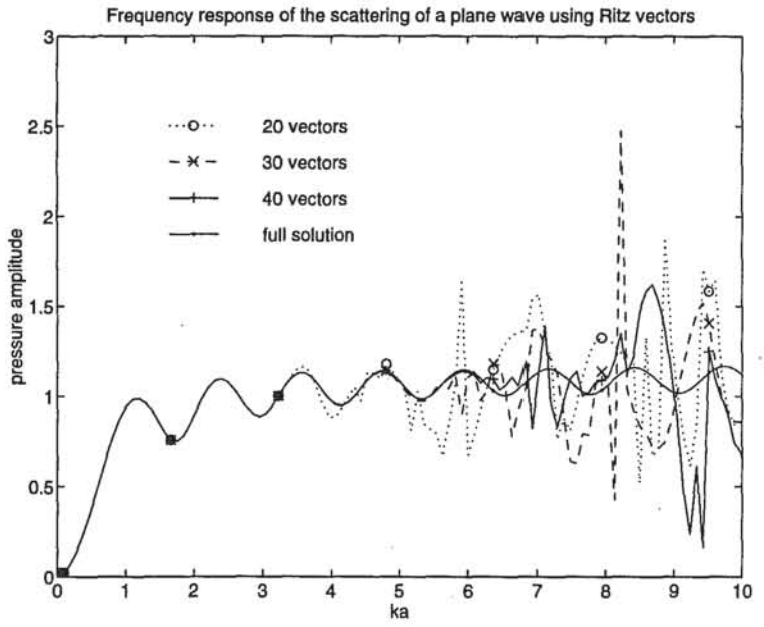

Figure 46: Radiated pressure at $(5a, 0, 0)$ for varying Ritz basis sizes, using order five wave envelope elements.

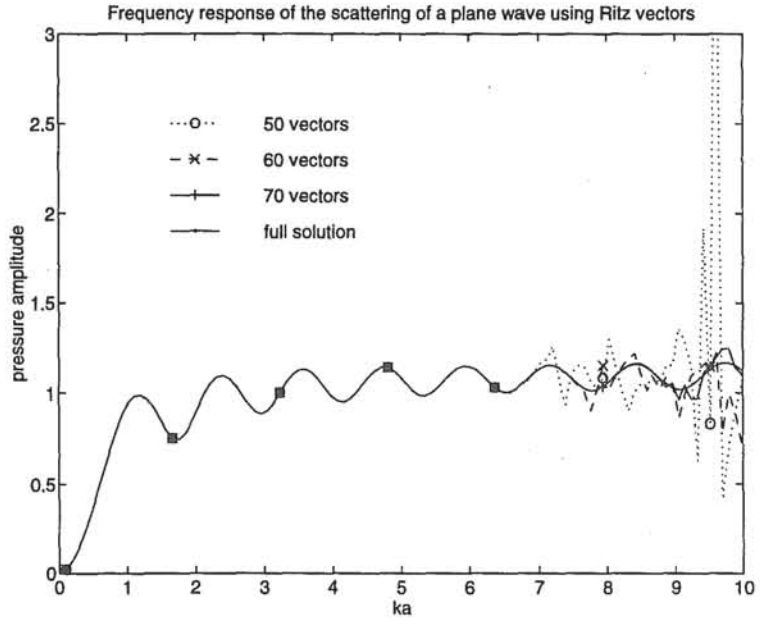

Figure 47: Radiated pressure at $(5a, 0, 0)$ for varying Ritz basis sizes, using order five wave envelope elements.

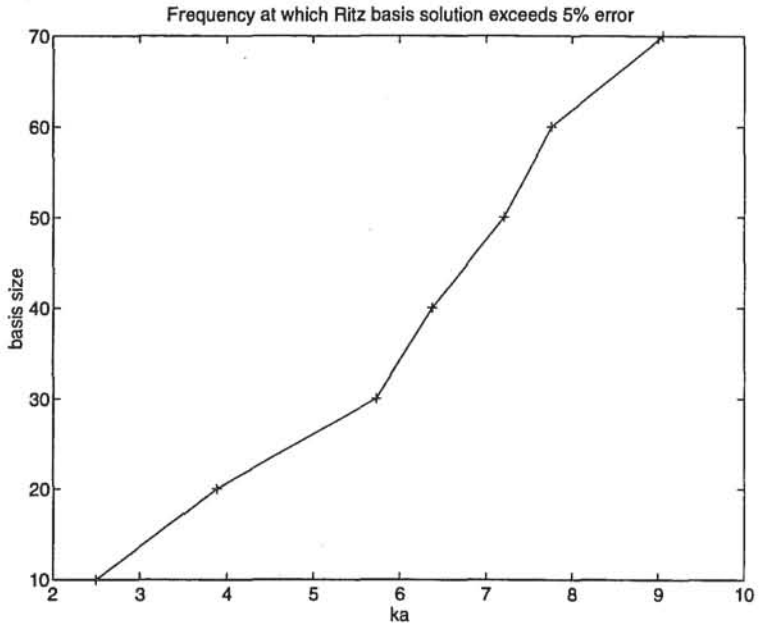

Figure 48: Errors derived from figures 46 and 47.

	Ritz vectors	full solution
assemble **K**, **C** and **M** matrices	9.0	9.0
generate 70 Ritz vectors	84.0	-
generate reduced system	81.6	-
solve reduced system	0.36	-
solve full system	-	12.0

Table 6: CPU times for the Ritz solution of the scattering model. Note: the first Ritz vector generated involves the decomposition of the **K** matrix, takes approximately 10 seconds and is not included in the above times. This is only necessary once per analysis. All times are in seconds.

which a solution is required (quite the opposite). Since CPU time savings are the main reason for using Ritz vectors, it is desirable to find a way to make Ritz vector solutions quicker than a full solution.

A simple and reasonably effective procedure is to use the same Ritz basis for several frequencies (options 2 and 3 of section 5.2). This is justified if the Ritz bases change slowly with frequency. The slower the change, the more widely spaced are the frequencies at which the Ritz bases need be calculated.

The scattering model of the previous section has been solved using Ritz bases of 70, 50 and 30 vectors at varying spacings, and the overall solution times are given in table 7. The number of Ritz bases at which the solution time becomes less than that required to solve the full problem is 6 (when using 70 Ritz vectors). This comparison is based on a solution being calculated over the range $ka = 0$ to $ka = 10.0$, in steps of $ka = 0.092$, giving a reasonably smooth frequency response curve. Decreasing the interval at which the solution is actually calculated will make the Ritz procedure appear more attractive, and conversely, increasing the same interval will favour the full solution. Choosing an appropriate value for this interval (irrespective of whether Ritz vectors are used) requires a balance to be found between excessive CPU time and obtaining smooth curves. With Ritz vectors this choice becomes less important because a smaller interval between solution frequencies does not significantly increase the CPU time provided that the Ritz basis is still recalculated at the same (larger) intervals.

The effect on the CPU times of reducing the size of the Ritz basis can be seen in table 7. The solution times are significantly reduced, but also reduced is the maximum frequency to which the solution is valid. As an example, the 30 Ritz vector basis is only valid to $ka \approx 5.5$ (see figures 46 and 47).

Decreasing the number of Ritz bases used in the solution will give greater CPU time savings, up to the point where the solution accuracy suffers. The frequency response curves in figure 49 show the behaviour of the solution when calculated using 2, 3 and 4 Ritz bases (containing 70 vectors) over the range from $ka = 0$ to $ka = 10$. It is interesting that the use of fewer Ritz bases lowers the frequency at which the solution becomes inaccurate, rather than degrading the solution over the entire frequency range. This occurs because the Ritz bases change more slowly at low frequencies than at high frequencies. The point where the solutions lose accuracy occurs as precipitously as before.

The solution calculated using two Ritz bases gives a good solution at frequencies higher than those obtained when using three or four Ritz bases. This behaviour can be explained by considering the particular ka values at which the Ritz bases are calculated. Table 8 gives the ka values at which the Ritz bases were calculated for the results given in figure 49. The 2 Ritz basis solution in the region of $ka = 7.0$ was generated from a Ritz basis that was calculated at $ka = 7.5$, while the 3 Ritz basis solution in the region of $ka = 7.0$ was calculated from a basis at $ka = 8.33$. The two bases (at $ka = 7.5$ and $ka = 8.33$) are significantly different because the solution at these two ka values have different dominant mode shapes. In particular, the basis calculated at $ka = 8.33$ does not

number of Ritz bases calculated	Ritz basis size		
	30	50	70
10	712	1315	1619
9	658	1197	1442
8	596	1091	1324
7	539	989	1163
6	485	891	1035
5	427	783	875
4	397	682	708
3	312	593	629
2	261	498	532
full solution	1121		

Table 7: CPU times (seconds) for varying Ritz basis spacings.

	Number of Ritz bases calculated		
	2	3	4
ka at which Ritz basis is calculated	2.5	1.66	1.25
	7.5	5.0	3.75
		8.33	6.25
			8.75

Table 8: Values of ka at which Ritz bases are calculated

accurately represent the true Ritz bases at ka values less than 8.33.

The abrupt change in some of the curves occurs when the Ritz basis used to calculate the solution changes from a basis calculated at one frequency to a basis calculated at another (higher) frequency. This is most obvious for the 3 Ritz basis curve, where the solution increases abruptly at $ka \approx 6.7$.

5.2.3 Interpolated Ritz bases

When using Ritz bases that are spread over a frequency range the question arises whether interpolation of these bases will allow greater spacings of the bases, while maintaining solution accuracy (option 4 of section 5.2) Unfortunately it does not. The accuracy of the solution is in fact considerably poorer than that obtained by using non-interpolated Ritz bases.

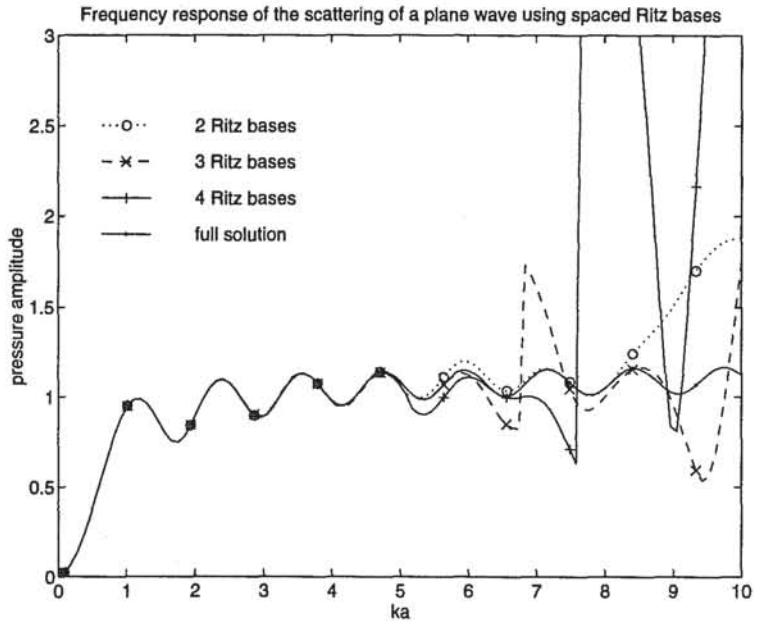

Figure 49: Radiated pressure at $(5a, 0, 0)$ for spaced Ritz bases containing 70 Ritz vectors.

A typical frequency response curve is shown in figure 50, for the scattering of a plane wave by a rigid sphere calculated with 5 Ritz vectors (at $ka = 0$, 2.5, 5.0, 7.5 and 10.0) over the interval $[0, 10]$. Large errors occur at localised points over the entire frequency range. This is because the interpolated Ritz basis at those points is made from a linear interpolation of two widely spaced and significantly different bases. Consider the error at $ka \approx 4.0$—the Ritz basis used at this frequency was constructed from a basis at $ka = 2.5$ and a basis at $ka = 5.0$, whereas in option 3 of section 5.2 with the same ka spacing the solution would depend only on the Ritz basis calculated at $ka = 5.0$. The two bases at $ka = 2.5$ and $ka = 5.0$ are completely different because the solution at these two frequencies have different dominant mode shapes, and interpolation between the two should not be expected to work. Quadratic interpolation using three Ritz bases gives similar results.

When using fewer Ritz bases, the basis at the upper end will differ even more from the basis at the lower end, giving worse results.

The effectiveness of Ritz basis interpolation is dependent upon how the dominant modes of the solution change, and when they change with respect to the Ritz bases. Every model will be different and no firm guidelines can be given to the use of interpolated Ritz bases.

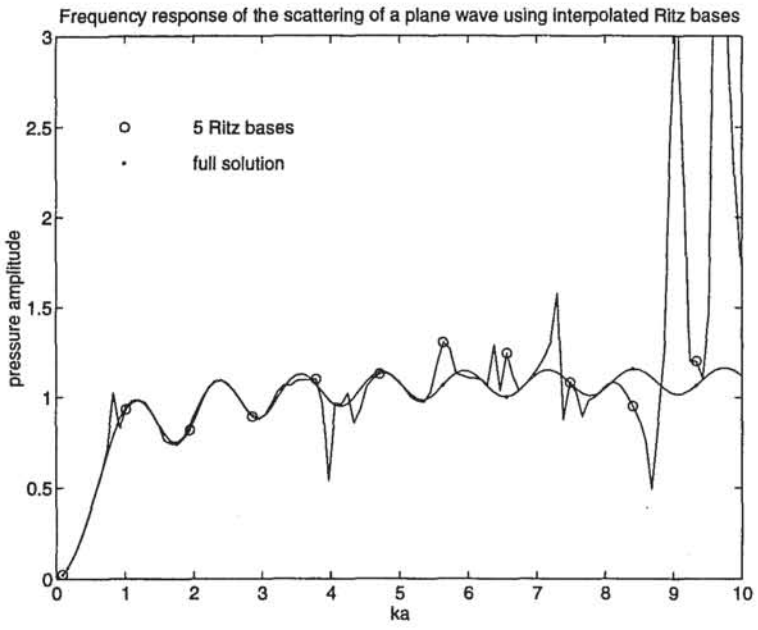

Figure 50: Radiated pressure at $(5a, 0, 0)$ for interpolated Ritz bases.

Chapter 6

Conclusions

A number of conclusions have been reached. These are;

1. Wave envelope elements of variable interpolation order have been successfully applied to acoustical radiation and scattering test cases. Although the test cases have been relatively simple, they incorporate the major aspects of more complicated and realistic models. Excellent agreement was observed between the wave envelope results and analytical solutions for moderate frequencies, and in some situations the results were accurate to very high frequencies. A test case involving more complex geometries and without an analytical solution has been compared to results from an acoustical boundary element package, and good agreement observed.

2. The wave envelope elements have been extended by the addition of variable basis function interpolation in the radial direction. Interpolations up to order ten are possible, allowing the wave envelope elements to model relatively complicated pressure fields. This permits good solutions to be obtained from meshes that consist solely of wave envelope elements.

3. Higher order wave envelope elements give matrices that are progressively more ill-conditioned. A limit appears to have been reached with order ten elements where the ill-conditioning becomes greater than the number of significant figures (16–17) used to represent the matrix elements. Working with more significant figures would raise the order ten restriction, but with an associated CPU time increase. Solving the system with Ritz vectors was found to alleviate this problem somewhat.

4. When the form of the prescribed velocity on the surface of the radiating or scattering body is independent of frequency, Ritz vectors can give CPU savings of two orders of magnitude. The accuracy of the solution is dependent upon the number of Ritz vectors used, but any degree of accuracy can be obtained by using more vectors.

5. When the form of the prescribed velocity is dependent upon frequency a single Ritz basis will not suffice for a multi-frequency analysis. A simplistic approach

whereby a basis is calculated at a particular frequency and then used for many adjacent frequencies and found to give surprisingly good results. Although a certain minimum spacing of the bases was required to achieve any CPU time savings when compared to solving the full system at every frequency, solution accuracy was maintained at spacings well above this minimum.

6. For both separable and non-separable excitations the highest frequency that a Ritz solution was accurate to was found to depend upon the number of vectors used.

Several areas exist which would benefit from further study. These are;

1. The only boundary conditions considered in this thesis were the acoustically hard surface and its vibrating counterpart. Consideration of other boundary conditions is necessary to cast wave envelope elements into a general tool for unbounded acoustical analysis. A more demanding aim is to allow for inhomogeneous mediums, and cater for moving flows.

2. The reasons behind the ill-conditioning of the element matrices require more attention, along with consideration of the improvement in solution accuracy obtained when using Ritz vectors on ill-conditioned systems.

3. The use of Ritz vectors with frequency dependent excitation problems is not completely satisfactory and further investigation is warranted.

Bibliography

[1] D. L. Anderson and R.L. Ungless. Infinite finite elements. In *International Symposium in Innovative numerical analysis in applied engineering science*, Versailles, France, May 1977.

[2] R.R. Arnold, R.L. Citerley, M. Chargin, and D. Galant. Application of R'itz vectors for dynamic analysis of large structures. *Computers and Structures*, 21(3):461–467, 1985.

[3] R.J. Astley. Wave envelope and infinite elements for acoustical radiation. *International Journal for Numerical Methods in Fluids*, 3:507–526, 1983.

[4] R.J. Astley. A finite element, wave envelope formulation for acoustical radiation in moving flows. *Journal of Sound and Vibration*, 103(4):471–485, 1985.

[5] R.J. Astley, P. Bettess, and P.J. Clark. Letter to the editor. *International Journal for Numerical Methods in Engineering*, 32:207–209, 1991.

[6] R.J. Astley, J.P. Coyette, and G.J. Macaulay. Mapped wave envelope elements for acoustical radiation and scattering. *Journal of Sound and Vibration*, 170(1):97–118, 1994.

[7] R.J. Astley and W. Eversman. A note on the utility of a wave envelope approach in finite element duct transmission studies. *Journal of Sound and Vibration*, 76(4):595–601, 1981.

[8] R.J. Astley and W. Eversman. Acoustic transmission in lined flow ducts. In R.H. Gallagher, D.H. Norrie, J.T. Oden, and O.C. zienkiewicz, editors, *Finite Elements in Fluids*, volume 4, chapter 28, pages 617–644. John Wiley and Sons, 1982.

[9] R.J. Astley and W. Eversman. Finite element formulations for acoustical radiation. *Journal of Sound and Vibration*, 88(1):47–64, 1983.

[10] K.J. Baumeister. Analysis of sound propagation in ducts using the wave envelope concept. Technical Report N-7719, NASA, 1974.

[11] K.J. Baumeister. Wave envelope of sound propagation in ducts with variable axial impedance. In I.R. Schwartz, H.T. Nagamatsu, and W Strahle, editors, *Progress in Astronautics and Aeronautics—Aeroacoustics: Fan Noise and Control; Duct Acoustics; Rotor Noise*, volume 44, pages 451–474. AIAA, 1976.

[12] K.J. Baumeister. Finite difference theory for sound propagation in a lined duct with uniform flow using the wave envelope technique. Technical Report 1001, NASA, 1977.

[13] K.J. Baumeister. Time-dependent wave envelope finite difference analysis of sound propagation. *AIAA Journal*, 24:32–38, January 1986.

[14] A. Bayless and E. Turkel. Radiation boundary conditions for wave-like equations. *Communications on Pure and Applied Mathematics*, 33:707–725, 1980.

[15] A. Bayliss, M. Gunzburger, and E. Turkel. Boundary conditions for the numerical solution of elliptic equations in exterior regions. *SIAM Journal on Applied Mathematics*, 42(2):430–450, 1982.

[16] A. Bayliss and E. Turkel. Far-field boundary conditions for compressible flows. *Journal of Computational Physics*, 48:182–199, 1982.

[17] E.P. Bayo and E.L. Wilson. Use of Ritz vectors in wave propagation and foundation response. *Earthquake Engineering and Structural Dynamics*, 12:499–505, 1984.

[18] G. Beer and J.L. Meek. Infinite domain elements. *International Journal for Numerical Methods in Engineering*, 17(1):43–52, 1981.

[19] P. Bettess. Infinite elements. *International Journal for Numerical Methods in Engineering*, 11:53–64, 1977.

[20] P. Bettess. More on infinite elements. *International Journal for Numerical Methods in Engineering*, 15:1613–1626, 1980.

[21] P. Bettess. A simple wave envelope test example. *Communications in Applied Numerical Methods*, 3:77–80, 1987.

[22] P. Bettess. *Infinite Elements*. Penshaw Press, 1992.

[23] P. Bettess and O.C. Zienkiewicz. Diffraction and refraction of surface waves using finite and infinite elements. *International Journal for Numerical Methods in Engineering*, 11:1271–1290, 1977.

[24] A. Boag, Y. Leviatan, and A. Boag. Analysis of acoustic scattering from fluid cylinders using a multifilament source model. *Journal of the Acoustical Society of America*, 83(1):1–8, 1987.

[25] C.A. Brebbia. *The Boundary Element Method for Engineers.* Pentech Press, London, 1978.

[26] D.S Burnett. *Finite Element Analysis.* Addison Wesley, 1987.

[27] A.J. Burton and G.F. Miller. The application of integral equation methods to the numerical solution of some exterior boundary-value problems. *Proceedings of the Royal Society London*, A323:201–210, 1971.

[28] C.L. Chang and J.J. Engblom. Reduced basis alternatives to the solution of nonlinear dynamical systems. *Journal of Aircraft*, 29(5):760–767, 1992.

[29] C.C. Chien, H. Rajiyah, and S.N. Atluri. An effective method for solving the hypersingular integral equations in 3-D acoustics. *Journal of the Acoustical Society of America*, 88:918–937, 1990.

[30] R.D. Cooke, D.S. Malkus, and M.E. Plesha. *Concepts and Applications of Finite Element Analysis.* John Wiley and Sons, 3rd edition, 1989.

[31] R. Cournat. Variational methods for the solution of problems of equilibrium and vibration. *Bulletin of the American Mathematical Society*, 49:1–23, 1943.

[32] J.P. Coyette. Evaluation of different computational strategies for acoustic finite element modelling. In *Proceedings of the Institute of Acoustics*, volume 12, pages 851–864, 1990.

[33] A. Craggs. The transient response of a coupled, plate-acoustic system using plate and acoustic finite elements. *Journal of Sound and Vibration*, 15(4):509–528, 1971.

[34] A. Craggs. The use of simple three-dimensional acoustic finite elements for determining the natural modes and frequencies of complex shaped enclosures. *Journal of Sound and Vibration*, 23(3):331–339, 1972.

[35] A. Craggs. A finite element method for modelling dissipative mufflers with a locally reactive lining. *Journal of Sound and Vibration*, 54(2):285–296, 1977.

[36] A. Craggs. The application of acoustic and absorption finite elements to sound fields in small enclosures. In M.M. Kamal and J.A. Wolf, Jr., editors, *Finite Element Applications in Acoustics.* ASME, 1981.

[37] L. Cremers, K.R. Fyfe, and J.P. Coyette. A variable order infinite acoustic wave envelope element. *Journal of Sound and Vibration*, 171(4):483–508, 1994.

[38] T.A. Cruse. A direct formulation and numerical solution of the general transient elastodynamic problem II. *J. Math. Anal. Appl.*, 22:341–355, 1968.

[39] T.A. Cruse and F.J. Rizzo. A direct formulation and numerical solution of the general transient elastodynamic problem I. *J. of Math. Anal. Appl.*, 22:244–259, 1968.

[40] B. Engquist and A. Majda. Absorbing boundary conditions for the numerical simulation of waves. *Mathematics of Computation*, 31(139):629–652, 1977.

[41] B. Engquist and A. Majda. Radiation boundary conditions for acoustic and elastic calculations. *Communications on Pure and Applied Mathematics*, 32:313–357, 1979.

[42] W. Eversman and R.J. Astley. Acoustic transmission in non-uniform ducts with mean flow, part II: The finite element method. *Journal of Sound and Vibration*, 74:103–121, 1981.

[43] M.B. Friedman and R.P. Shaw. Diffraction of a plane shock wave by an arbitrary rigid cylindrical obstacle. *Journal of Applied Mechanics*, 29:40–46, 1962.

[44] H. Gan, P.L. Levin, and R. Ludwig. Finite element formulation of acoustic scattering phenomena with absorbing boundary condition in the frequency domain. *Journal of the Acoustical Society of America*, 94:1651–1662, September 1993.

[45] D. Givoli. *Numerical Methods for Problems in Infinite Domains*. Studies in Applied Mechanics. Elsevier, 1992.

[46] G.M.L. Gladwell. A finite element method for acoustics. In *Proceedings of the 5th International Congress in Acoustics*, 1965.

[47] G.M.L. Gladwell and G. Zimmermann. On energy and complementary energy formulations of acoustic and structural vibration problems. *Journal of Sound and Vibration*, 3(3):233–241, 1966.

[48] G.H. Golub and C.F. Van Loan. *Matrix Computations*. The John Hopkins University Press, Baltimer and London, 1989.

[49] I. Harari and T.J.R. Hughes. Analysis of continuous formulations underlying the computation of time-harmonic acoustics in exterior domains. *Computer Methods in Applied Mechanics and Engineering*, 97:103–124, 1992.

[50] I. Harari and T.J.R. Hughes. A cost comparison of boundary element and finite element methods for problems of time-harmonic acoustics. *Computer Methods in Applied Mechanics and Engineering*, 97:77–102, 1992.

[51] T.J.R. Hughes. *The Finite Element Method*. Prentice-Hall, 1987.

[52] A. Ibrahimbegovic, H.C. Chen, E.L. Wilson, and R.L. Taylor. Ritz method for dynamic analysis of large discrete linear systems with non–proportional damping. *Earthquake Engineering and Structural Dynamics*, 19:877–889, 1990.

[53] A. Ibrahimbegovic and E.L. Wilson. Automated truncation of Ritz basis in modal transformation. *Journal of Engineering Mechanics*, 116(11):2506–2520, 1990.

[54] B.P. Jacob and N.F.F. Ebecken. Adaptive reduced integration method for nonlinear structural dynamic analysis. *Computers and Structures*, 45(2):333–347, 1992.

[55] M.A. Jaswon and G.T. Symm. *Integral equation methods in potential theory and elastostatics*. Academic Press, London, 1977.

[56] X. Jiaxian. An improved method for partial eigensolution of large structures. *Computers and Structures*, 32(5):1055–1060, 1989.

[57] K. Joo and E.L. Wilson. Ritz vectors and generation criteria for mode superposition analysis. *Earthquake Engineering and Structural Dynamics*, 18:149–167, 1989.

[58] M.C Junger and D. Feit. *Sound, Structures and their Interaction*. MIT, 1972.

[59] Y. Kagawa, T. Yamabuchi, and K. Sugihara. A finite element approach to a coupled structural-acoustic radiation system with application to loudspeaker characteristic calculation. *Journal of Sound and Vibration*, 69(2):229–243, 1980.

[60] J.E. Kaiser and A.H. Nayfeh. A wave envelope technique for wave propagation in nonuniform ducts. *AIAA Journal*, 15:533–537, April 1977.

[61] S. Kaniel. Estimates for some computation techniques in linear algebra. *Mathematical Computations*, 20:369–378, 1966.

[62] W. Kanok-Nukulchai and S.F. Lin. Nonlinear analysis using Ritz vector reduced basis. *Computers and Structures*, 44(1):117–124, 1992.

[63] H. Kardestuncer, editor. *The Finite Element Handbook*. McGraw Hill, New York, 1987.

[64] L.E. Kinsler, A.R. Frey, A.B. Coppens, and J.V. Sanders. *Fundamentals of Acoustics*. John Wiley & Sons, Inc, 3rd edition, 1982.

[65] R.E. Klienman and G.F. Roach. Boundary integral equations for the three-dimensional helmholtz equation. *SIAM Review*, 16:214–236, 1974.

[66] P.S. Kondapalli and D.J. Shippy. The method of fundamental solutions for transmission and scattering of elastic waves. *Computer Methods in Applied Mechanics and Engineering*, 96:255–269, 1992.

[67] G.H. Koopmann, L. Song, and J.B. Fahnline. A method for computing acoustic fields based on the principle of wave superposition. *Journal of the Acoustical Society of America*, 86(6):2433–2438, 1989.

[68] C. Lanczos. An iteration method for the solution of the eigenvalue problem of linear differential and integral operators. *Journal of Research of the National Bureau of Standards*, 45:255–281, 1950.

[69] P. Léger and E.L. Wilson. Generation of load dependent Ritz transformation vectors in structural dynamics. *Engineering Computations*, 4:309–318, 1987.

[70] Y. Leviatan and A. Boag. Analysis of electromagnetic scattering from dielectric cylinders using a multifilament current model. *IEEE Transactions on Antennas and Propagation*, AP-35(10):1119–1127, 1987.

[71] Y. Leviatan, A. Boag, and A. Boag. Analysis of TE scattering from dielectric cylinders using a multifilament magnet current model. *IEEE Transactions on Antennas and Propagation*, 36(7):1020–1031, 1988.

[72] J.M.M.C. Marques and D.R.J. Owen. Infinite elements in quasi-static materially non-linear problems. *Computers and Structures*, 18(4):739–751, 1984.

[73] A.H. Nayfeh, B.J. Shaker, and J.E. Kaiser. Transmission of sound through nonuniform circular ducts with compressible mean flows. *AIAA Journal*, 18:515–525, May 1980.

[74] D.J. Nefske, J.A. Wolfe Jr, and L.J. Howell. Structural-acoustic finite element analysis of the automobile passenger compartment. A review of current practice. *Journal of Sound and Vibration*, 80(2):247–266, 1982.

[75] B. Nour-Omid, B.N. Parlett, and R.L. Taylor. Lanczos versus subspace iteration for solution of eigenvalue problems. *International Journal for Numerical Methods in Engineering*, 19:859–871, 1983.

[76] Numerical Integration Technologies, Ambachtenlaan 11a B-3001 Leuven Belgium. *Sysnoise reference manual*, 4.4 edition, 1992.

[77] A.M. Ondet and J.L. Barbry. Modelling of sound propagation in fitted workshops using ray tracing. *Journal of the Acoustical Society of America*, 85:787–796, February 1989.

[78] C.C. Paige. *The Computation of Eigenvalues and Eigenvectors of Very Large Sparse Matrices*. Ph.D. thesis, London University, 1971.

[79] A.V. Parrett. *Applications of finite and wave envelope element approximations to acoustic radiation from turbofan engine inlets in flight.* Ph.D. thesis, University of Missouri-Rolla, 1984.

[80] M. Petyt, J. Lea, and G.H. Koopmann. A finite element method for determining the acoustic modes of irregular shaped cavities. *Journal of Sound and Vibration*, 45(4):495–502, 1976.

[81] T.L. Richards and S.K. Jha. A simplified finite element method for studying acoustic characteristics inside a car cavity. *Journal of Sound and Vibration*, 63(1):61–72, 1979.

[82] Y. Saad. On the rates of convergence of the Lanczos and the block Lanczos methods. *SIAM Journal of Numerical Analysis*, 17:687–706, 1980.

[83] H.A. Schenck. Improved integral formulation for acoustic radiation problems. *Journal of the Acoustical Society of America*, 44:41–58, 1968.

[84] E. Skudrzyk. *The Foundations of Acoustics.* Springer-Verlag, Wien New York, 1971.

[85] A. Sommerfeld. *Partial Differential Equations in Physics.* Academic Press Inc, New York, 1949. Translated by Ernst G. Straus.

[86] G.T. Symm. Integral equation methods in potential theory. *Proceedings of the Royal Society*, 275(II):33–46, 1963.

[87] B.A. Szabo and G.C. Lee. Derivation of stiffness matrices for problems in plane elasticity by Galerkin's method. *International Journal for Numerical Methods in Engineering*, 1:301–310, 1961.

[88] Yu-Chuing Teng. Three-dimensional finite element analysis of waves in an acoustic medium with inclusion. *Journal of the Acoustical Society of America*, 86:414–422, July 1989.

[89] M.J. Turner, R.W. Clough, H.C. Martin, and L.J. Topp. Stiffness and deflection analysis of complex structures. *Journal of the Aeronautical Sciences*, 23(9):805–823, 1956.

[90] R.L. Ungless. An infinite finite element. Master's thesis, University of British Columbia, 1973.

[91] E.L. Wilson and E.P. Bayo. Use of special Ritz vectors in dynamic substructure analysis. *Journal of Structural Engineering*, 112(8):1944–1954, 1986.

[92] E.L. Wilson and T. Itoh. An eigensolution strategy for large systems. *Computers and Structures*, 16(1–4):259–265, 1983.

[93] E.L. Wilson, Ming-Wu Yuan, and J.M. Dickens. Dynamic analysis by direct superposition of Ritz vectors. *Earthquake Engineering and Structural Dynamics*, 10:813–821, 1982.

[94] H. Xia and J.L. Humar. Frequency dependent Ritz vectors. *Earthquake Engineering and Structural Dynamics*, 21:215–231, 1992.

[95] O.C. Zienkiewicz, K. Bando, P. Bettess, C. Emson, and T.C. Chiam. Mapped infinite elements for exterior wave problems. *International Journal for Numerical Methods in Engineering*, 21(7):1229–1252, 1985.

[96] O.C. Zienkiewicz and P. Bettess. Infinite elements in the study of fluid structure interaction problems. In *Proceedings of the 2nd International Symposium on Computer Methods in Applied Science*, Versailles, 1975.

[97] O.C. Zienkiewicz, P. Bettess, T.C. Chiam, and C. Emson. Numerical methods for unbounded field problems and a new infinite element formulation. *AMSE, AMD*, 46:115–148, 1981.

[98] O.C Zienkiewicz and Y.K. Cheung. Finite elements in the solution of field problems. *The Engineer*, 220:507–510, 1965.

[99] O.C. Zienkiewicz, C. Emson, and P. Bettess. A novel boundary infinite element. *International Journal for Numerical Methods in Engineering*, 19:393–404, 1983.

[100] O.C. Zienkiewicz and R.L. Taylor. *The Finite Element Method*, volume 1. McGraw Hill, 4th edition, 1989.

[101] O.C. Zienkiewicz and R.L. Taylor. *The Finite Element Method*, volume 2. McGraw Hill, 4th edition, 1991.

Appendix A

Element library

This appendix details the elements used in the wave envelope program.

A.1 Conventional elements

A.1.1 Two-dimensional

These are the basis functions for the linear (4 noded) two-dimensional conventional element. The node numbering is shown in figure 51.

$$\begin{aligned} N_1 &= \frac{1}{4}(1-\varepsilon)(1-\psi), \\ N_2 &= \frac{1}{4}(1+\varepsilon)(1-\psi), \\ N_3 &= \frac{1}{4}(1+\varepsilon)(1+\psi), \\ N_4 &= \frac{1}{4}(1-\varepsilon)(1+\psi). \end{aligned}$$

Quadratic (8 noded) elements were not implemented.

A.1.2 Three-dimensional

Linear

These are the basis functions for conventional three-dimensional linear (8 noded) finite elements. The node numbering is shown in figure 52 (Note that the origin of the coordinate system is at the centre of the element).

$$N_1 = \frac{1}{8}(1+\varepsilon)(1-\eta)(1-\psi),$$

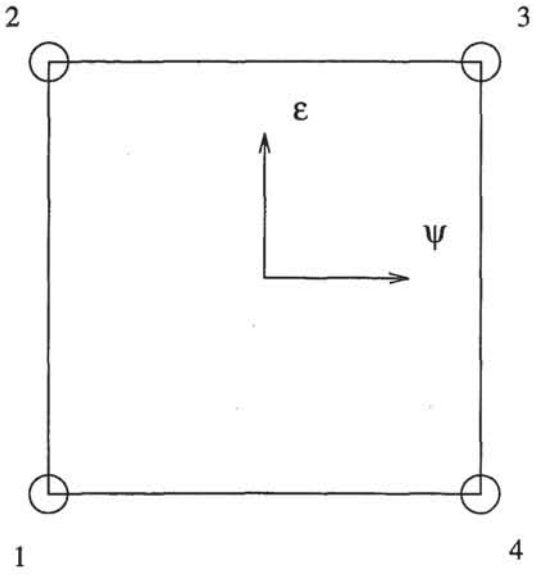

Figure 51: Two-dimensional linear conventional element

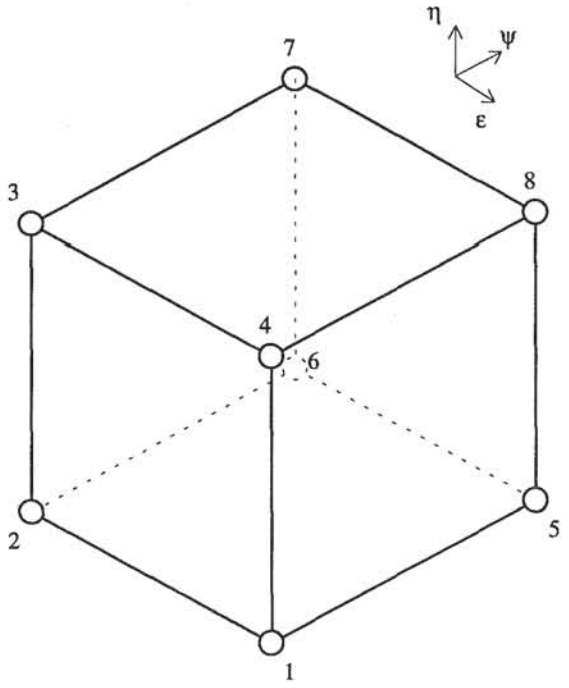

Figure 52: Three-dimensional linear conventional element

$$
\begin{aligned}
N_2 &= \frac{1}{8}(1-\varepsilon)(1-\eta)(1-\psi), \\
N_3 &= \frac{1}{8}(1-\varepsilon)(1+\eta)(1-\psi), \\
N_4 &= \frac{1}{8}(1+\varepsilon)(1+\eta)(1-\psi), \\
N_5 &= \frac{1}{8}(1+\varepsilon)(1-\eta)(1+\psi), \\
N_6 &= \frac{1}{8}(1-\varepsilon)(1-\eta)(1+\psi), \\
N_7 &= \frac{1}{8}(1-\varepsilon)(1+\eta)(1+\psi), \\
N_8 &= \frac{1}{8}(1+\varepsilon)(1+\eta)(1+\psi).
\end{aligned}
$$

Quadratic

These are the basis functions for conventional three-dimensional quadratic (20 noded) finite elements. The node numbering is shown in figure 53.

$$
\begin{aligned}
N_i &= (1+\varepsilon_0)(1+\eta_0)(1+\psi_0)(\varepsilon_0+\eta_0+\psi_0-2)\,;\, i=1,\ldots,8, \\
N_i &= \frac{1}{4}(1-\varepsilon^2)(1+\eta_0)(1+\psi_0)\,;\, i=9,11,17,19, \\
N_i &= \frac{1}{4}(1-\eta^2)(1+\varepsilon_0)(1-\psi_0)\,;\, i=10,12,18,20, \\
N_i &= \frac{1}{4}(1-\psi^2)(1+\varepsilon_0)(1+\eta_0)\,;\, i=13,14,15,16,
\end{aligned}
$$

where $\varepsilon_0 = \varepsilon_i\varepsilon$, $\eta_0 = \eta_i\eta$ and $\psi_0 = \psi_i\psi$.

A.2 Wave envelope elements

A.2.1 Two-dimensional

These are the basis functions for the linear (4 noded) two-dimensional wave envelope element (shown in figure 9) with order 2 interpolation in the radial direction. Note how they approach zero as ψ approaches 1. The basis functions are of the form

$$N_i = P_i e^{-ika(\varepsilon)\left(\frac{1+\psi}{1-\psi}\right)},$$

where

$$P_1 = \frac{-1}{\sqrt{8}}(1-\varepsilon)\psi\sqrt{1-\psi},$$

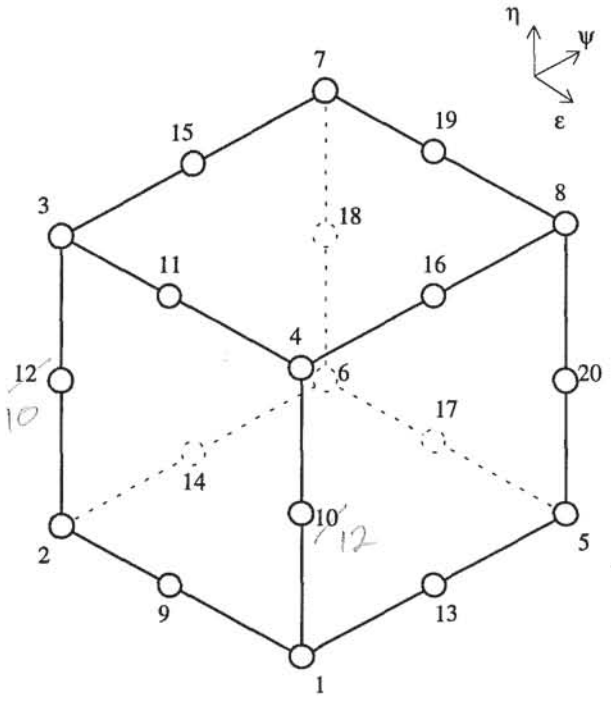

Figure 53: Three-dimensional quadratic conventional element

$$
\begin{aligned}
P_2 &= \frac{-1}{\sqrt{8}}(1+\varepsilon)\psi\sqrt{1-\psi}, \\
P_3 &= \frac{1}{2}(1+\varepsilon)(1+\psi)\sqrt{1-\psi}, \\
P_4 &= \frac{1}{2}(1-\varepsilon)(1+\psi)\sqrt{1-\psi}.
\end{aligned}
$$

For higher interpolation orders in the radial direction a general form of the above equation was developed (see section A.2.3). It applies equally well for two- or three-dimensional elements and linear or quadratic angular interpolation.

A.2.2 Three-dimensional

These are the basis functions for the linear (8 nodes) three–dimensional wave envelope element (shown in figure 10) with quadratic interpolation in the radial direction. The basis functions are of the form

$$N_i = P_i e^{-ika(\varepsilon)\left(\frac{1+\psi}{1-\psi}\right)},$$

where

$$
\begin{aligned}
P_1 &= \frac{1}{8}(1+\varepsilon)(1-\eta)(\psi^2-\psi), \\
P_2 &= \frac{1}{8}(1-\varepsilon)(1-\eta)(\psi^2-\psi), \\
P_3 &= \frac{1}{8}(1-\varepsilon)(1+\eta)(\psi^2-\psi), \\
P_4 &= \frac{1}{8}(1+\varepsilon)(1+\eta)(\psi^2-\psi), \\
P_5 &= \frac{1}{4}(1+\varepsilon)(1-\eta)(1-\psi^2), \\
P_6 &= \frac{1}{4}(1-\varepsilon)(1-\eta)(1-\psi^2), \\
P_7 &= \frac{1}{4}(1-\varepsilon)(1+\eta)(1-\psi^2), \\
P_8 &= \frac{1}{4}(1+\varepsilon)(1+\eta)(1-\psi^2).
\end{aligned}
$$

A.2.3 Variable order interpolation wave envelope elements

This section details the mechanism used to generate the basis functions for the variable order wave envelope element.

An arbitrary integration order wave envelope element is one in which the infinite edge can have any number of nodes on it. The other dimensions have the conventional two or

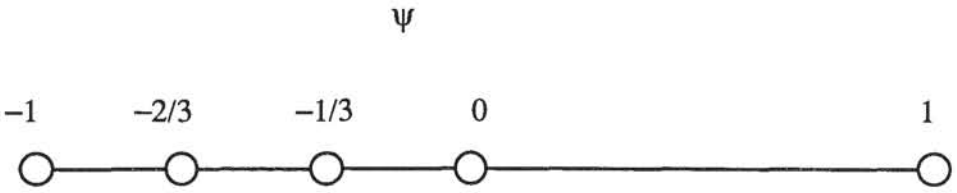

Figure 54: An infinite edge

three nodes on them. These elements are of the Lagrangian type, since they are formed from multiplies of one-dimensional Lagrange polynomials.

Consider just one infinite edge as shown in figure 54. The simplest node arrangement is to have one at $\psi = -1$ and another at $\psi = 1$. This gives a linear interpolation in the element. The simplest interpolation used in the wave envelope program is quadratic and this type has a third node at $\psi = 0$. Higher order interpolations have additional nodes distributed evenly between $\psi = -1$ and $\psi = 0$. The figure shows an infinite edge with 5 nodes, giving a quartic interpolation. The interpolation function along an infinite edge is given by

$$P_l' = \prod_{\substack{j=1,n+1 \\ j \neq l}} \frac{(\psi - \psi_j)}{(\psi_l - \psi_j)},$$

where $\psi_{n+1} = 1$, ψ_l is the ψ coordinate of the l^{th} node along the edge (starting at $\psi = -1$) and n is one less than the number of nodes along the edge.

For two-dimensional radiation a $1/\sqrt{r}$ factor is used to correctly model the radiation decay, hence P_l' becomes

$$P_l' = \left[\prod_{\substack{j=1,n+1 \\ j \neq l}} \frac{(\psi - \psi_j)}{(\psi_l - \psi_j)} \right] \sqrt{\frac{1 - \psi_l}{1 - \psi}}.$$

The extra term originates from

$$\sqrt{r} = \sqrt{\frac{2a}{1 - \psi}}$$

and is such that at $\psi = \psi_l$ it evaluates to one. This keeps the desirable property of P_l' equating to 1 at its own node.

A numbering scheme for the wave envelope elements was chosen so that the important corner nodes always had the same ordering in the element numbering scheme. For example, figure 55 part(a) shows a linear two-dimensional wave envelope element with six nodes (excluding the two that are mapped to infinity). Compare this numbering to

that of the 12 noded element in 55 part(b). A similar methodology was used for the three-dimensional elements, and two examples are shown in figure 56.

The complete wave envelope element basis functions are given by

$$N_i = P_i e^{-ika(\varepsilon,\eta)\left(\frac{1+\psi}{1-\psi}\right)},$$

where $P_i = P_l' f$, and $f = f(\varepsilon)$ or $f = f(\varepsilon, \eta)$ for two- and three-dimensional elements respectively. P_l' is as given above for the two- or three-dimensional elements as appropriate. The relationship between the indices i and l is dependent upon the element numbering scheme, and is most easily explained with an example. Consider figure 55 part(a), where the node numbers correspond to the index i in the above equation. Node 1 has an l value of 1, node 5 a value of 2, and node 4 an l value of 3. Likewise, node 2 has an l value of 1, node 6 a value of 2 and node 3 and value of 3. That is, the number l refers to the radial position of the node. This numbering method for l applies to all wave envelope elements. The f functions are given below.

Two-dimensional linear

$$\text{if node is on } \begin{cases} \varepsilon = -1, & f = \frac{1}{2}(1-\varepsilon) \\ \varepsilon = 1, & f = \frac{1}{2}(1+\varepsilon) \end{cases}$$

Three-dimensional linear

$$\text{if node is on } \begin{cases} \varepsilon = -1, & \eta = -1, & f = \frac{1}{4}(1-\varepsilon)(1-\eta) \\ \varepsilon = -1, & \eta = 1, & f = \frac{1}{4}(1-\varepsilon)(1+\eta) \\ \varepsilon = 1, & \eta = -1, & f = \frac{1}{4}(1+\varepsilon)(1-\eta) \\ \varepsilon = 1, & \eta = 1, & f = \frac{1}{4}(1+\varepsilon)(1+\eta) \end{cases}$$

Three-dimensional quadratic

$$\text{if node is on } \begin{cases} \varepsilon = 1, & \eta = -1, & f = \frac{1}{4}(1+\varepsilon)(1-\eta)(\varepsilon-\eta-1) \\ \varepsilon = -1, & \eta = -1, & f = \frac{1}{4}(1-\varepsilon)(1-\eta)(-\varepsilon-\eta-1) \\ \varepsilon = -1, & \eta = 1, & f = \frac{1}{4}(1-\varepsilon)(1+\eta)(-\varepsilon+\eta-1) \\ \varepsilon = 1, & \eta = 1, & f = \frac{1}{4}(1+\varepsilon)(1+\eta)(\varepsilon+\eta-1) \\ \varepsilon = 0, & \eta = -1, & f = \frac{1}{2}(1-\varepsilon^2)(1-\eta) \\ \varepsilon = -1, & \eta = 0, & f = \frac{1}{2}(1-\varepsilon)(1-\eta^2) \\ \varepsilon = 0, & \eta = 1, & f = \frac{1}{2}(1-\varepsilon^2)(1+\eta) \\ \varepsilon = 1, & \eta = 0, & f = \frac{1}{2}(1+\varepsilon)(1-\eta^2) \end{cases}$$

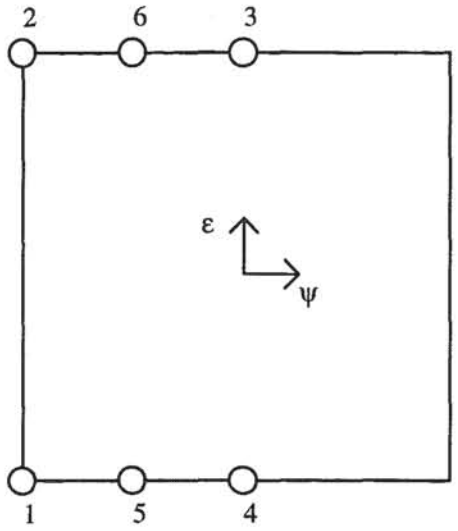

(a)

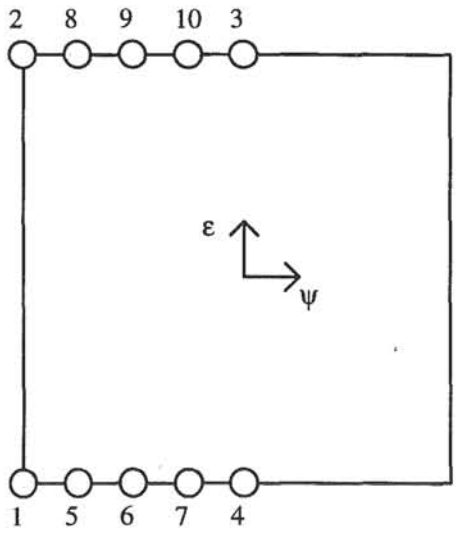

(b)

Figure 55: Two-dimensional wave envelope element numbering scheme. (a) order three element, (b) order five element

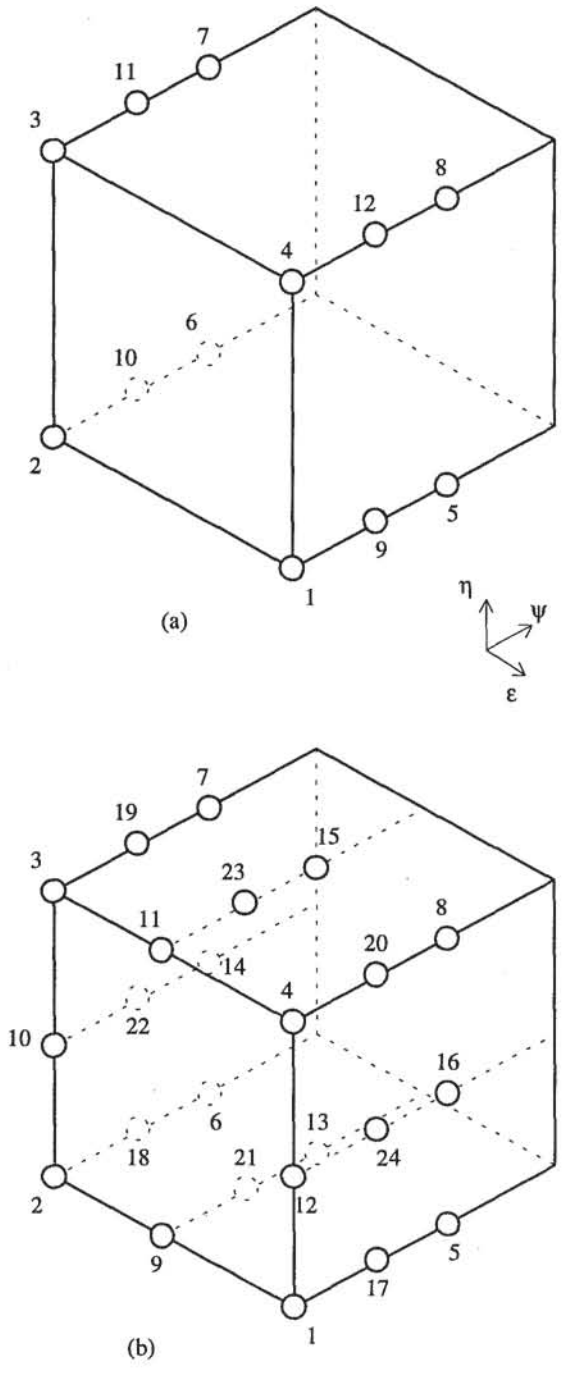

Figure 56: Three-dimensional wave envelope element numbering scheme. (a) order three element with linear angular interpolation, (b) order three element with quadratic angular interpolation

Derivatives

Derivatives are obtained from

$$\begin{aligned}\frac{\partial P_i}{\partial \varepsilon} &= \frac{\partial f}{\partial \varepsilon} P_l', \\ \frac{\partial P_i}{\partial \eta} &= \frac{\partial f}{\partial \eta} P_l', \\ \frac{\partial P_i}{\partial \psi} &= f \frac{\partial P_l'}{\partial \psi}.\end{aligned}$$

The derivatives $\partial f/\partial \varepsilon$ and $\partial f/\partial \eta$ are trivial and are easily gleaned from the above expressions for f. The $\partial P_l'/\partial \psi$ term for two-dimensional elements is

$$\begin{aligned}\frac{\partial P_l'}{\partial \psi} &= \left[\sum_{k=1}^{n+1} \frac{\prod_{j=1,n+1}^{j\neq k}(\psi - \psi_j)}{\prod_{j=1,n+1}^{j\neq l}(\psi_l - \psi_j)}\right] \sqrt{\frac{1-\psi_l}{1-\psi}} \\ &\quad + \left[\prod_{j=1,n+1}^{j\neq l} \frac{\psi - \psi_j}{\psi_l - \psi_j}\right] \frac{1}{2}\sqrt{1-\psi_l}\,(1-\psi)^{-\frac{3}{2}},\end{aligned}$$

and for three-dimensional elements is

$$\frac{\partial P_l'}{\partial \psi} = \sum_{k=1}^{n+1} \frac{\prod_{j=1,n+1}^{j\neq k}(\psi - \psi_j)}{\prod_{j=1,n+1}^{j\neq l}(\psi_l - \psi_j)}.$$

Appendix B

Wave envelope mapping functions

Mapping functions are tabulated for the wave envelope elements used in the wave envelope program.

B.1 Two-dimensional

B.1.1 Linear

This element uses four mapping nodes. See figure 55.

$$
\begin{aligned}
M_1 &= \frac{(1-\varepsilon)(-\psi)}{1-\psi}, \\
M_2 &= \frac{(1+\varepsilon)(-\psi)}{1-\psi}, \\
M_3 &= \frac{(1+\varepsilon)(1+\psi)}{2(1-\psi)}, \\
M_4 &= \frac{(1-\varepsilon)(1+\psi)}{2(1-\psi)}.
\end{aligned}
$$

B.1.2 Quadratic

This element requires six mapping nodes but was not implemented in the wave envelope program.

B.2 Three-dimensional

B.2.1 Linear

This element has eight mapping nodes, as shown in figure 56, part(a).

$$
\begin{aligned}
M_1 &= \frac{(1+\varepsilon)(1-\eta)(-\psi)}{2(1-\psi)}, \\
M_2 &= \frac{(1-\varepsilon)(1-\eta)(-\psi)}{2(1-\psi)}, \\
M_3 &= \frac{(1-\varepsilon)(1+\eta)(-\psi)}{2(1-\psi)}, \\
M_4 &= \frac{(1+\varepsilon)(1+\eta)(-\psi)}{2(1-\psi)}, \\
M_5 &= \frac{(1+\varepsilon)(1-\eta)(1+\psi)}{4(1-\psi)}, \\
M_6 &= \frac{(1-\varepsilon)(1-\eta)(1+\psi)}{4(1-\psi)}, \\
M_7 &= \frac{(1-\varepsilon)(1+\eta)(1+\psi)}{4(1-\psi)}, \\
M_8 &= \frac{(1+\varepsilon)(1+\eta)(1+\psi)}{4(1-\psi)}.
\end{aligned}
$$

B.2.2 Quadratic

The three-dimensional quadratic mapping function requires 16 nodes. Figure 56 part(b) illustrates the node numbering scheme.

$$
\begin{aligned}
M_i &= -\frac{1}{2}(1+\varepsilon_0)(1+\eta_0)(\varepsilon_0+\psi_0-1)\frac{\psi}{1-\psi} \; ; i = 1,2,3,4, \\
M_i &= -(1-\varepsilon^2)(1+\psi^2)\frac{\psi}{1-\psi} \; ; i = 9,11, \\
M_i &= -(1-\eta^2)(1+\varepsilon_0)\frac{\psi}{1-\psi} \; ; i = 10,12, \\
M_i &= \frac{1}{4}(1+\varepsilon_0)(1+\eta_0)(\varepsilon_0+\eta_0-1)\left(\frac{1+\psi}{1-\psi}\right) \; ; i = 5,6,7,8, \\
M_i &= \frac{1}{2}(1-\varepsilon^2)(1+\eta_0)\left(\frac{1+\psi}{1-\psi}\right) \; ; i = 13,15, \\
M_i &= \frac{1}{2}(1-\eta^2)(1+\varepsilon_0)\left(\frac{1+\psi}{1-\psi}\right) \; ; i = 14,16,
\end{aligned}
$$

where $\varepsilon_0 = \varepsilon_i \varepsilon$ and $\eta_0 = \eta_i \eta$ and $\psi_0 = \psi_i \psi$.

Appendix C

Inner products

An inner product on a complex vector space V is a function that associates a complex number $\langle \mathbf{u}, \mathbf{v} \rangle$ with each pair of vectors $\mathbf{u}$ and $\mathbf{v}$ in such a way that the following axioms are satisfied for all vectors $\mathbf{u}$, $\mathbf{v}$, and $\mathbf{w}$ in V and all scalars k.

symmetry axiom $\langle \mathbf{u}, \mathbf{v} \rangle = \overline{\langle \mathbf{v}, \mathbf{u} \rangle}$

additivity axiom $\langle \mathbf{u} + \mathbf{v}, \mathbf{w} \rangle = \langle \mathbf{u}, \mathbf{w} \rangle + \langle \mathbf{v}, \mathbf{w} \rangle$

homogeneity axiom $\langle k\mathbf{u}, \mathbf{v} \rangle = k \langle \mathbf{u}, \mathbf{v} \rangle$

positivity axiom $\langle \mathbf{v}, \mathbf{v} \rangle \geq 0$ and $\langle \mathbf{v}, \mathbf{v} \rangle = 0$ if and only if $\mathbf{v} = 0$

where a bar over an object indicates the complex conjugate of that object.

Appendix D

Acoustic boundary conditions

D.1 Rigid body boundary condition

Consider the linearised inviscid momentum equation,

$$\rho \frac{\partial \mathbf{u}}{\partial t} = -\nabla P, \tag{84}$$

where ρ is the fluid density, $\mathbf{u}$ the particle velocity P the acoustic pressure, and t represents time.

For time harmonic waves the time dependence of $\mathbf{u}$ can be taken to be

$$\mathbf{u} = \Re(\mathbf{U}e^{i\omega t}),$$

where $\mathbf{U}$ is a complex velocity amplitude vector. Now,

$$\frac{\partial \mathbf{u}}{\partial t} = \Re(\mathbf{U}i\omega e^{i\omega t}).$$

The time dependence of P can also be stated as

$$P(t) = \Re(pe^{i\omega t}),$$

where p is a complex pressure amplitude. Substituting these two equations into 84 gives

$$\rho \mathbf{U}(i\omega)e^{i\omega t} = -\nabla p e^{i\omega t}.$$

Cancellation of the exponential terms results in

$$i\omega\rho\mathbf{U} = -\nabla p.$$

If $\omega = kc$, where k is the acoustic wavenumber and c the wave speed, this becomes

$$\nabla p = -ik\rho c\mathbf{U}.$$

By resolving the above equation normal to a surface S defined by the vector $\hat{\mathbf{n}}$, we obtain

$$\nabla p \cdot \hat{\mathbf{n}} = -ik\rho cU.$$

where

$$U = \mathbf{U} \cdot \hat{\mathbf{n}},$$

giving boundary condition 4 of section 2.1.1.

D.2 Sommerfeld radiation condition

The Sommerfeld radiation condition is

$$r^{\frac{1}{2}} \left(\frac{\partial p}{\partial r} + ikp \right) \rightarrow 0 \text{ as } r \rightarrow \infty \quad \text{(for 2D)},$$
$$r \left(\frac{\partial p}{\partial r} + ikp \right) \rightarrow 0 \text{ as } r \rightarrow \infty \quad \text{(for 3D)}.$$

In physical terms this condition means that the wave amplitude must vanish at a rate greater than $1/r$ as r approaches infinity (or $1/r^{1/2}$ for two-dimensional functions).

If we consider the Sommerfeld radiation condition as it approaches a far but finite boundary S_2, it is clear that the above condition is satisfied in an approximate sense if

$$\frac{\partial p}{\partial r} + ikp = 0 \text{ on } S_2.$$

The derivative of p with respect to r can be interpreted as the directional derivative of the pressure with respect to the outward radial direction r. This can be replaced with the more general expression, $\nabla p \cdot \hat{\mathbf{n}}$ to give

$$\nabla p \cdot \hat{\mathbf{n}} + ikp = 0 \text{ on } S_2,$$

where $\hat{\mathbf{n}}$ is the unit normal to the surface S_2.

Appendix E

Two-dimensional wave envelope results

E.1 Introduction

The results presented here are the two-dimensional analogues of the three-dimensional results presented in chapter 4. Two excitation types are considered; multi-pole radiation and scattering by a plane wave. Both include an infinitely long cylinder as the radiating or scattering body.

The conclusions reached for the three-dimensional results are equally valid for these two-dimensional results.

E.2 Multi-pole radiation

By setting the normal velocity on the surface of a circular cylinder to

$$U(\theta) = U_0 \cos(n\theta),$$

where U_0 is the maximum normal velocity amplitude, θ the cylindrical polar angle and n a positive integer we obtain an analytic solution for the resulting pressure field of the form,

$$p(r,\theta) = -i\rho c U_0 \cos(n\theta) \frac{H_n^{(2)}(kr)}{H_n^{(2)'}(ka)},$$

where $H_n^{(2)}(z)$ is a Hankel function of order n of the second kind, $H_n^{(2)'}(z)$ the derivative of $H_n^{(2)}(z)$ with respect to z and a the radius of the cylinder.

The mesh used to calculate a wave envelope element solution to the analytic solution given above is shown in figure 57. The model represents a two-dimensional cylinder or radius 0.1m, and consists of 150 linear wave envelope elements, with a common wave envelope origin at the centre of the cylinder. A symmetry plane was used, and only half of the region was meshed.

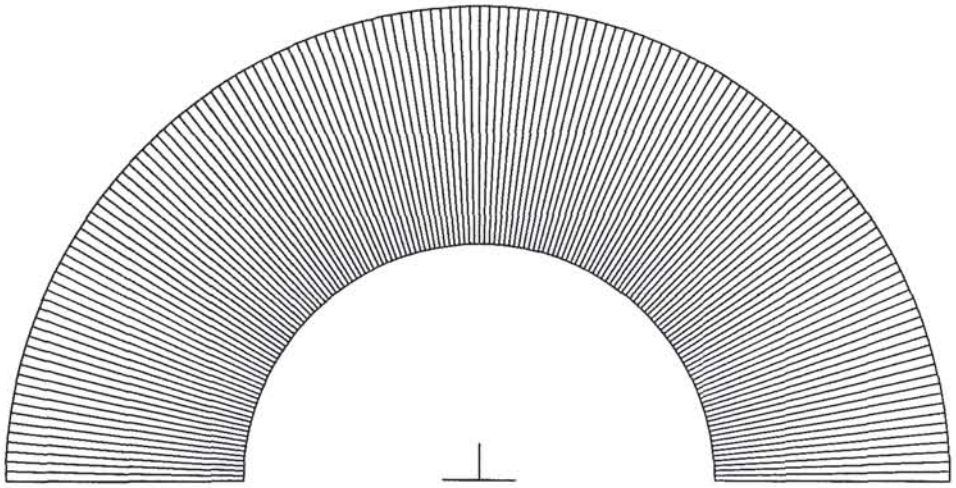

Figure 57: Wave envelope mesh surrounding a two-dimensional cylinder of radius 0.1 m.

Figures 58, 59, 60 and 61 show the pressure amplitude at $x = 5a$, $y = 0$ plotted against wavenumber ka, for multi-poles of order 2, 10, 20 and 25 respectively, up to $ka = 30$.

In figure 61 the order 10 interpolation wave envelope element gave acceptable results for the order 25 multi-pole. To obtain acceptable results for higher order multi-poles, higher order wave envelope interpolations are required. However, because of the ill-conditioning of the element matrices for interpolations beyond order 10 already discussed in section 4.6, this is not practical unless the numerical precision of the calculations is increased. Hence, an order 25 multi-pole (and therefore an order 25 Hankel function) is the highest order currently representable with two-dimensional wave envelope elements.

E.3 Scattering of a plane wave

Figure 62 plots the scattered pressure amplitude at $x = 5a$, $y = 0$ for the scattering of a plane wave by the cylinder, for which the analytical solution is given by [58]

$$p(r,\theta) = P_0 \sum_{n=0}^{\infty} \epsilon\, i^n \frac{J_n'(ka)}{H_n^{(2)}(ka)} H_n^{(2)}(kr)\cos(n\theta),$$

where $\epsilon = 1$ for $n = 0$ and $\epsilon = 2$ otherwise.

As can been seen from the multi-pole results, an order 10 wave envelope element will adequately represent an order 25 multi-pole, and hence an order 25 Hankel function. When calculating the scattering analytical solution, order 25 Hankel functions make a significant contribution to the analytic solution beyond $ka \approx 18$. This is the point where the numerical scattering solution begins to differ from the analytical solution.

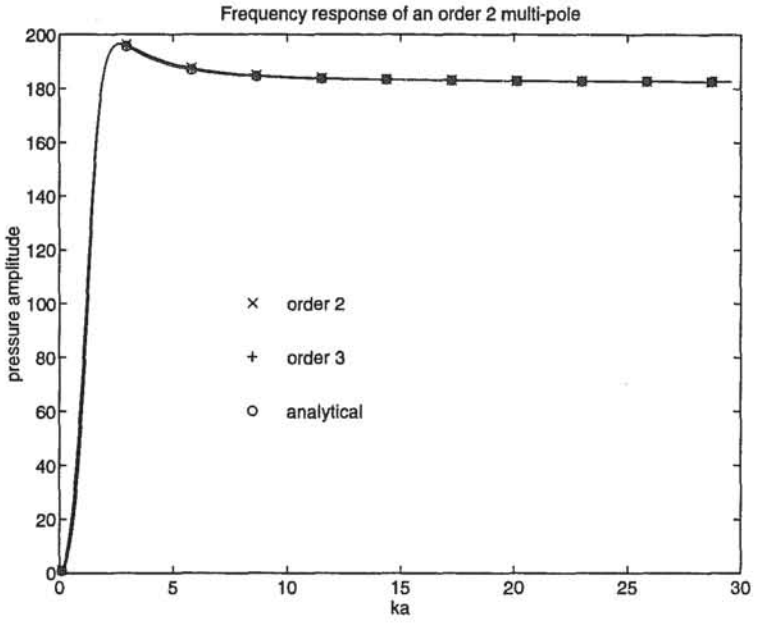

Figure 58: Radiated pressure at $(5a, 0)$ for varying wave envelope interpolation orders. Model is a 2D cylinder with 150 linear wave envelope elements.

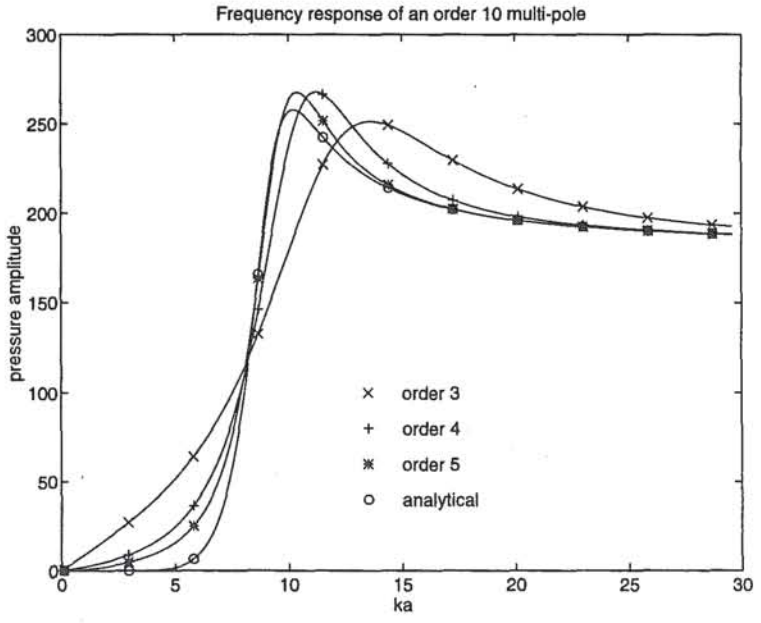

Figure 59: Radiated pressure at $(5a, 0)$ for varying wave envelope interpolation orders. Model is a 2D cylinder with 150 linear wave envelope elements.

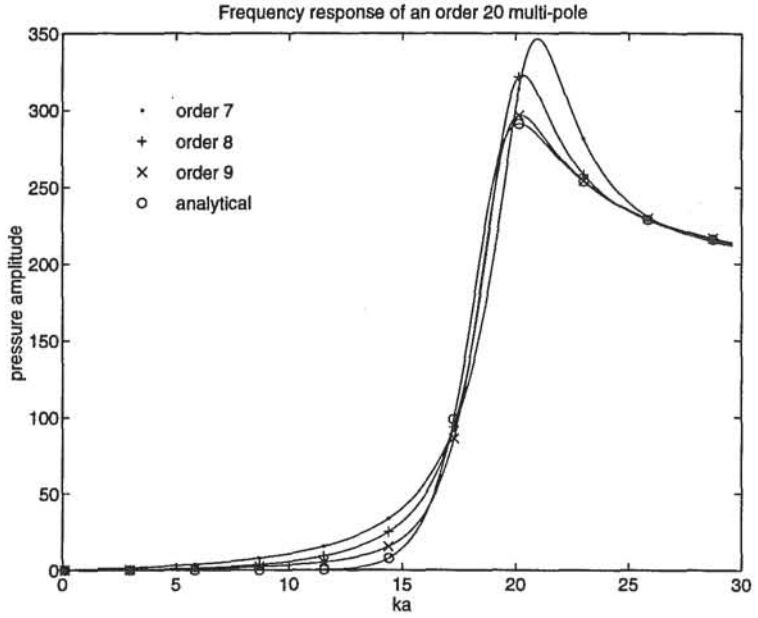

Figure 60: Radiated pressure at $(5a, 0)$ for varying wave envelope interpolation orders. Model is a 2D cylinder with 150 linear wave envelope elements.

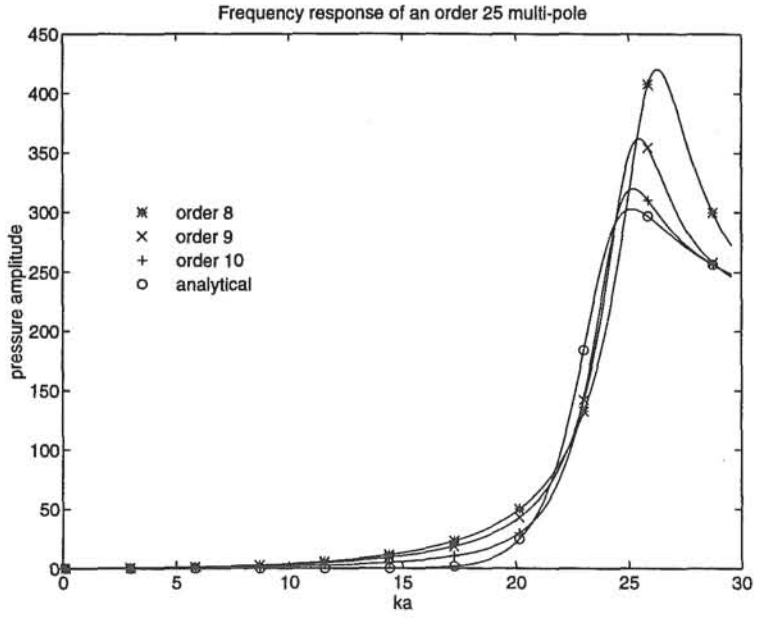

Figure 61: Radiated pressure at $(5a, 0)$ for varying wave envelope interpolation orders. Model is a 2D cylinder with 150 linear wave envelope elements.

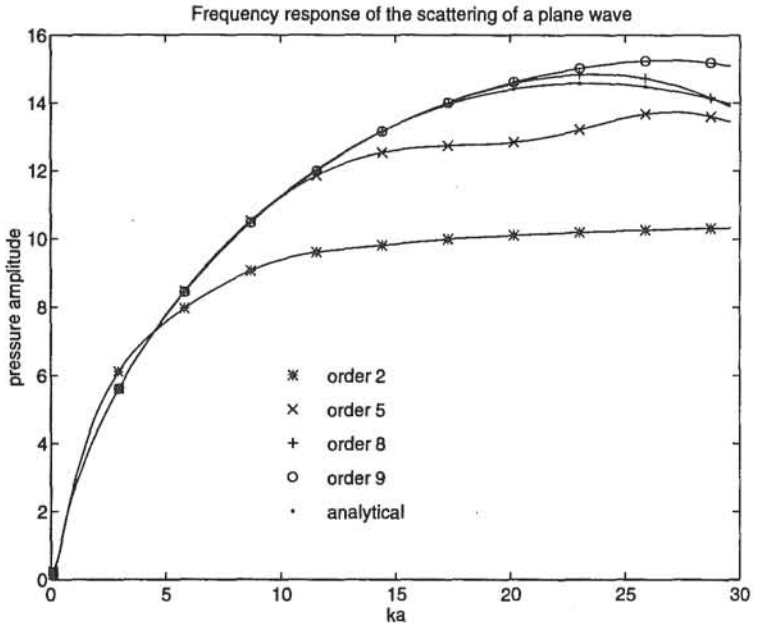

Figure 62: Scattered pressure at $(5a, 0)$ for varying wave envelope interpolation orders for a plane wave travelling in the positive x direction. Model is a 2D cylinder with 150 linear wave envelope elements.

Appendix F

The wave envelope program

A computer program has been written to provide a means for testing the wave envelope concept and the use of Ritz vectors. The Fortran 77 source code, along with numerous input and output files are on the enclosed diskette in MSDOS format. Instructions are provided in the `read.me` file on the diskette.

The main features of the program are:

- allows both wave envelope and conventional elements
- the wave envelope element interpolation can be varied up to order 10
- allows both two- and three-dimensional models
- allows solutions to be calculated at multiple frequencies
- can use variable numbers of Ritz vectors to solve the system
- accepts mesh definitions in a standard format
- uses skyline storage to store sparse matrices
- will automatically minimise the matrix bandwidth
- written in ANSI C and Fortran 77, with some VAX Fortran extensions
- will output results at given field points, or on a display mesh
- includes analytical solutions for some models and excitations
- unfriendly user interface
- has the characteristics of a lumbering elephant
- definitely unmodifiable, except by the original author

And a final note: trying to single-handedly write a program of this size (11000 lines) is hazardous to ones' health.